Atlas of Formability

Ti-6Al-4V ELI

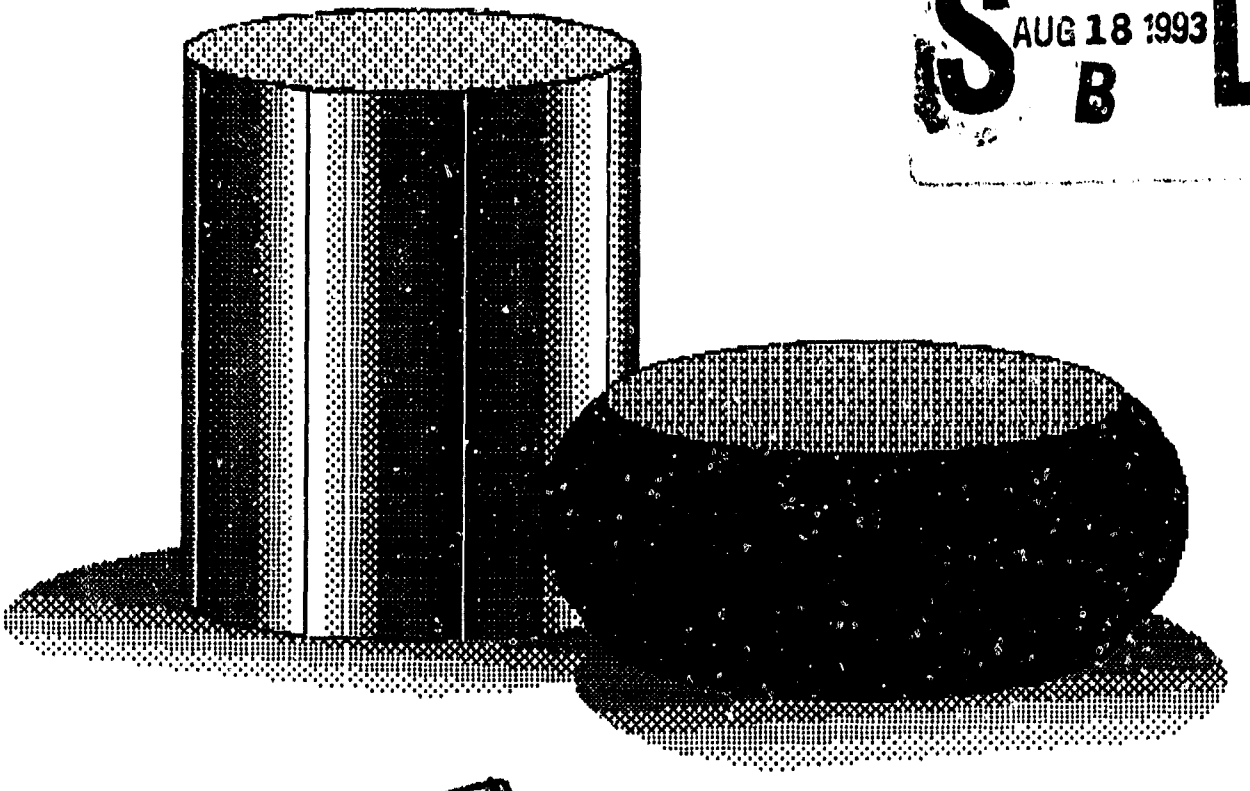

NCEMT

DISCLAIMER NOTICE

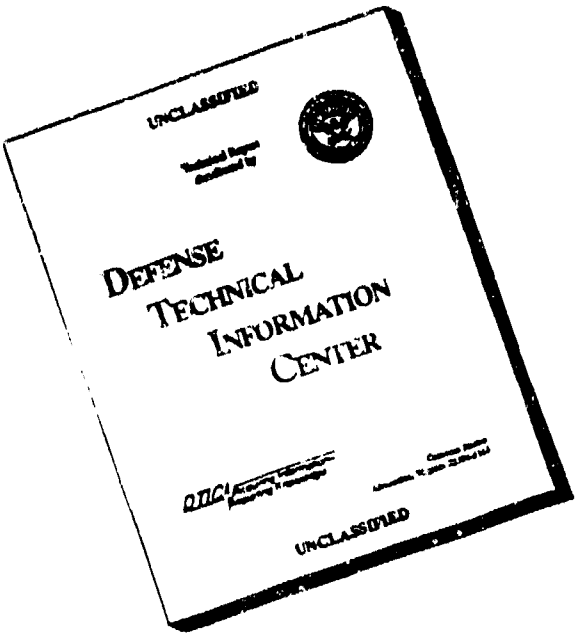

THIS DOCUMENT IS BEST QUALITY AVAILABLE. THE COPY FURNISHED TO DTIC CONTAINED A SIGNIFICANT NUMBER OF PAGES WHICH DO NOT REPRODUCE LEGIBLY.

ATLAS OF FORMABILITY

TI-6AL-4V ELI

by

Prabir K. Chaudhury and Dan Zhao

National Center for Excellence in Metalworking Technology
1450 Scalp Avenue
Johnstown, PA 15904

for

Naval Industrial Resource Support Activity
Building 75-2, Naval Base
Philadelphia, PA 19112-5078

October 31, 1992

REPORT DOCUMENTATION PAGE

Form Approved
OMB No. 0704-0188

1. AGENCY USE ONLY (Leave blank)	2. REPORT DATE	3. REPORT TYPE AND DATES COVERED
	October 31, 1992	Final, July 31, 1992-October 31, 1992

4. TITLE AND SUBTITLE

Atlas of Formability
Ti-6Al-4V ELI

5. FUNDING NUMBERS

C-N00140-88-C-RC21

6. AUTHOR(S)

Prabir Chaudhury
Dan Zhao

7. PERFORMING ORGANIZATION NAME(S) AND ADDRES*(ES)

National Center for Excellence in Metalworking
Tehcnology (NCEMT)
1450 Scalp Avenue
Johnstown, PA 15904

8. PERFORMING ORGANIZATION REPORT NUMBER

9. SPONSORING/MONITORING AGENCY NAME(S) AND ADDRESS(ES)

Naval Industrial Resources Support Activity
Building 75-2, Naval Base
Philadelphia, PA 19112-5078

10. SPONSORING/MONITORING AGENCY REPORT NUMBER

11. SUPPLEMENTARY NOTES

12a. DISTRIBUTION/AVAILABILITY STATEMENT

12b. DISTRIBUTION CODE

13. ABSTRACT *(Maximum 200 words)*

In this investigation, flow behavior of Ti-6Al-4V ELI alloy was studied by conducting compression tests over a wide range of temperatures and strain rates. Constitutive relations were determined from the flow behavior, and a dynamic material modeling was conducted on this alloy. Thus, the optimum processing condition in terms of temperature and strain rate was identified. Microstructural changes during high temperature deformation were also characterized.

14. SUBJECT TERMS

Ti-6Al-4V ELI, Deformation Processing, High Temperature Deformation, Processing Map, Metalworking

15. NUMBER OF PAGES

55

16. PRICE CODE

17. SECURITY CLASSIFICATION OF REPORT	18. SECURITY CLASSIFICATION OF THIS PAGE	19. SECURITY CLASSIFICATION OF ABSTRACT	20. LIMITATION OF ABSTRACT
Unclassified	Unclassified	Unclassified	

GENERAL INSTRUCTIONS FOR COMPLETING SF 298

The Report Documentation Page (RDP) is used in announcing and cataloging reports. It is important that this information be consistent with the rest of the report, particularly the cover and title page. Instructions for filling in each block of the form follow. It is important to ***stay within the lines*** to meet ***optical scanning requirements***.

Block 1. Agency Use Only *(Leave blank)*.

Block 2. Report Date. Full publication date including day, month, and year, if available (e.g. 1 Jan 88). Must cite at least the year.

Block 3. Type of Report and Dates Covered. State whether report is interim, final, etc. If applicable, enter inclusive report dates (e.g. 10 Jun 87 - 30 Jun 88).

Block 4. Title and Subtitle. A title is taken from the part of the report that provides the most meaningful and complete information. When a report is prepared in more than one volume, repeat the primary title, add volume number, and include subtitle for the specific volume. On classified documents enter the title classification in parentheses.

Block 5. Funding Numbers. To include contract and grant numbers; may include program element number(s), project number(s), task number(s), and work unit number(s). Use the following labels:

C	- Contract	PR	- Project
G	- Grant	TA	- Task
PE	- Program Element	WU	- Work Unit Accession No.

Block 6. Author(s). Name(s) of person(s) responsible for writing the report, performing the research, or credited with the content of the report. If editor or compiler, this should follow the name(s).

Block 7. Performing Organization Name(s) and Address(es). Self-explanatory.

Block 8. Performing Organization Report Number. Enter the unique alphanumeric report number(s) assigned by the organization performing the report.

Block 9. Sponsoring/Monitoring Agency Name(s) and Address(es). Self-explanatory.

Block 10. Sponsoring/Monitoring Agency Report Number. *(If known)*

Block 11. Supplementary Notes. Enter information not included elsewhere such as: Prepared in cooperation with...; Trans. of...; To be published in.... When a report is revised, include a statement whether the new report supersedes or supplements the older report.

Block 12a. Distribution/Availability Statement. Denotes public availability or limitations. Cite any availability to the public. Enter additional limitations or special markings in all capitals (e.g. NOFORN, REL, ITAR).

- **DOD** - See DoDD 5230.24, "Distribution Statements on Technical Documents."
- **DOE** - See authorities.
- **NASA** - See Handbook NHB 2200.2.
- **NTIS** - Leave blank.

Block 12b. Distribution Code.

- **DOD** - Leave blank.
- **DOE** - Enter DOE distribution categories from the Standard Distribution for Unclassified Scientific and Technical Reports.
- **NASA** - Leave blank.
- **NTIS** - Leave blank.

Block 13. Abstract. Include a brief *(Maximum 200 words)* factual summary of the most significant information contained in the report.

Block 14. Subject Terms. Keywords or phrases identifying major subjects in the report.

Block 15. Number of Pages. Enter the total number of pages.

Block 16. Price Code. Enter appropriate price code *(NTIS only)*.

Blocks 17. - 19. Security Classifications. Self-explanatory. Enter U.S. Security Classification in accordance with U.S. Security Regulations (i.e., UNCLASSIFIED). If form contains classified information, stamp classification on the top and bottom of the page.

Block 20. Limitation of Abstract. This block must be completed to assign a limitation to the abstract. Enter either UL (unlimited) or SAR (same as report). An entry in this block is necessary if the abstract is to be limited. If blank, the abstract is assumed to be unlimited.

TABLE OF CONTENTS

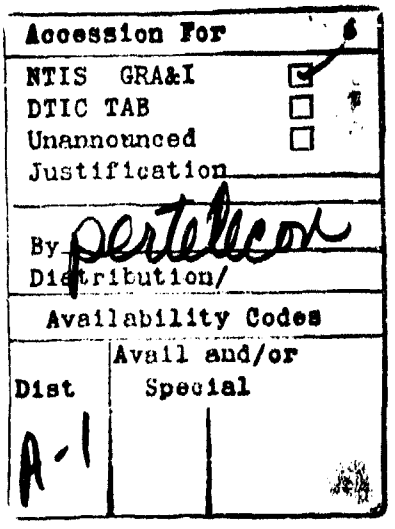

LIST OF TABLE

Ti-6Al-4V ELI

Introduction

Ti-6Al-4V is one of the conventional titanium alloys with a variety of applications in the aerospace industry. The understanding of mechanical and microstructural behavior during high temperature deformation is very important for this alloy since the microstructure and mechanical properties are strongly affected by the thermomechanical processing history. In this investigation, the flow behavior of Ti-6Al-4V, ELI grade was studied by conducting compression testing at various temperatures and strain rates. Constitutive relations were determined from the flow behavior and then, a dynamic material modeling for this alloy was performed. Thus, the optimum processing conditions in terms of temperature and strain rate were determined. Microstructural changes during high temperature deformation were also characterized to aid process design engineers to select processing conditions in terms of resulting microstructure.

Experimental Procedure

The material used in this investigation was commercially available Ti-6Al-4V ELI in the form of hot rolled and annealed bar with a 0.687 inch diameter. The typical microstructure of the as-received materials consisted of elongated α grains with an aspect ratio of 1.8 containing very fine intergranular β as shown in Figure 1. The composition of this alloy is as follows:

C	N	Fe	Al	V	Y	O	H
0.01	0.011	.20	5.80	3.82	<50PPM	0.124	62PPM

Cylindrical compression test specimens with a diameter of 12.7 mm and a height of 15.9 mm were machined from the bars. Isothermal compression tests in vacuum environment were conducted on an MTS machine. The test matrix was as follows:

Temperature, C (F): 800 (1472), 850 (1562), 900 (1652), 950 (1742), 1000 (1832), 1040 (1904), 1080 (1976);
Strain rate, s^{-1}: 0.001, 0.01, 0.1, 1, 5 and 25.

Load and stroke data from the testing was acquired by a computer and later converted to true stress-true strain curves. Immediately after the compression test, the specimens were quenched with forced helium gas in order to retain the deformed microstructure. Longitudinal section of the specimens were examined with optical microscope and photomicrographs were taken from the center of the longitudinal section of the specimens.

Results

Table 1 gives a list of the figures, testing conditions and the observed microstructures. The true stress-true strain flow curves with the corresponding deformed microstructure are shown in Figure 2 to Figure 43. True stress versus strain rate was plotted in a log-log scale in Figure 44 at a true strain of approximately 0.3. The slope of the plot gives the strain rate sensitivity m, which is not constant over the range of strain rate tested. Log stress vs. 1/T at the same true strain is shown in Figure 45. A processing map at this strain was developed and is shown in Figure 46. The optimum processing condition from the map can be obtained by selecting the temperature and strain rate combination which provides the maximum efficiency in the stable region. This condition is approximately 896 C and 0.001 s^{-1} for this material.

Table 1. List of figures, testing conditions and microstructural observations for Ti-6Al-4V ELI

Figure No	Temperature C (F)	Strain Rate s^{-1}	Microstructure Optical M croscopy	Page No
1	As received		Elongated α grains with an aspect ratio of 1.8 containing very fine intergranular β.	4
2	800 (1472)	0.001	Equiaxed α grains with a uniform size of ~5.5 μm containing ~10-15% of very fine intergranular β.	5
3	800 (1472)	0.01		6
4	800 (1472)	0.1	Equiaxed α grains with a uniform size of ~5μm containing ~10-15% of very fine intergranular β	7
5	800 (1472)	1	Equiaxed α grains with a size of ~5μm, but there is a small proportion of α elongated grains. Very fine β is present at the grain boundaries.	8
6	800 (1472)	5		9
7	800 (1472)	25	Elongated and equiaxed α grains. the equiaxed grains (~20%) have a size of ~4μm. Very fine intergranular β.	10
8	850 (1562)	0.001	Equiaxed α grains with an irregular size. The smaller grains are in a proportion of 10-12% and have a size of 1-3μm. The larger α grains have an average size of ~10μm. β is fine and intergranular.	11
9	850 (1562)	0.01	Equiaxed α grains with an average size of ~7μm and a small proportion (~3%) of α grains with a size between 1-3 μm. β is intergranular.	12
10	850 (1562)	0.1	Small equiaxed α grains (~5μm). There are some larger α grains with a size of ~7μm. β is intergranular.	13
11	850 (1562)	1		14
12	850 (1562)	5	Same as above.	15
13	850 (1562)	25	Equiaxed α grains with a duplex size. The larger grains have a size of ~5 μm. The smaller grains are in a proportion of ~5% and have a size of ~1-2 μm. β is very fine and is intergranular.	16
14	900 (1652)	0.001	Uniform equiaxed α grains with an average size of 5.4 μm and ~3-5% of very fine acicular α (transformed β). There is also some intergranular β.	17
15	900 (1652)	0.01		18

16	900 (1652)	0.1	Equiaxed α grains with a uniform size (~5 μm). There is a small proportion of very fine acicular α (transformed β grains of ~3 μm). There is also the presence of intergranular β.	19
17	900 (1652)	1	Equiaxed α grains with an irregular size. Although the larger proportion of the α grains have a size of ~4 μm. The smaller α grains have a size of ~2μm. There is ~1% of transformed β containing very fine acicular α and, β is very fine and intergranular.	20
18	900 (1652)	5		21
19	900 (1652)	25	Equiaxed α grains with a uniform size (~7 μm). There is very fine transformed β at the grain boundary triple points, in addition to a small proportion of intergranular β.	22
20	950 (1742)	0.001	Equiaxed α grains with a uniform size (7.1±0.6 μm). There is ~10% of acicular α (transformed β) and intergranular β.	23
21	950 (1742)	0.01	Equiaxed α grains with a uniform size (~6 μm). There is ~10-12% of acicular α (transformed β) with intergranular β.	24
22	950 (1742)	0.1	Same as above	25
23	950 (1742)	1	Same as above. But the grain size is smaller (~4.5μm) and 15-20% of acicular α. The acicular spacing is ~1.7 μm.	26
24	950 (1742)	5	Same as above	27
25	950 (1742)	25	Equiaxed α grains with a uniform size (7.8 ± 0.5 μm). There is ~15% of acicular α (transformed β) and intergranular β.	28
26	1000 (1882)	0.001	Large equiaxed transformed β grains (~194 ±30 μm) into plate-like α+β , and α at prior β grain boundaries. The α plate spacing is ~1.8 μm.	29
27	1000 (1882)	0.01	Same as above, but the prior β grains are ~180 μm and the interplate or interlamellar spacing is approximately 1.6 μm.	30
28	1000 (1882)	0.1	Same as above, but the prior β grains are slightly smaller.	31
29	1000 (1882)	1	Large equiaxed transformed β grains into plate-like α+β and some coarse acicular α, and α at prior β grain boundaries.	32
30	1000 (1882)	5		33
31	1000 (1882)	25	Same as above, but smaller grain size.	34
32	1040 (1904)	0.001	Large equiaxed transformed β grains (~ 280μm) into plate-like α+β and some coarse acicular α, and α at prior β grain boundaries.	35

33	1040 (1904)	0.01	Same as above, but the grain size is approximately 200μm, while the interlamellar spacing was found to be ~2μm.	36
34	1040 (1904)	0.1		37
35	1040 (1904)	1	Same as above, but smaller grain size (270μm).	38
36	1040 (1904)	5		39
37	1040 (1904)	25	Same as above, but smaller grain size (240μm).	40
38	1080 (1976)	0.001	Very large equiaxed transformed β grains into a very fine plate-like α + β , The α–phase at prior β grain boundaries is relatively thicker than at the strain rates analyzed below.	41
39	1080 (1976)	0.01		42
40	1080 (1976)	0.1	Same as above, but thinner prior β grain boundaries.	43
41	1080 (1976)	1	Very large equiaxed transformed β grains into plate-like α+β and, α at prior β grain boundaries.	44
42	1080 (1976)	5		45
43	1080 (1976)	25	Large equiaxed transformed β grain into plate-like α+ β and, α at prior β grain boundaries.	46

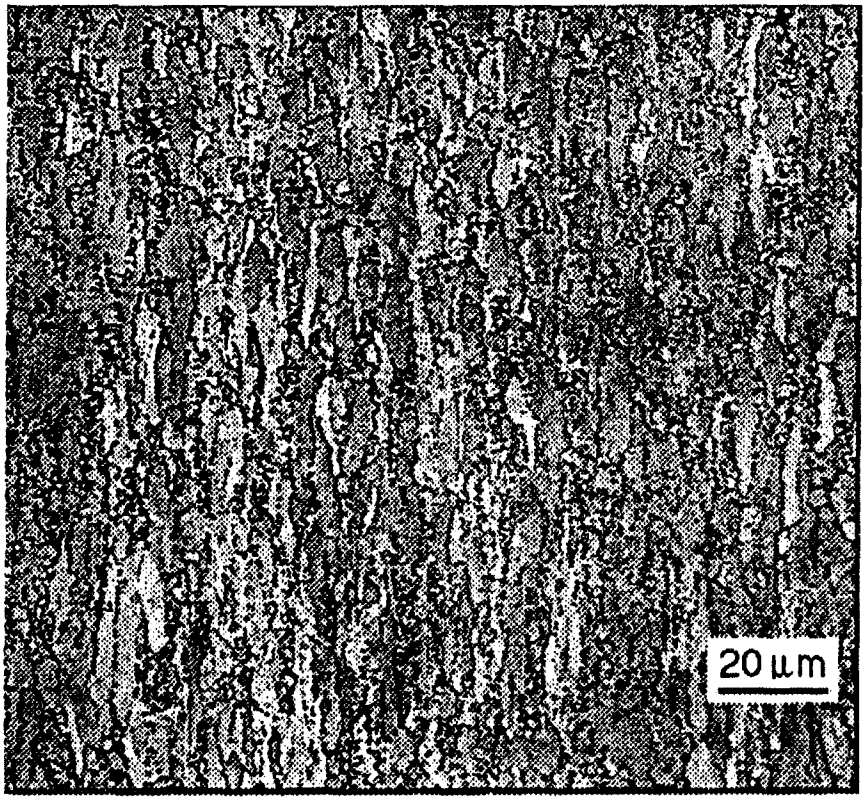

Figure 1. As-received microstructure of Ti-6Al-4V ELI.

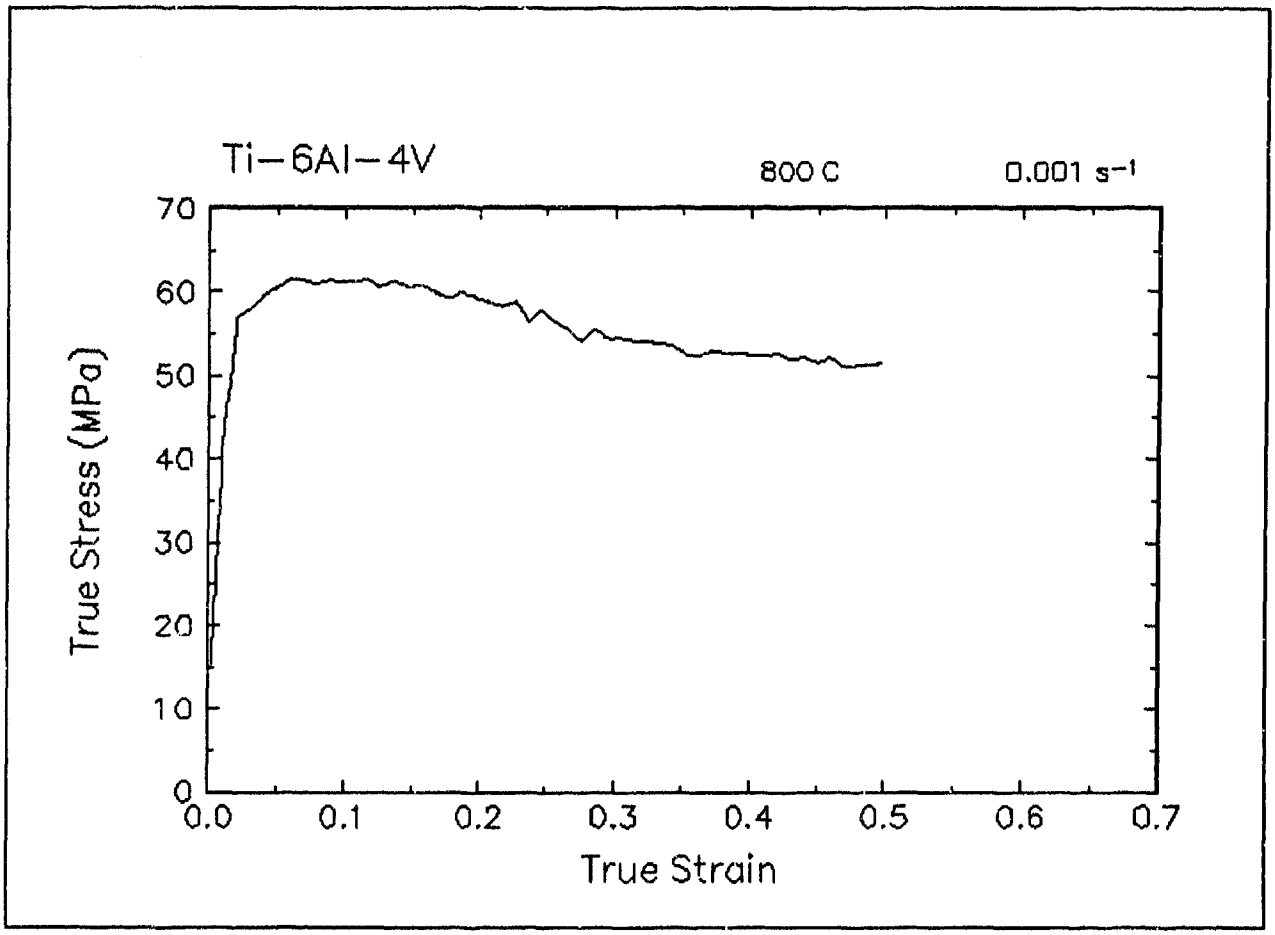

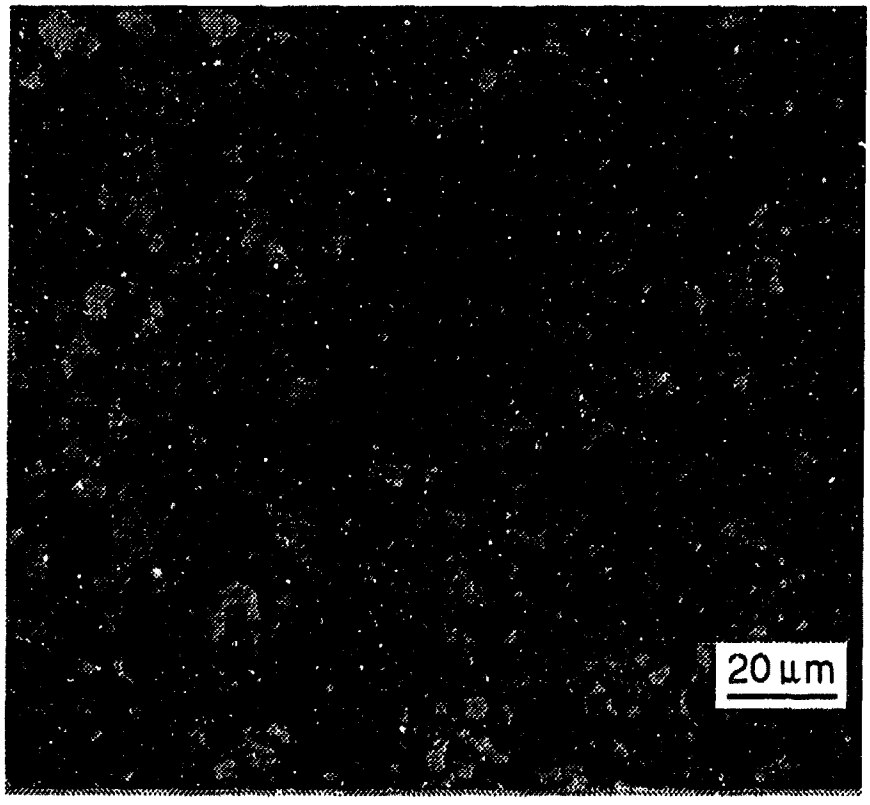

Figure 2. True stress-true strain curve and an optical micrograph from the center of the compressed sample cut through the compression axis, 800 C and 0.001 s^{-1}.

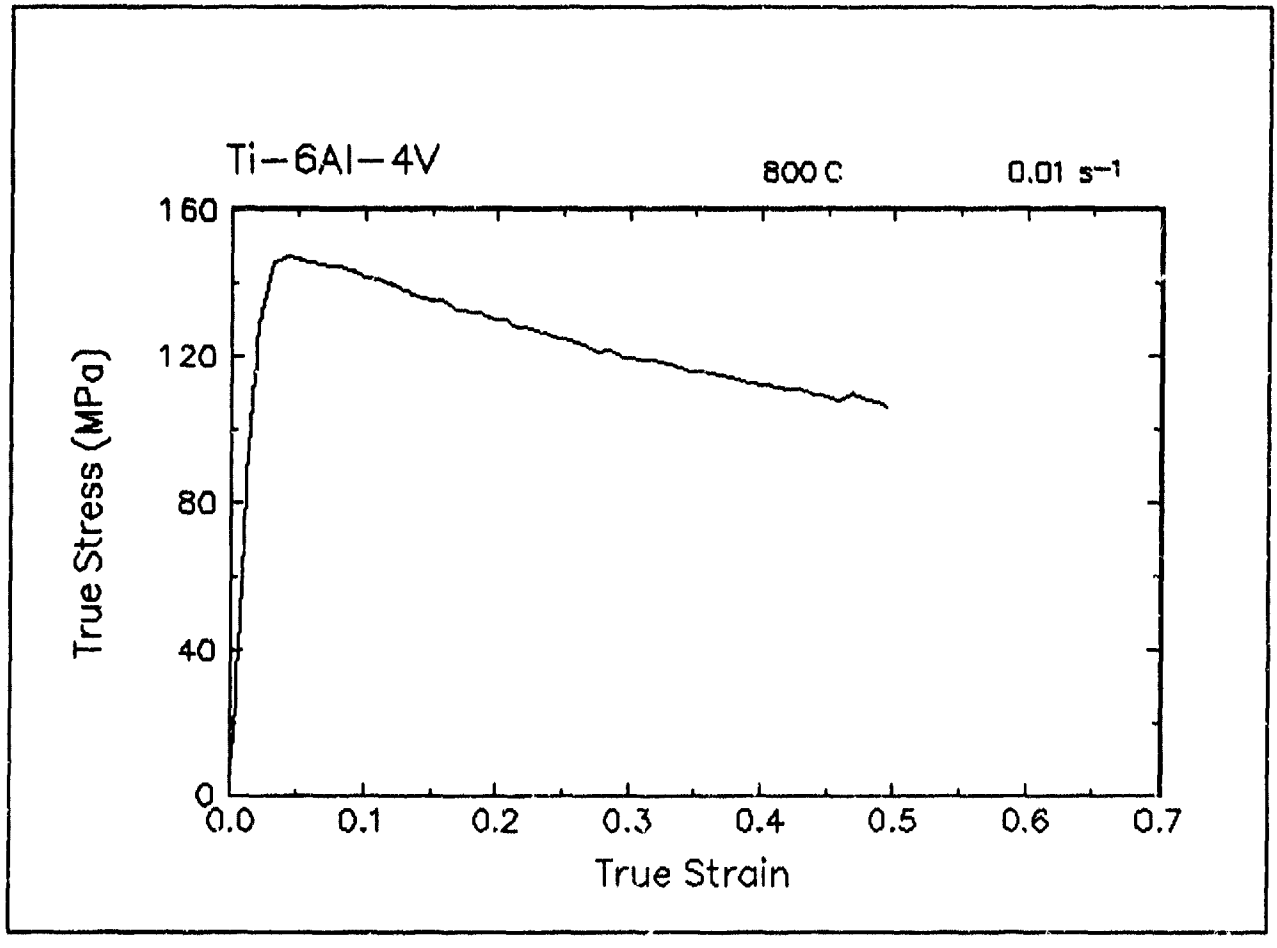

Figure 3. True stress-true strain curve, 800 C and 0.01 s^{-1}.

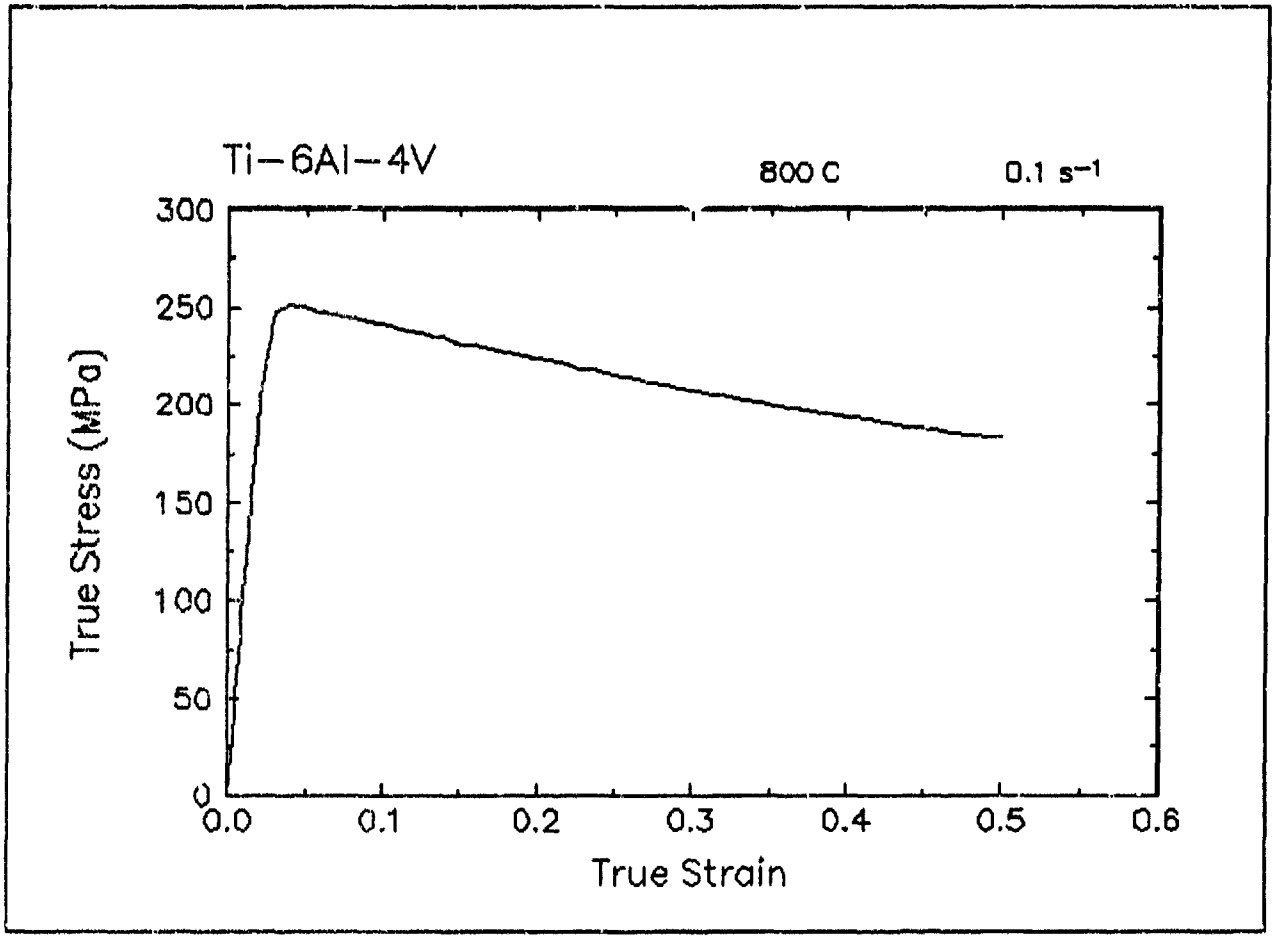

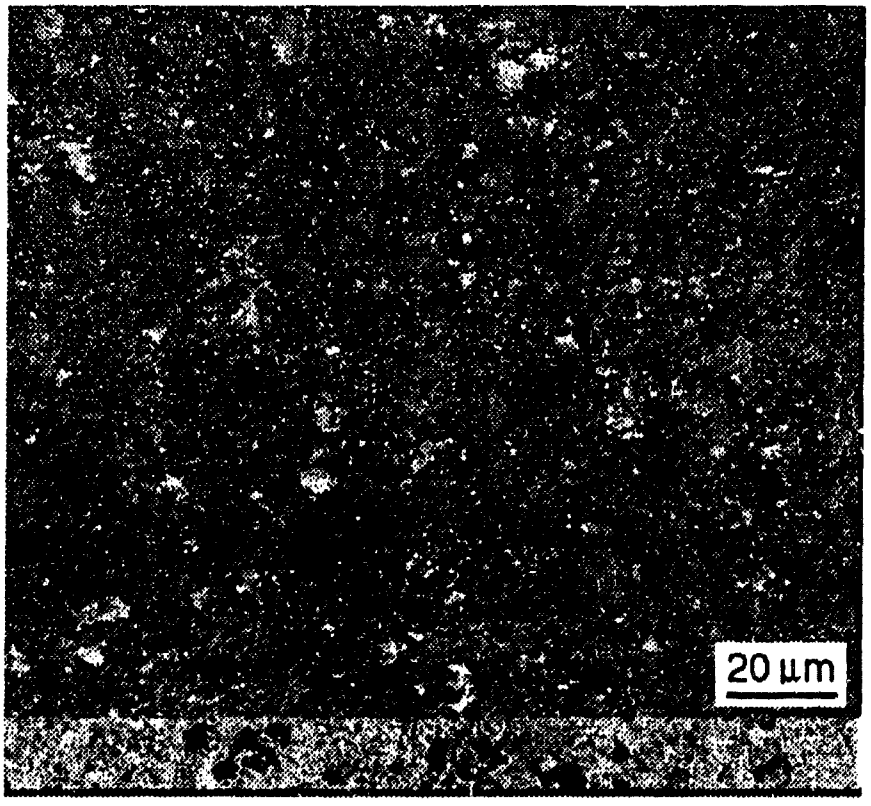

Figure 4. True stress-true strain curve and an optical micrograph from the center of the compressed sample cut through the compression axis, 800 C and 0.1 s^{-1}.

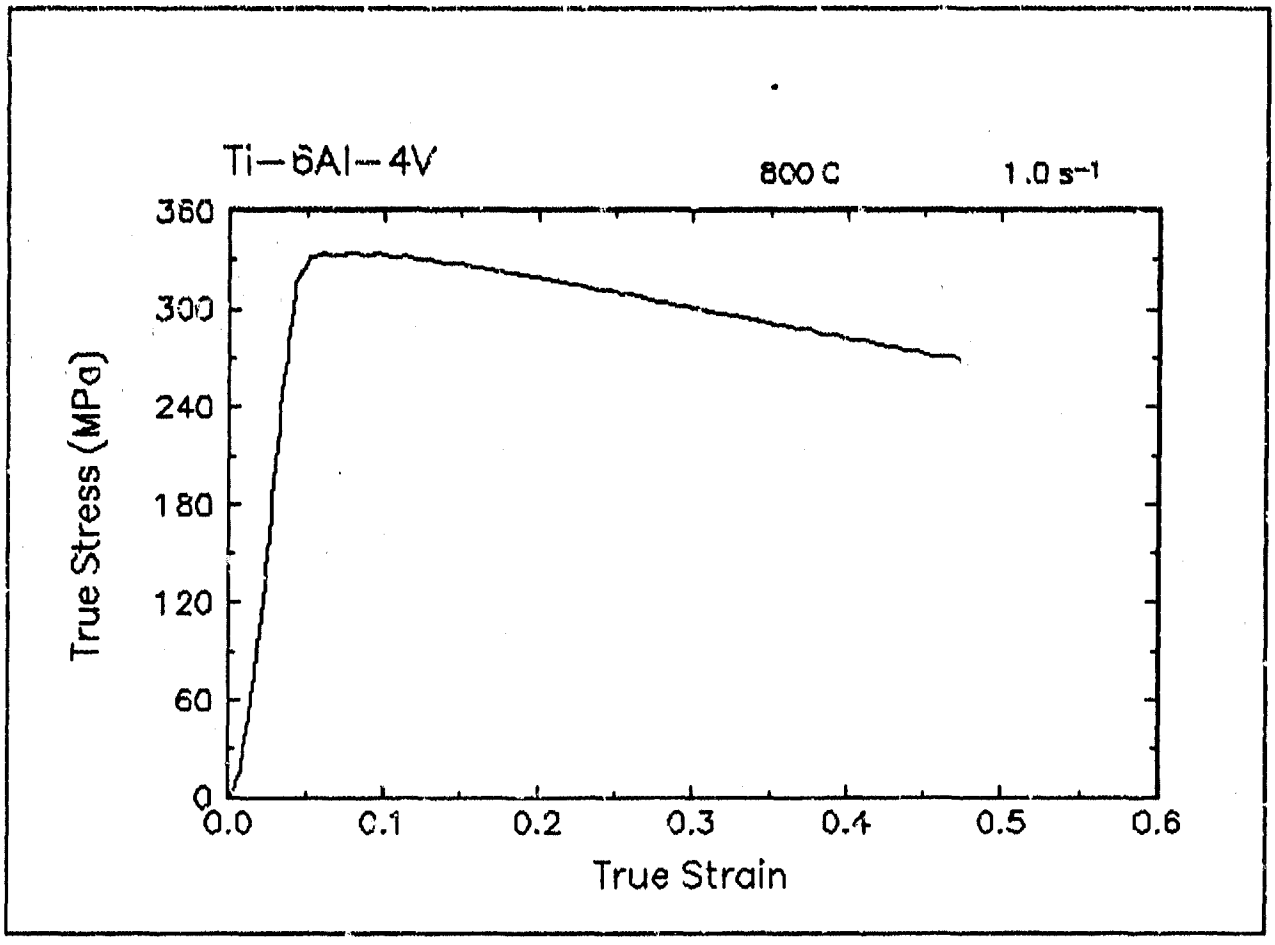

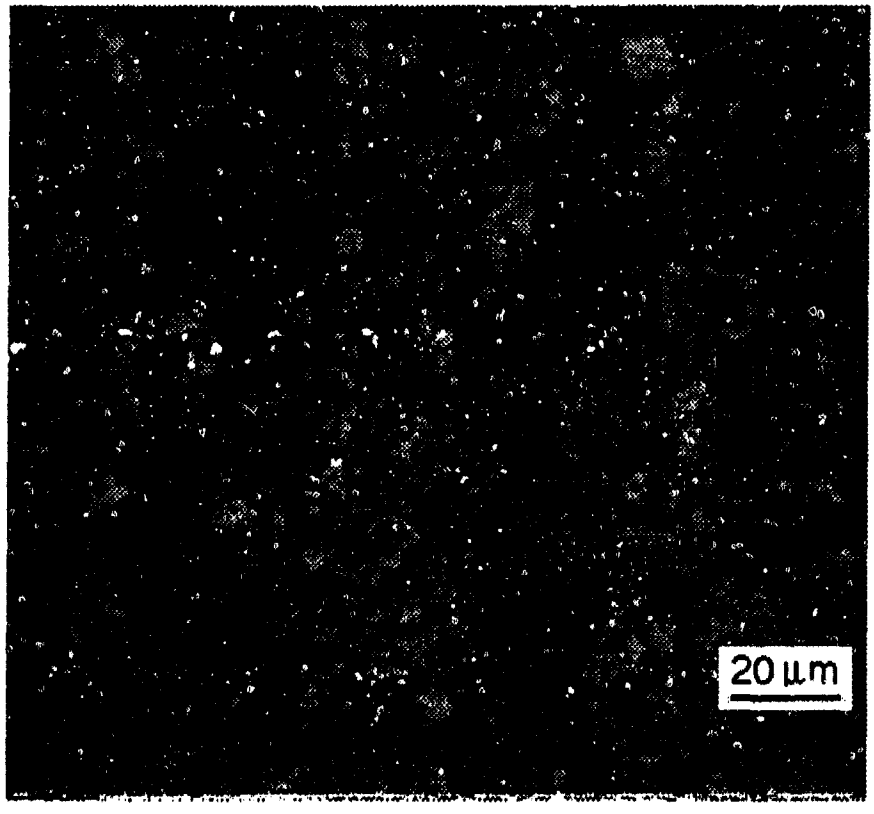

Figure 5. True stress-true strain curve and an optical micrograph from the center of the compressed sample cut through the compression axis, 800 C and 1 s^{-1}.

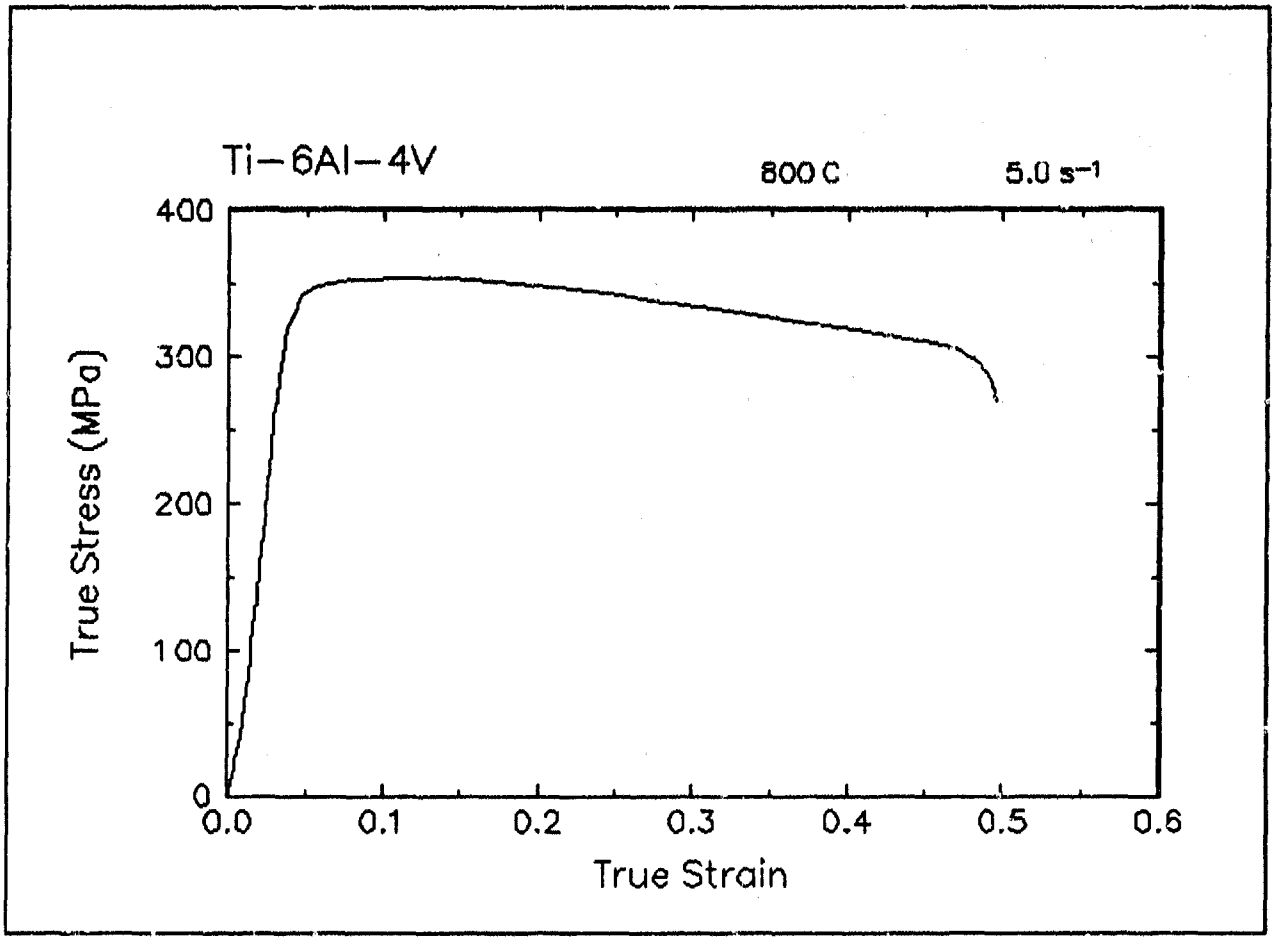

Figure 6. True stress-true strain curve, 800 C and 5 s^{-1}.

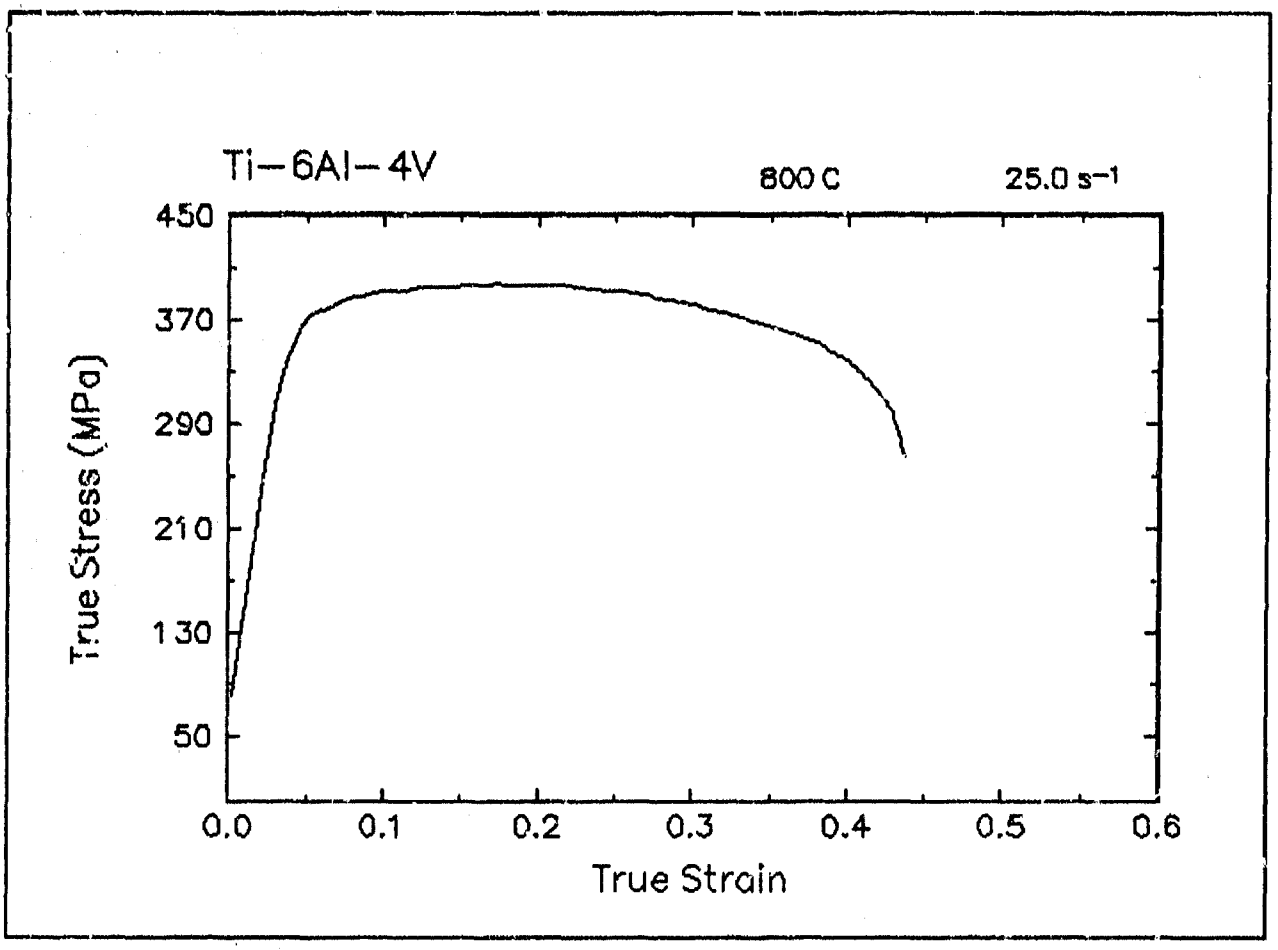

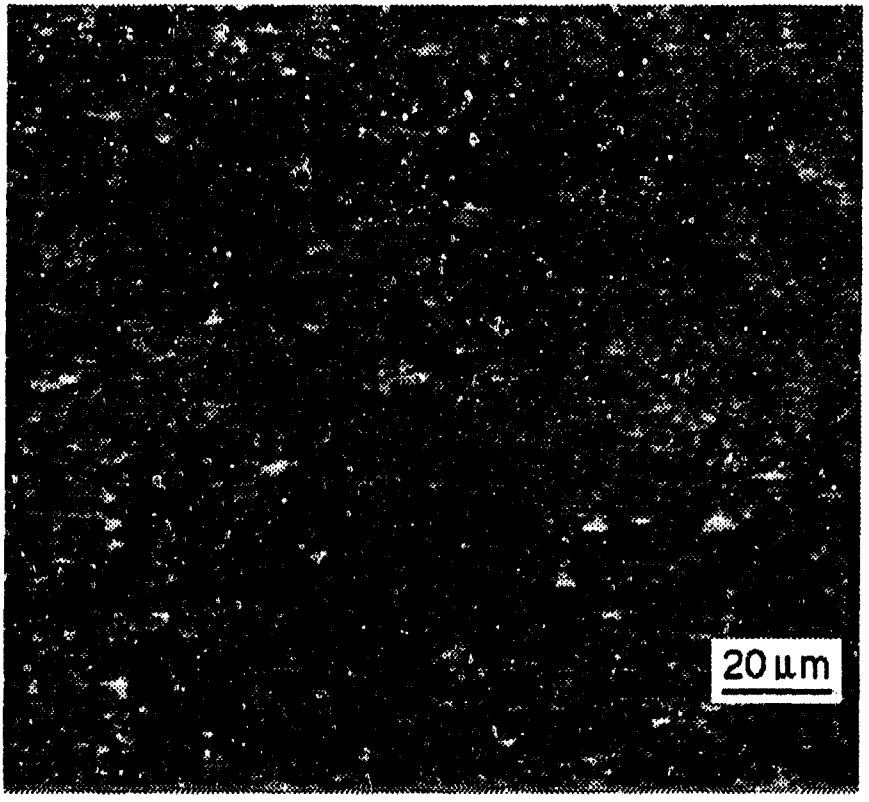

Figure 7. True stress-true strain curve and an optical micrograph from the center of the compressed sample cut through the compression axis, 800 C and 25 s^{-1}.

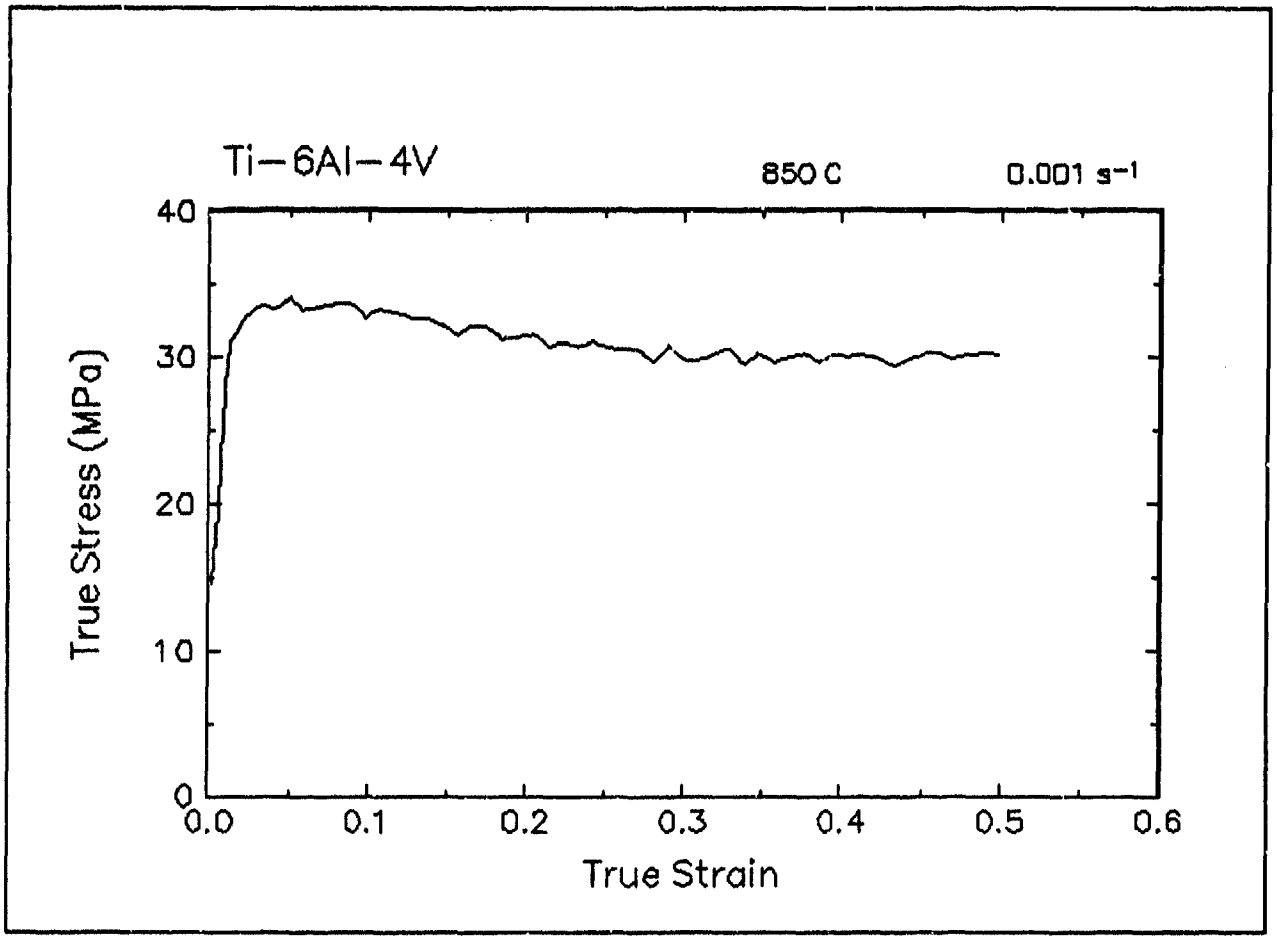

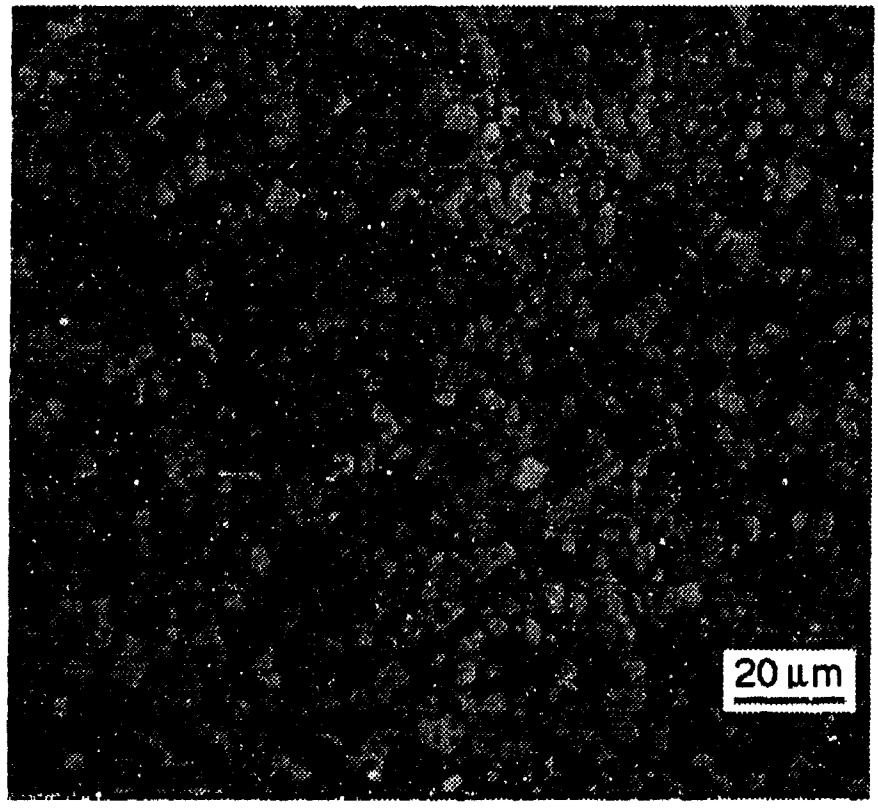

Figure 8. True stress-true strain curve and an optical micrograph from the center of the compressed sample cut through the compression axis, 850 C and 0.001 s^{-1}.

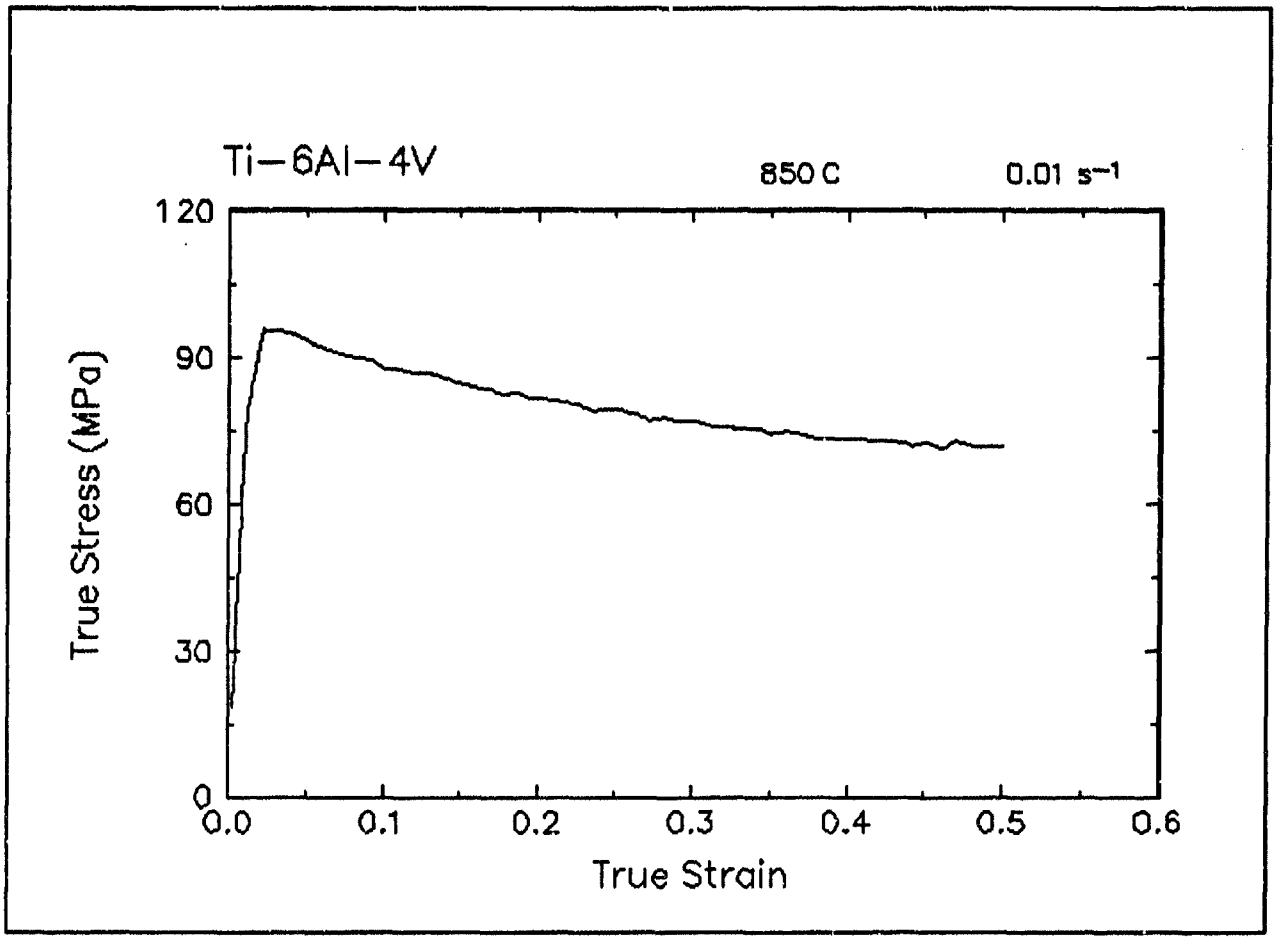

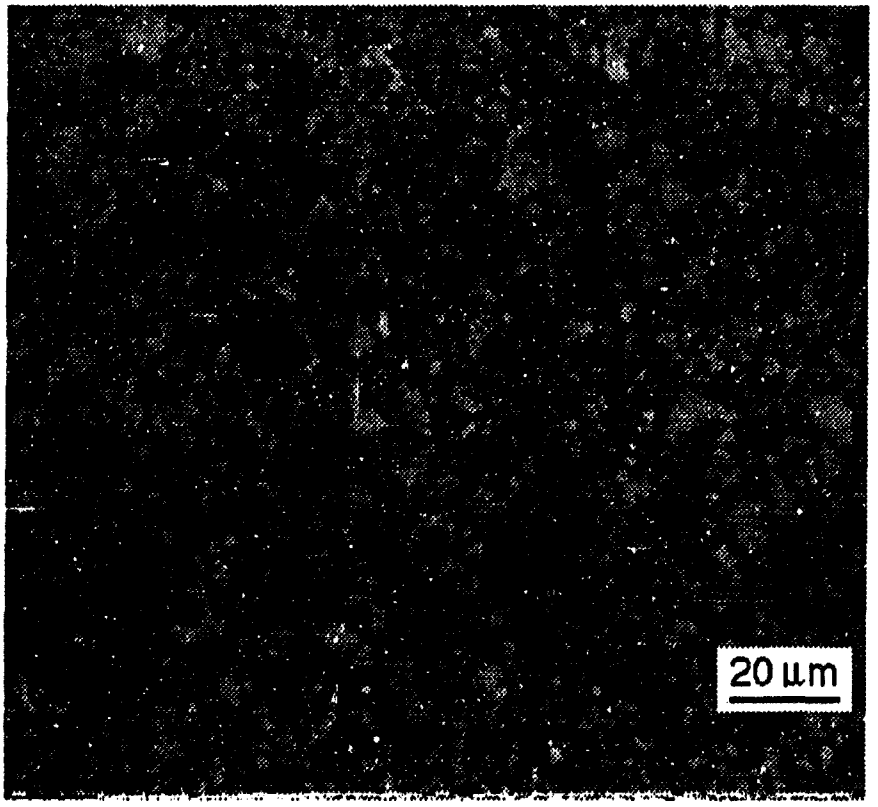

Figure 9. True stress-true strain curve and an optical micrograph from the center of the compressed sample cut through the compression axis, 850 C and 0.01 s^{-1}.

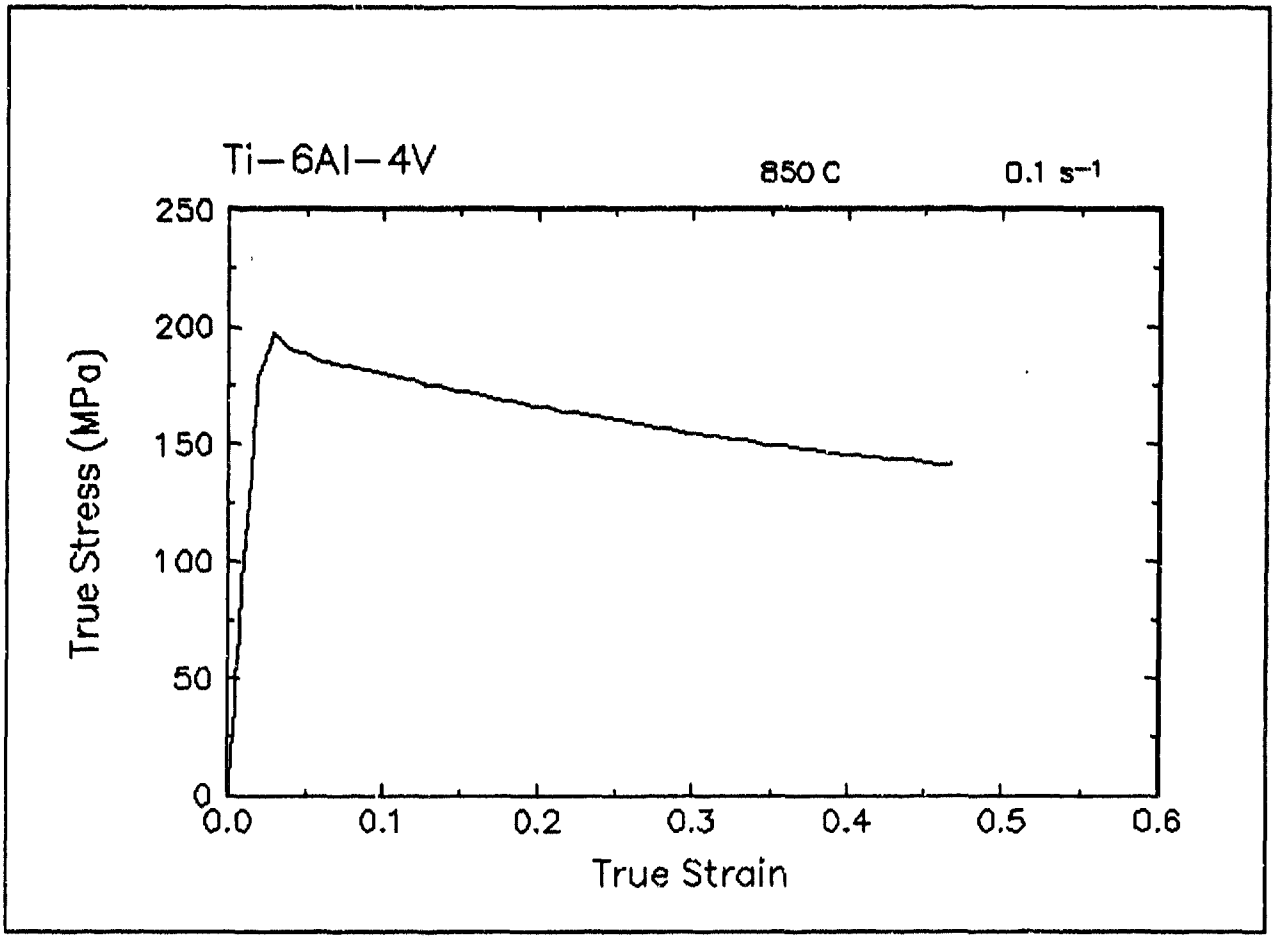

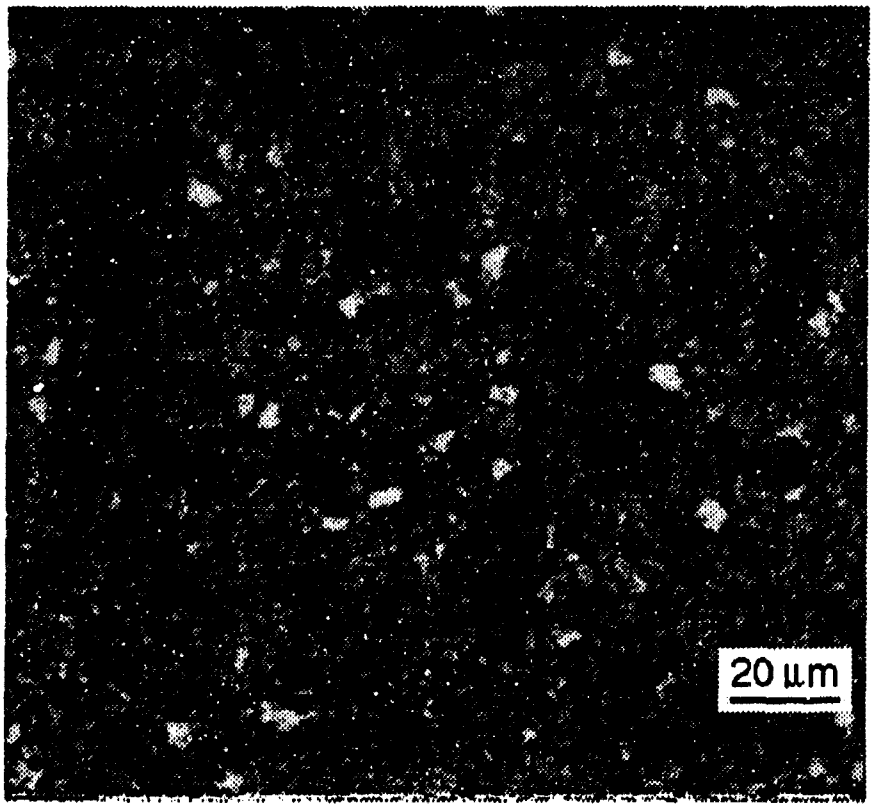

Figure 10. True stress-true strain curve and an optical micrograph from the center of the compressed sample cut through the compression axis, 850 C and 0.1 s^{-1}.

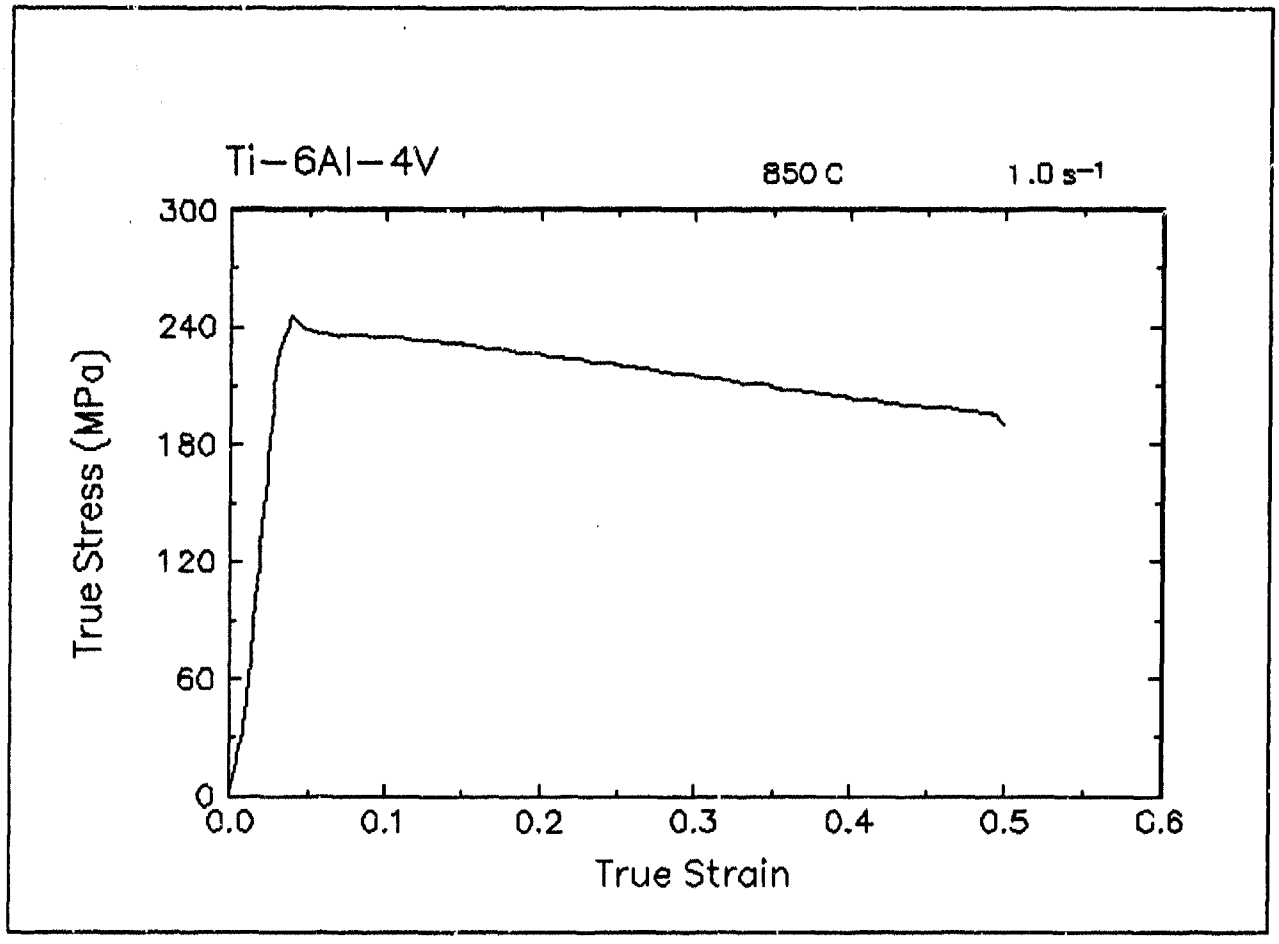

Figure 11. True stress-true strain curve, 850 C and 1 s^{-1}.

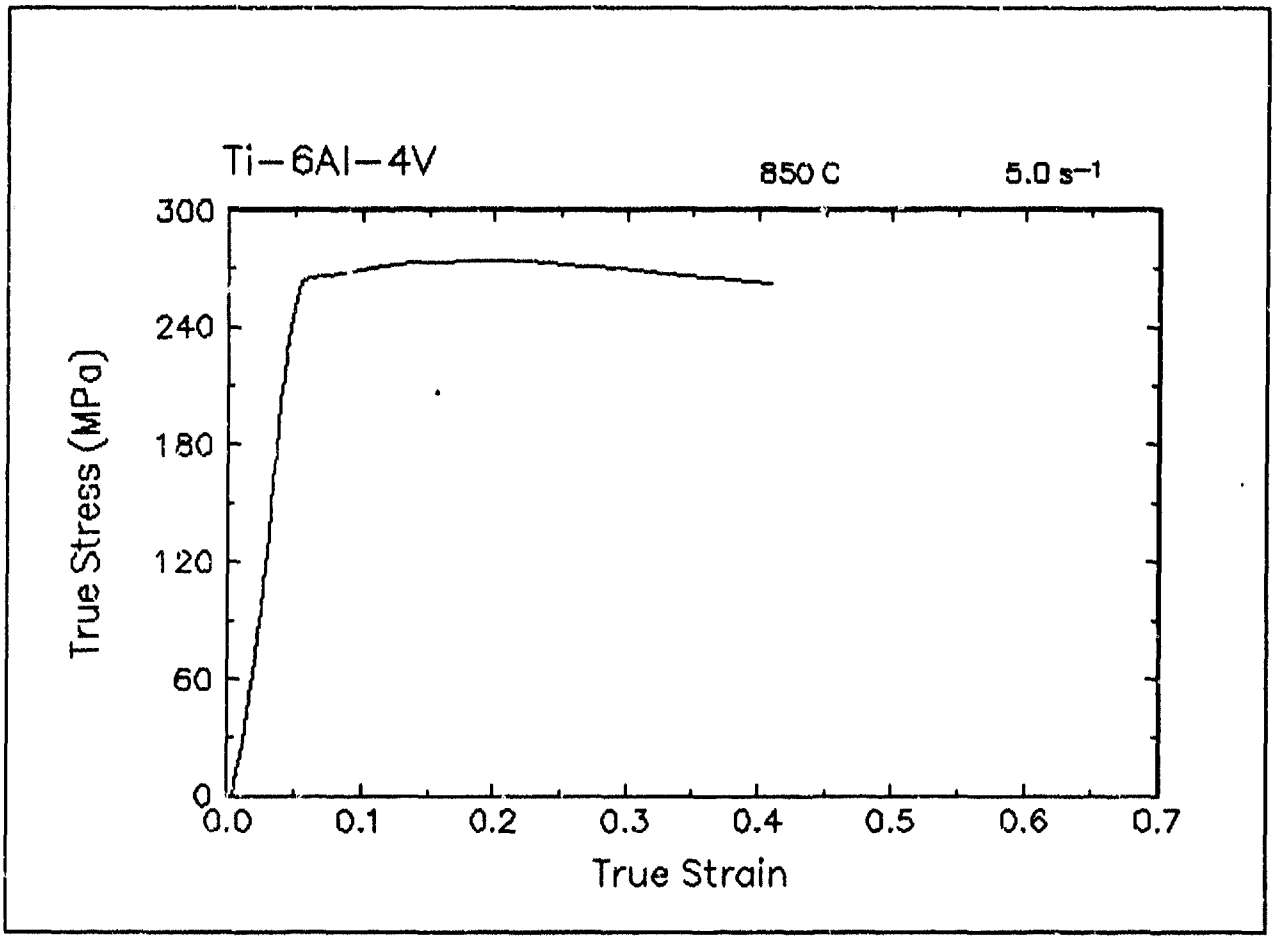

Figure 12. True stress-true strain curve, 850 C and 5 s^{-1}.

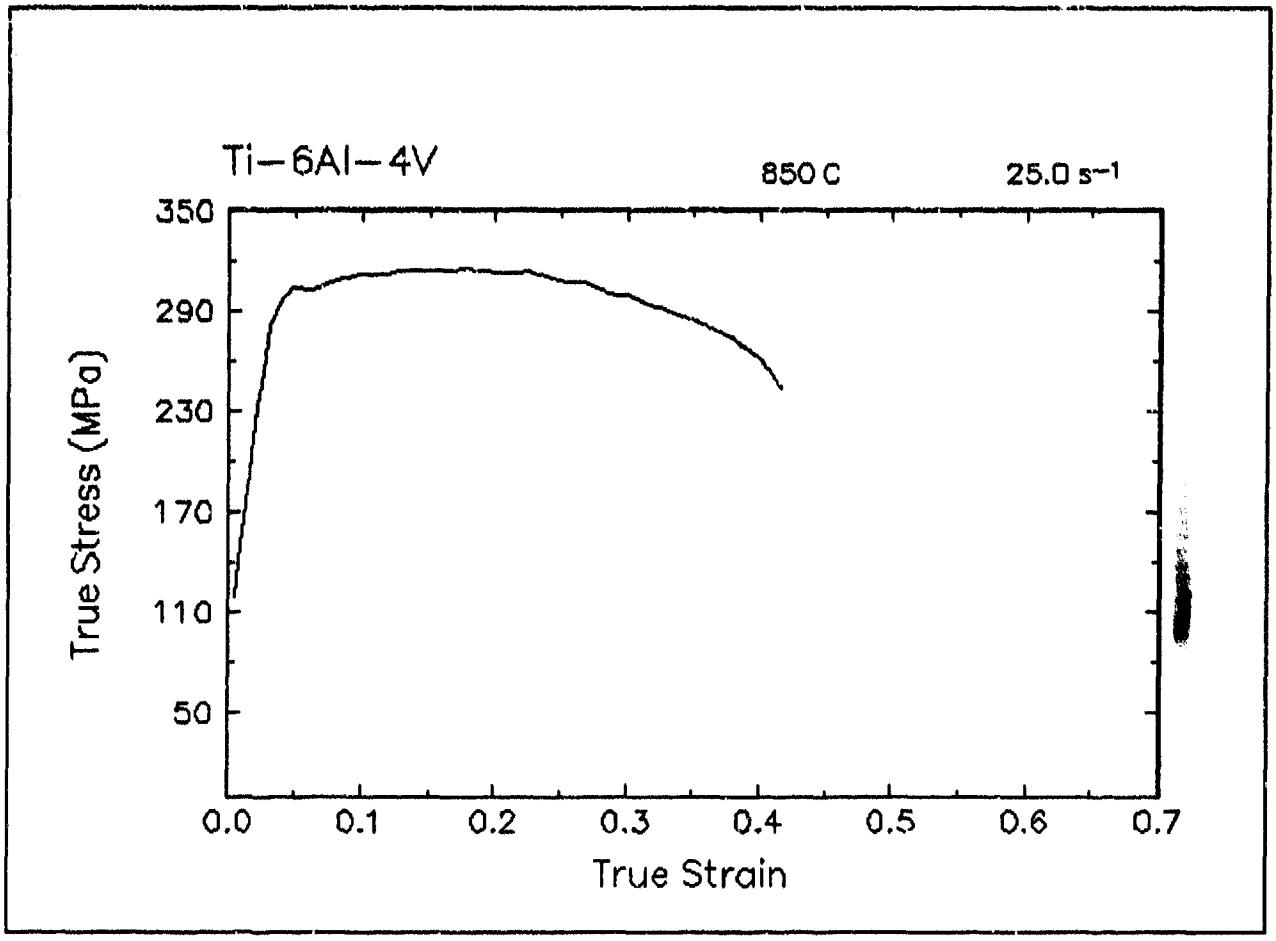

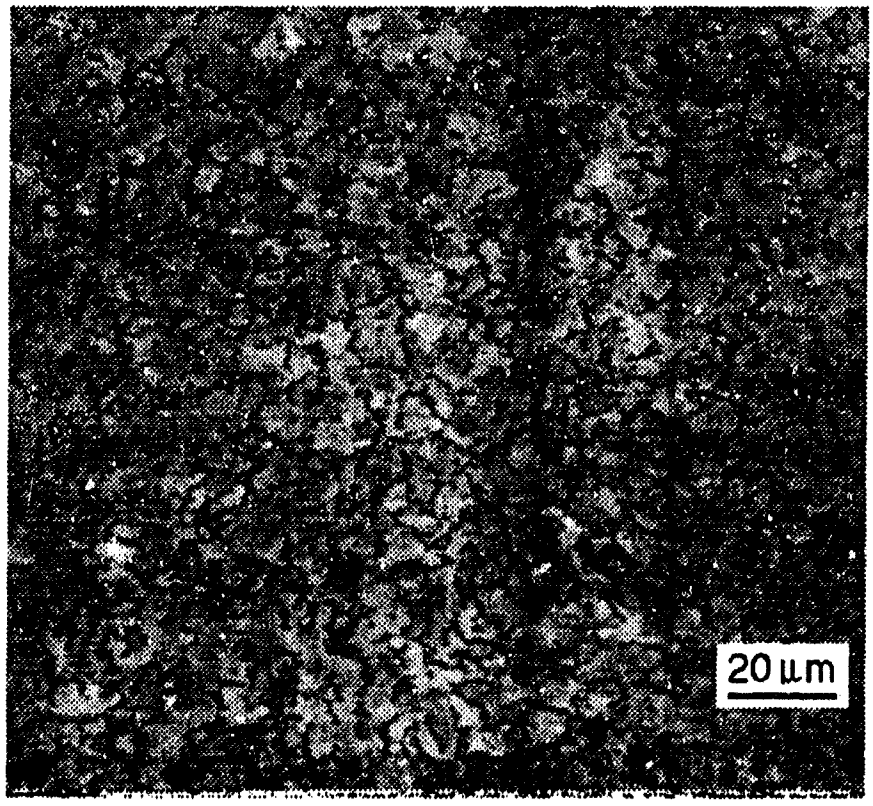

Figure 13. True stress-true strain curve and an optical micrograph from the center of the compressed sample cut through the compression axis, 850 C and 25 s^{-1}.

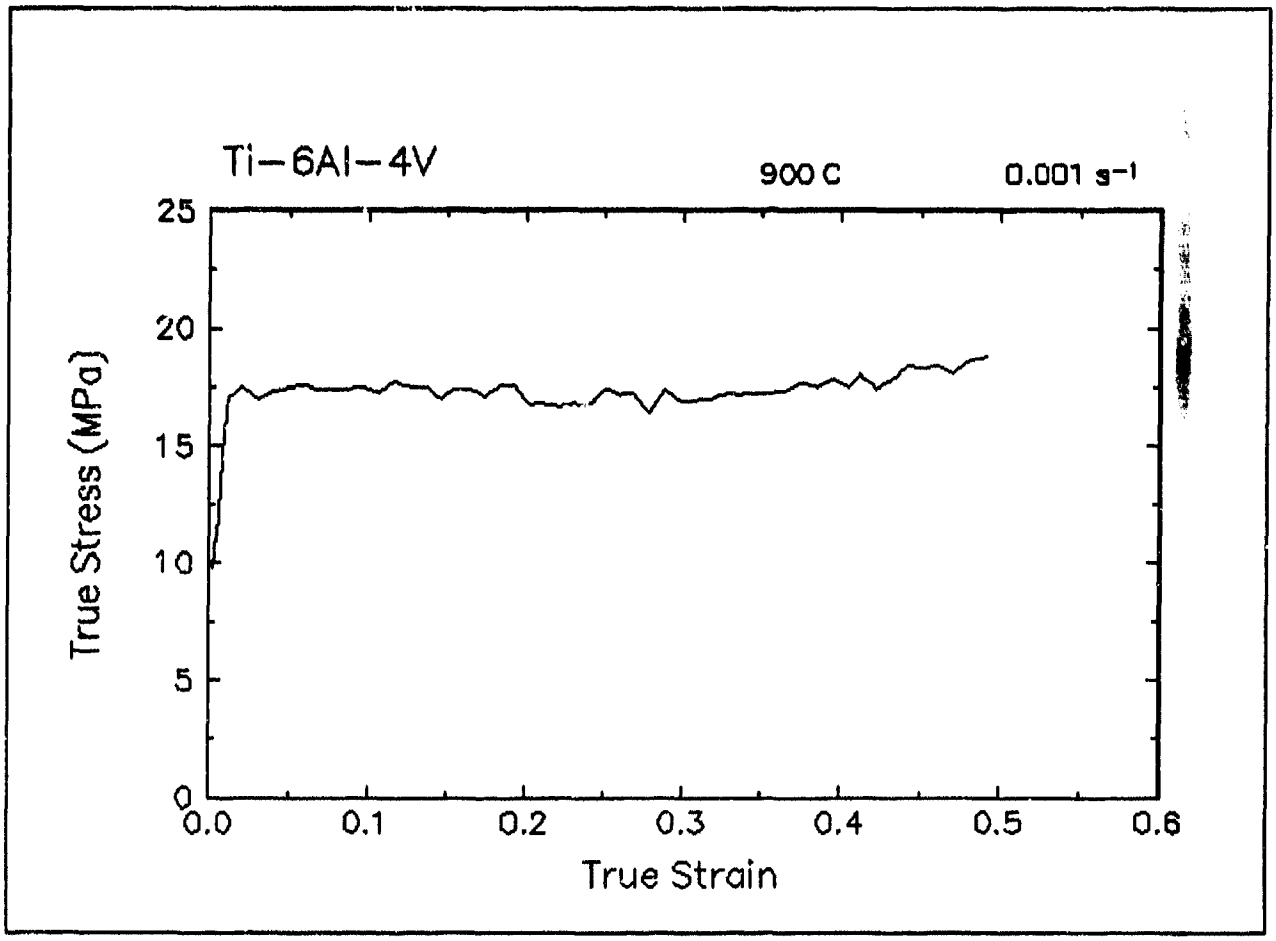

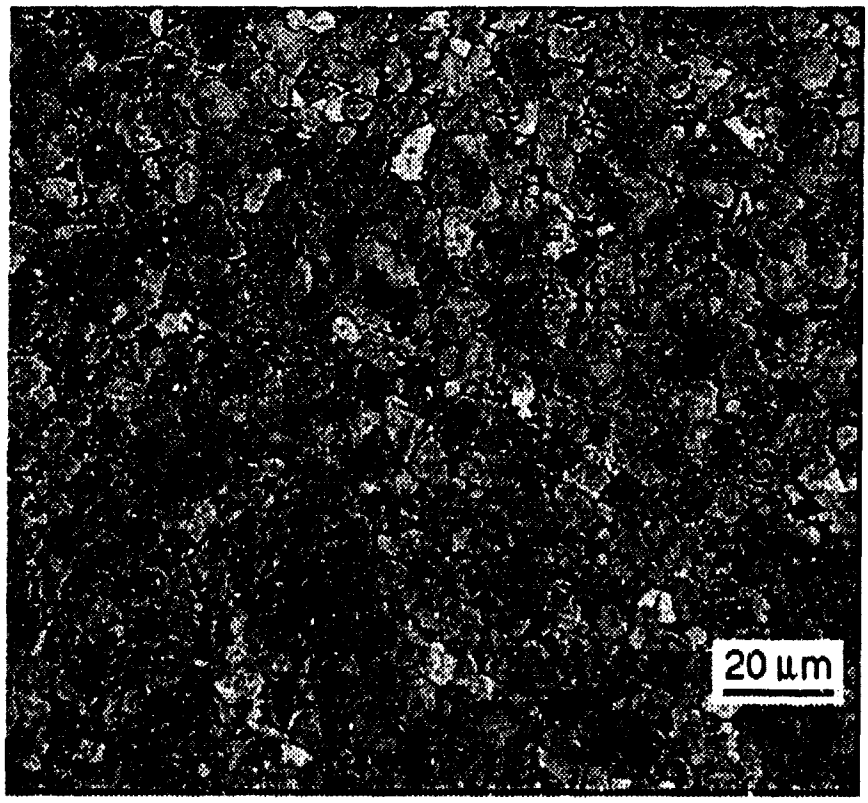

Figure 14. True stress-true strain curve and an optical micrograph from the center of the compressed sample cut through the compression axis, 900 C and 0.001 s^{-1}.

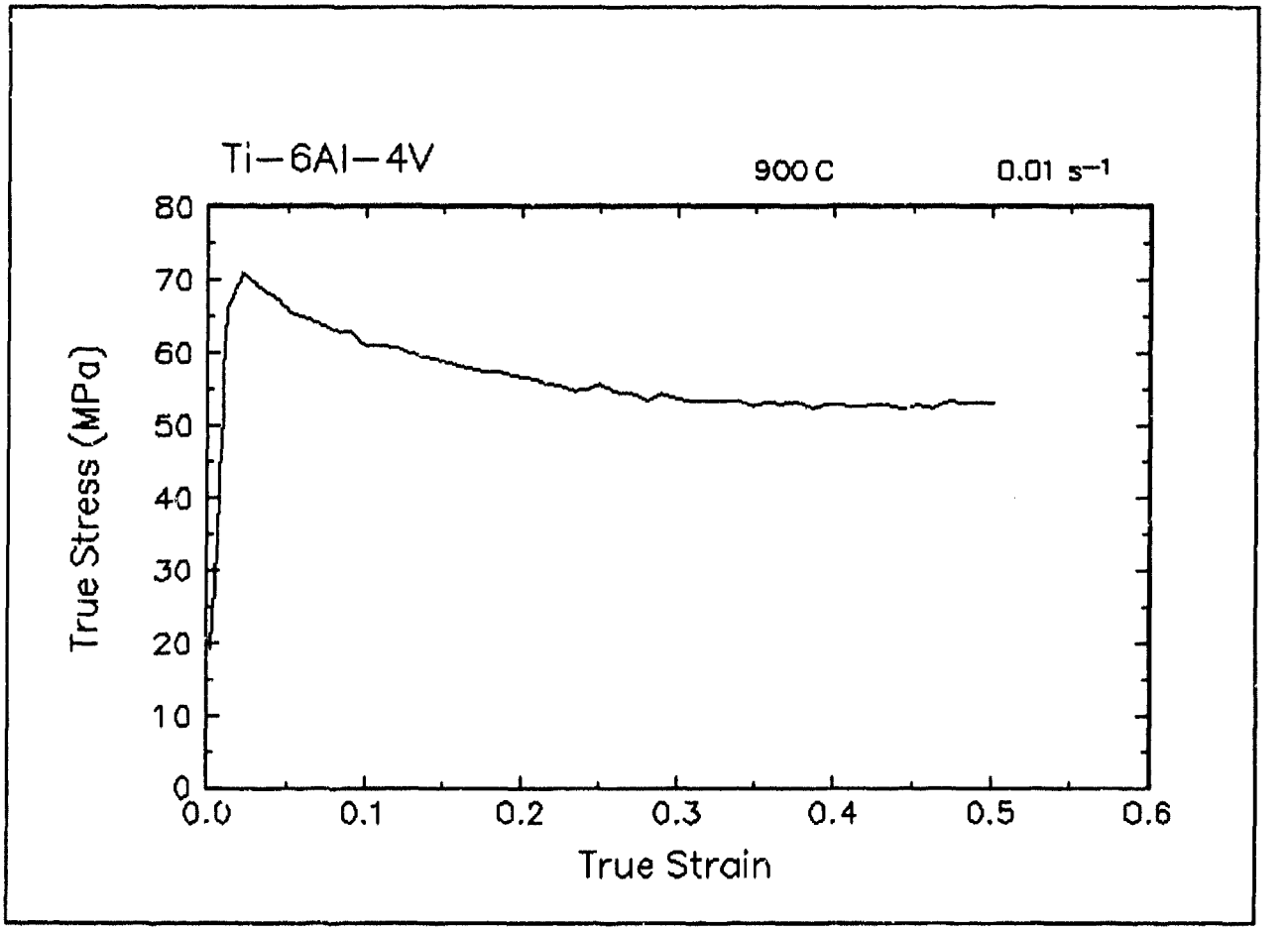

Figure 15. True stress-true strain curve, 900 C and 0.01 s^{-1}.

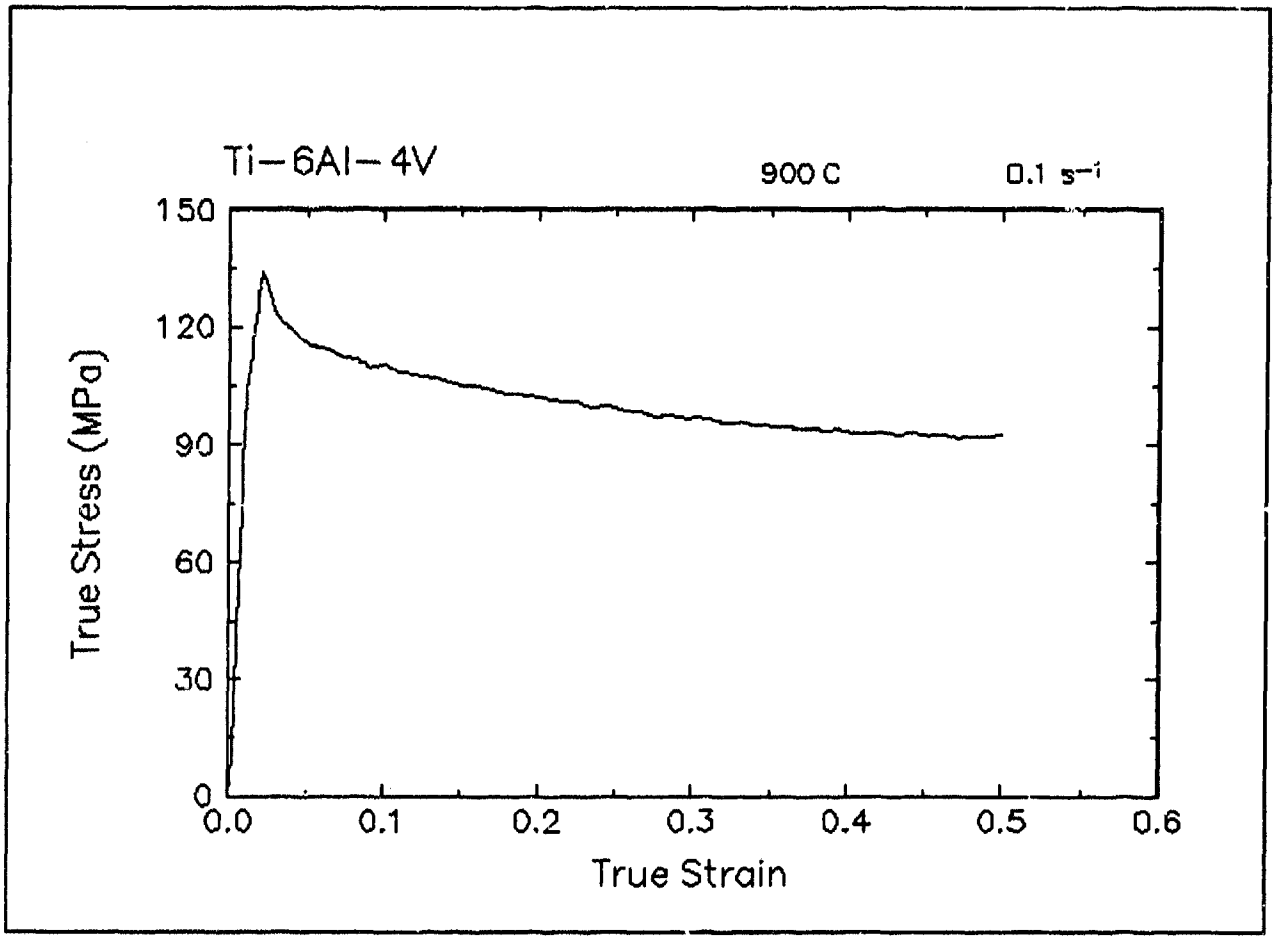

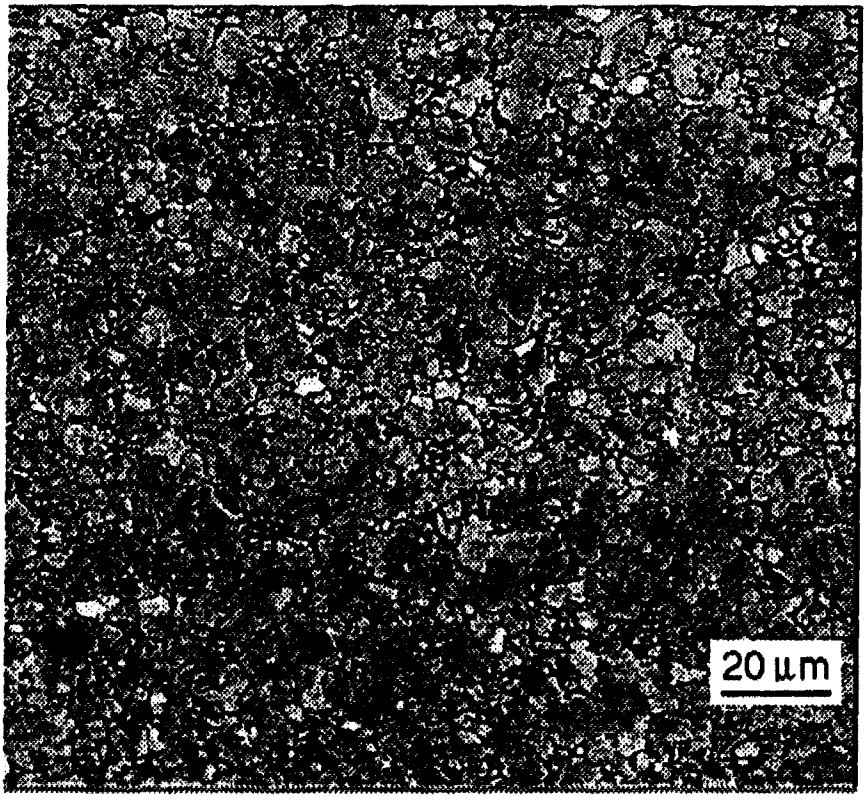

Figure 16. True stress-true strain curve and an optical micrograph from the center of the compressed sample cut through the compression axis, 900 C and 0.1 s^{-1}.

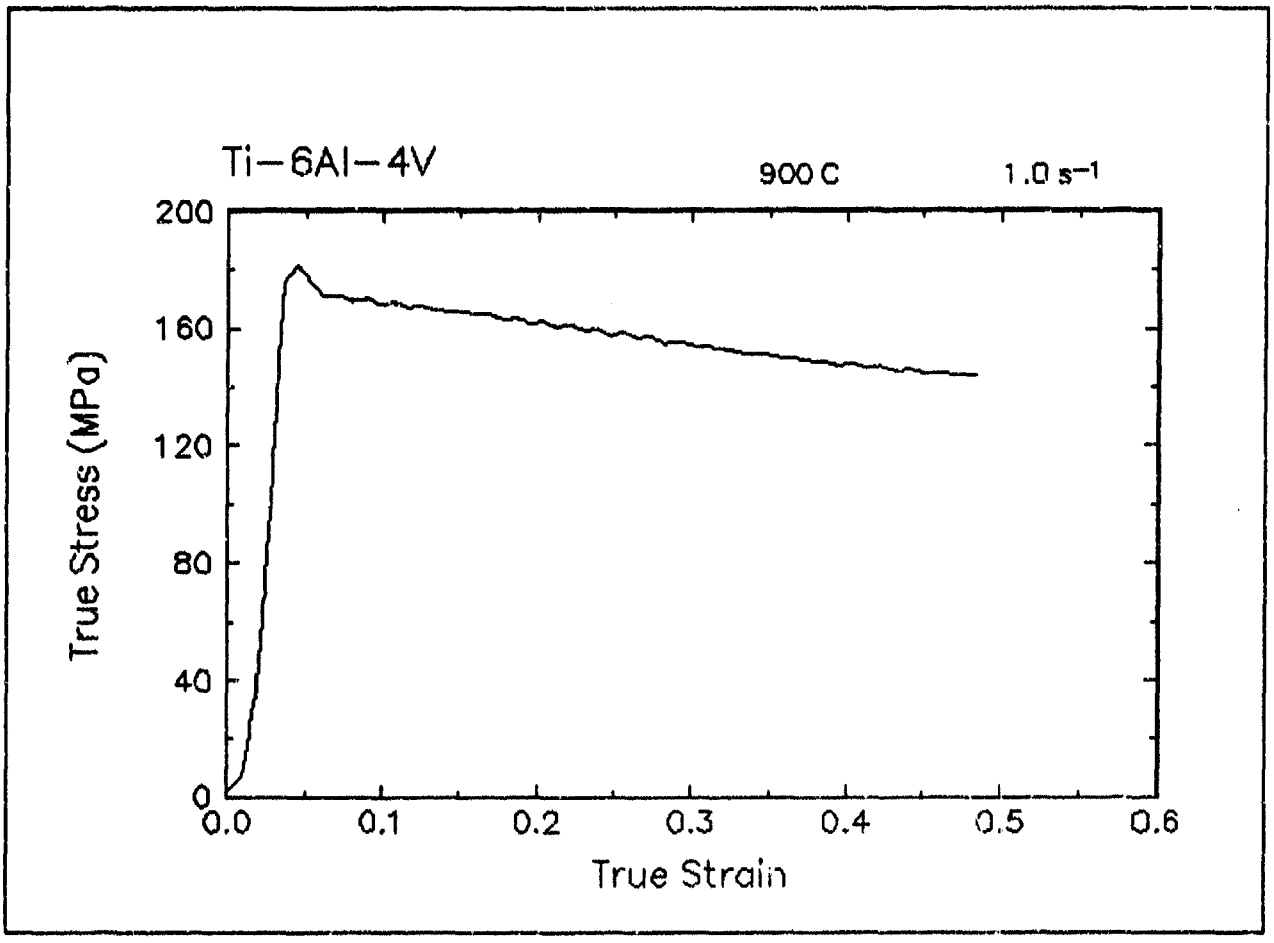

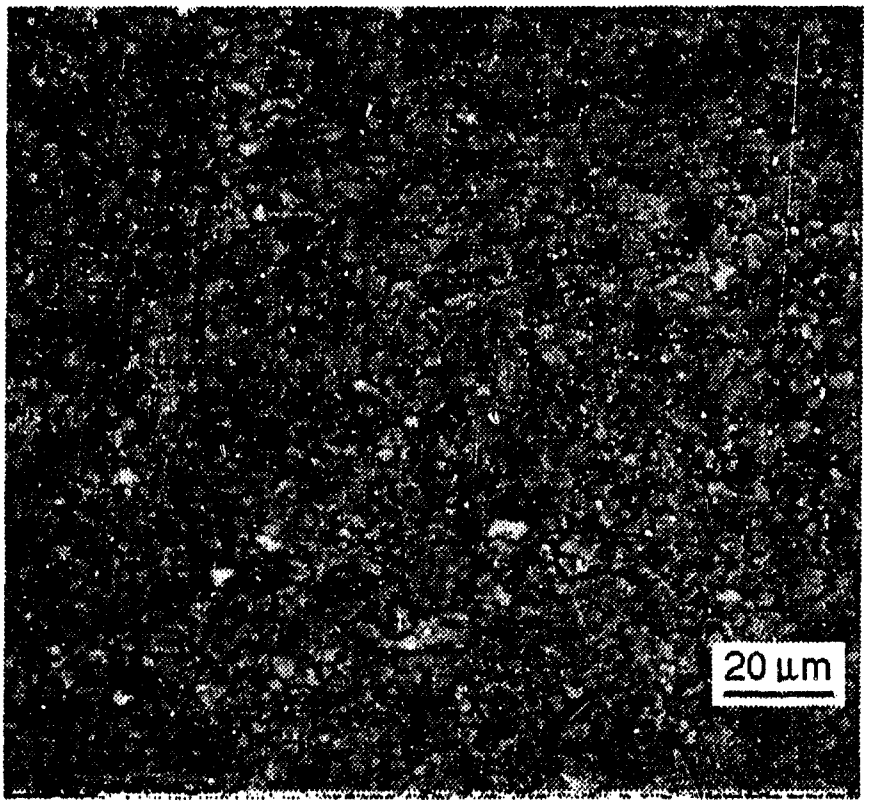

Figure 17. True stress-true strain curve and an optical micrograph from the center of the compressed sample cut through the compression axis, 900 C and 1 s^{-1}.

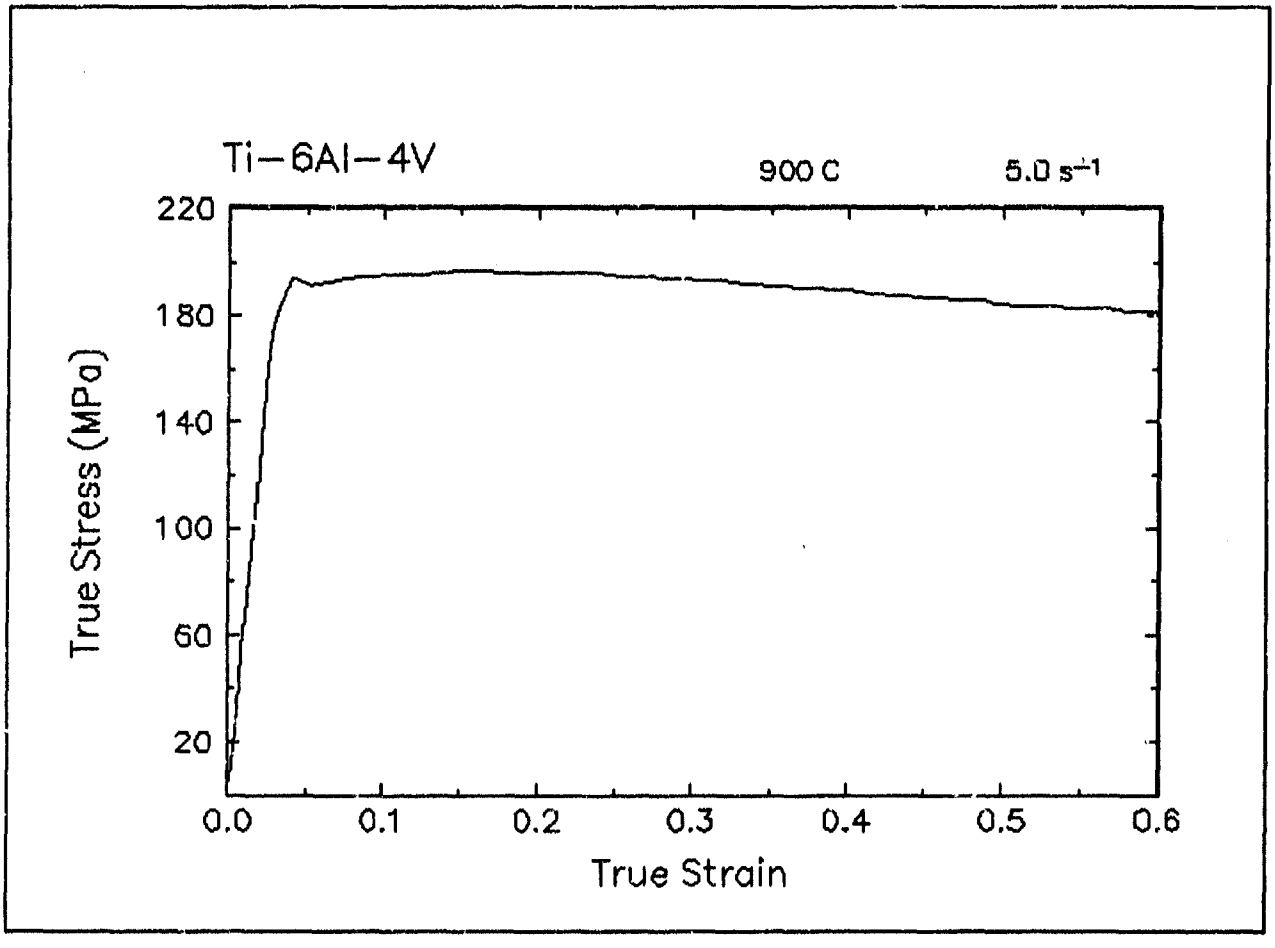

Figure 18. True stress-true strain curve, 900 C and 5 s^{-1}.

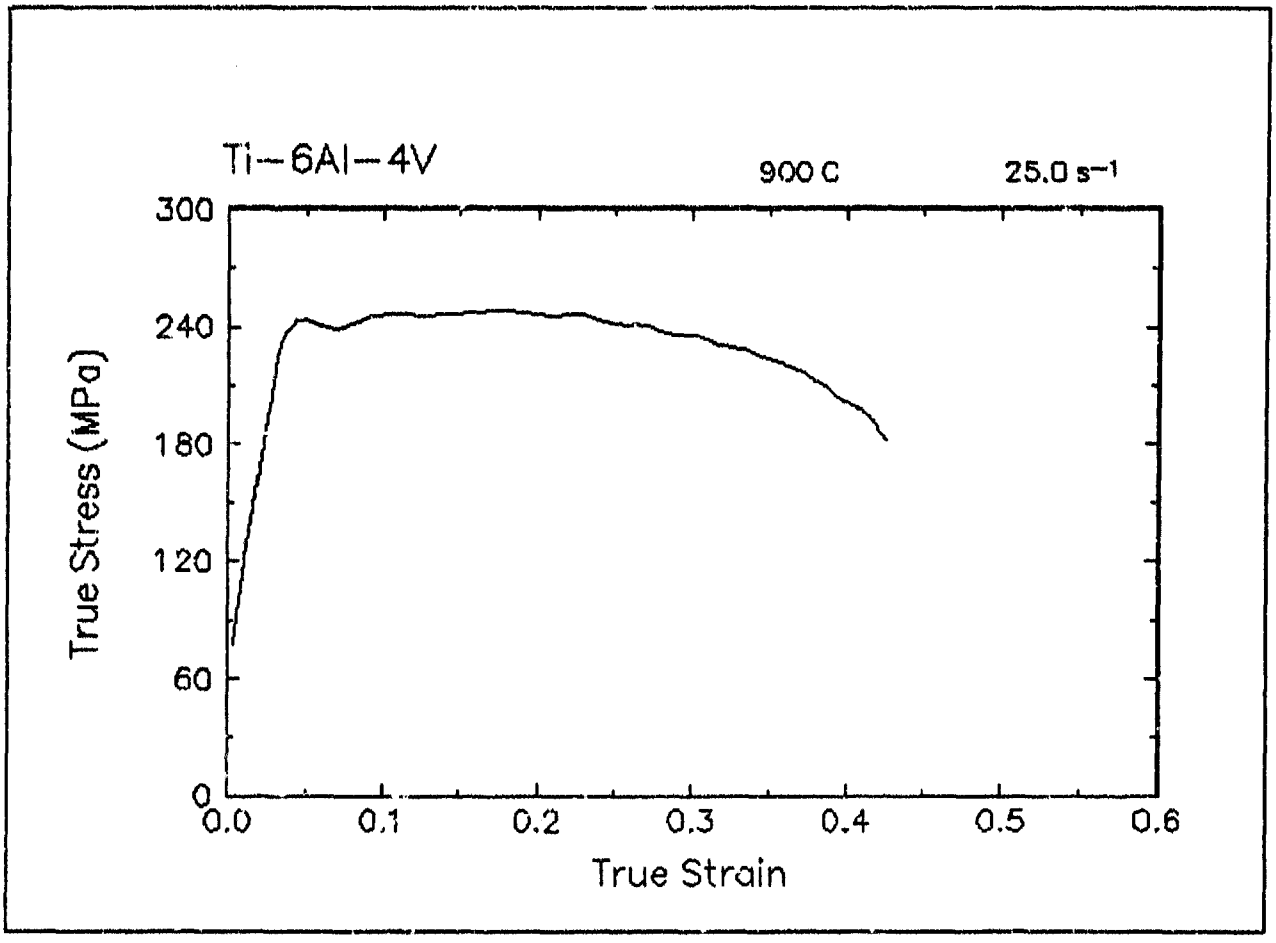

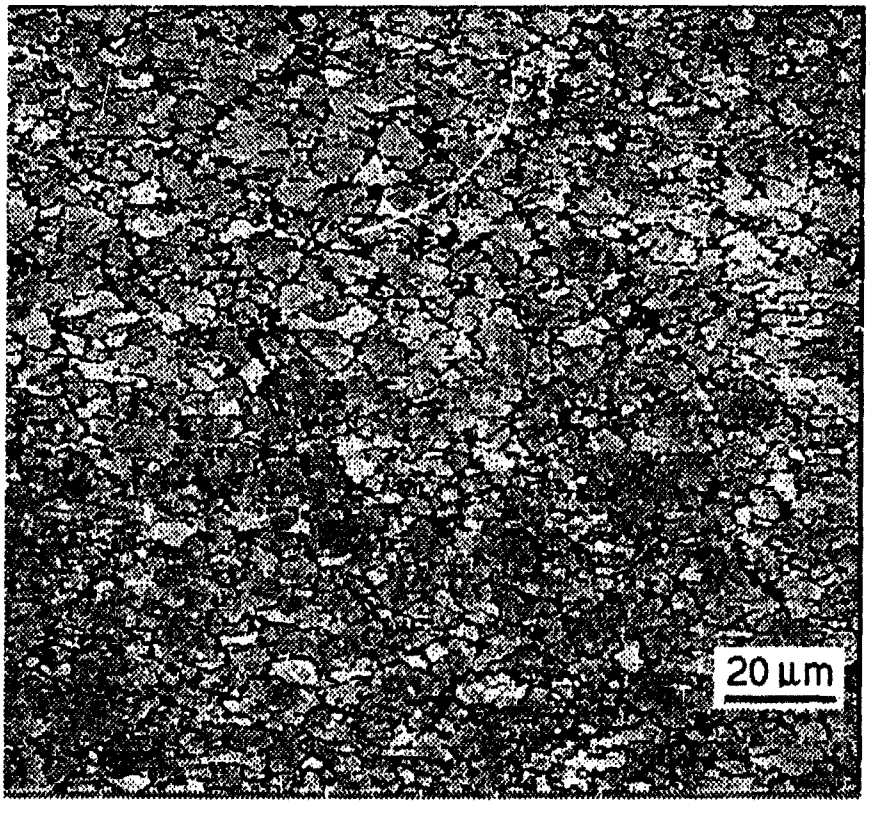

Figure 19. True stress-true strain curve and an optical micrograph from the center of the compressed sample cut through the compression axis, 900 C and 25 s^{-1}.

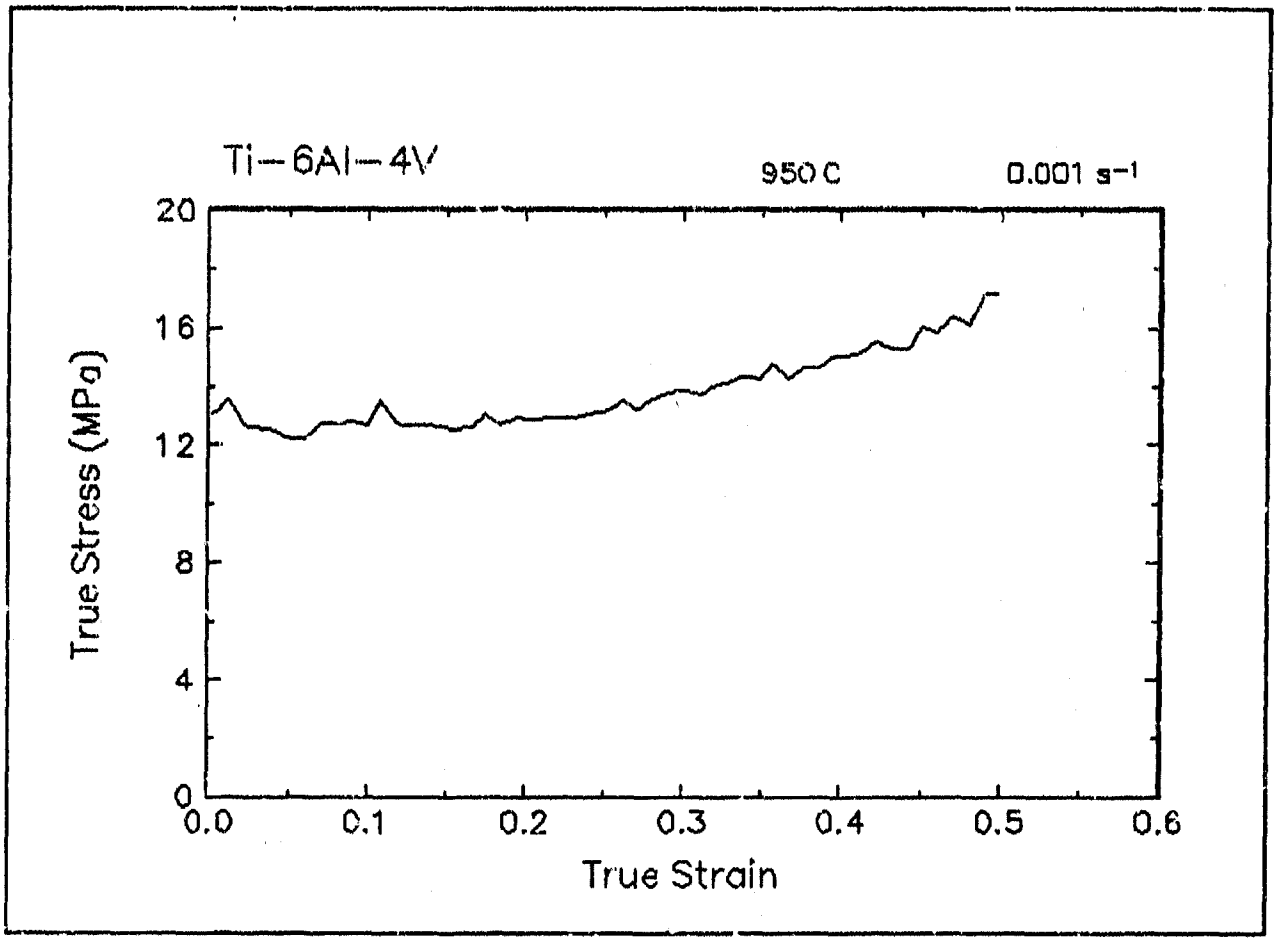

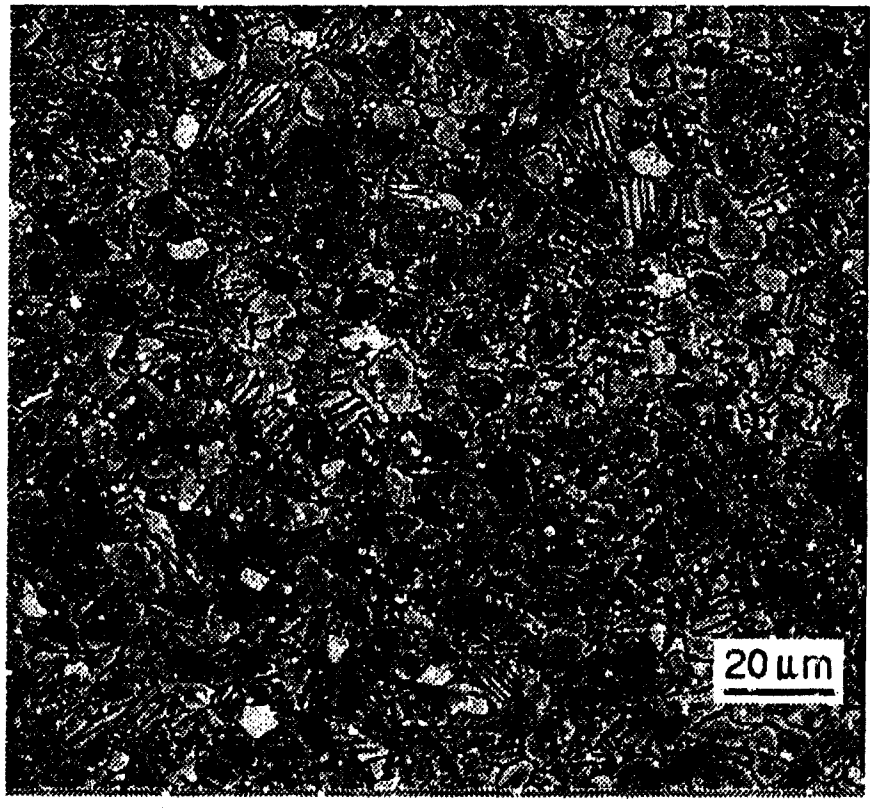

Figure 20. True stress-true strain curve and an optical micrograph from the center of the compressed sample cut through the compression axis, 950 C and 0.001 s^{-1}.

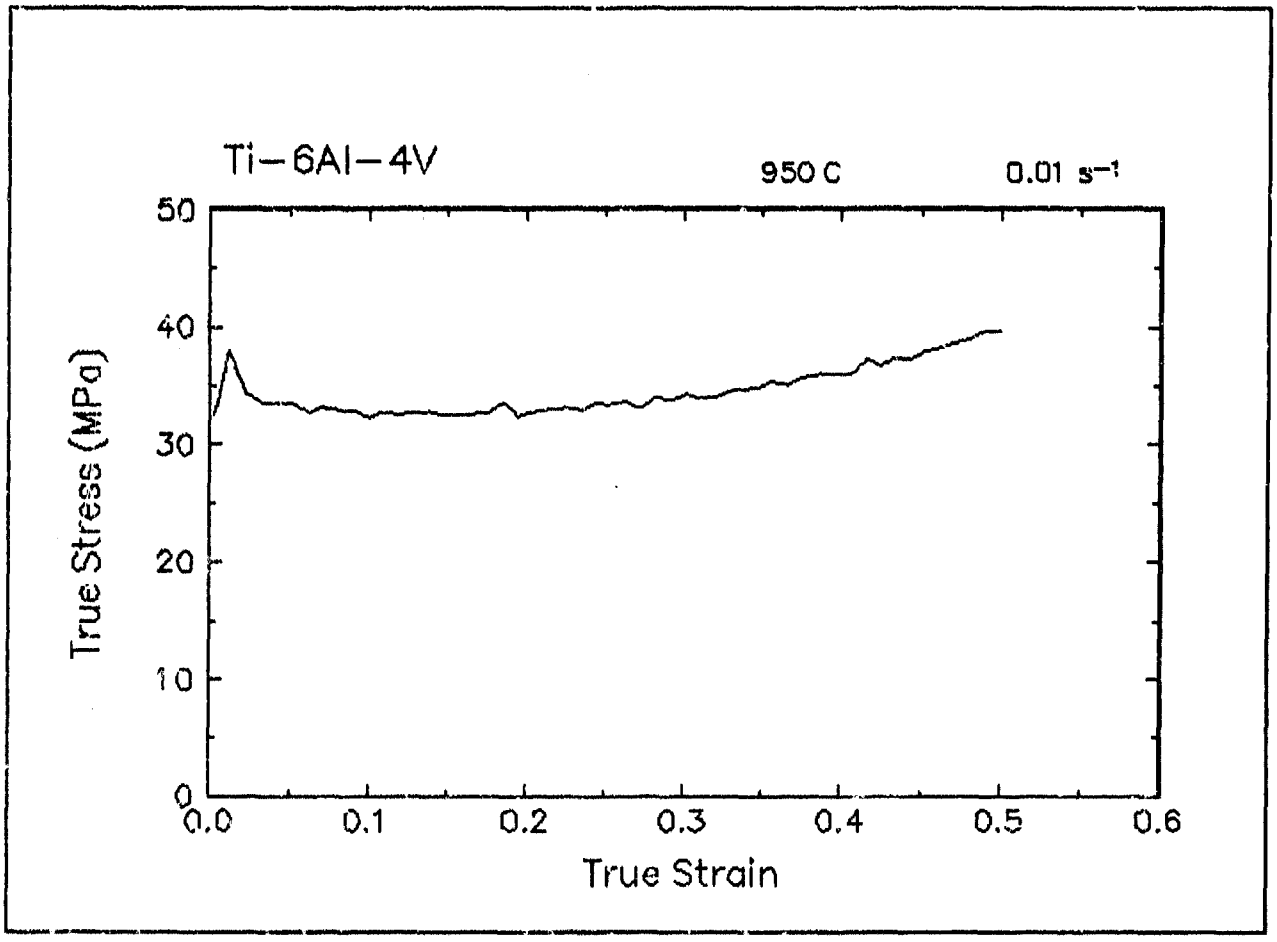

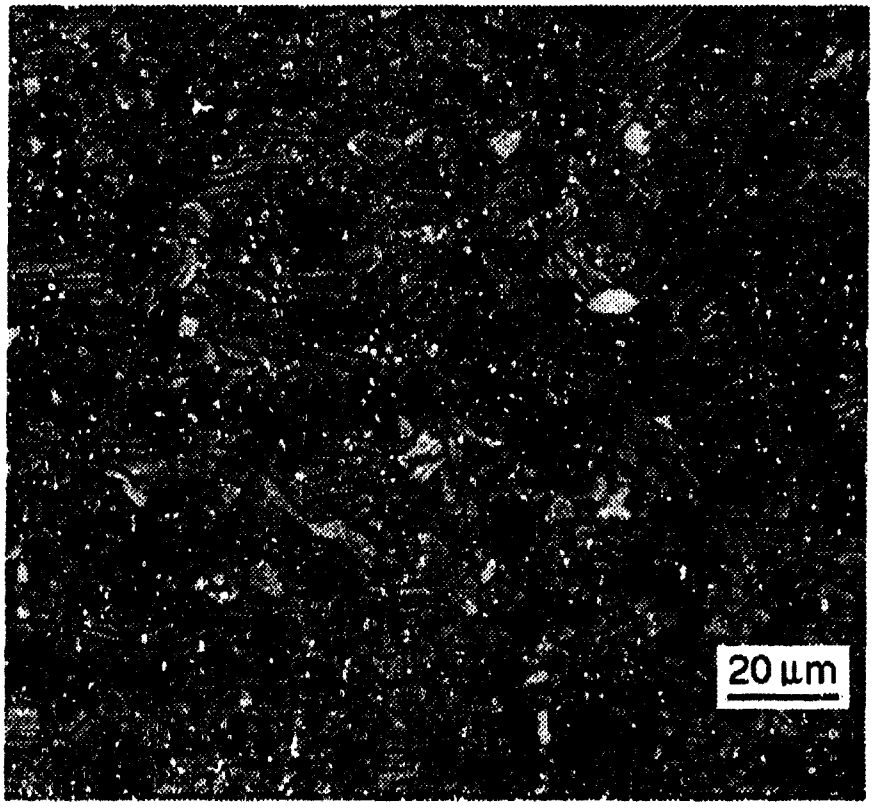

Figure 21. True stress-true strain curve and an optical micrograph from the center of the compressed sample cut through the compression axis, 950 C and 0.01 s^{-1}.

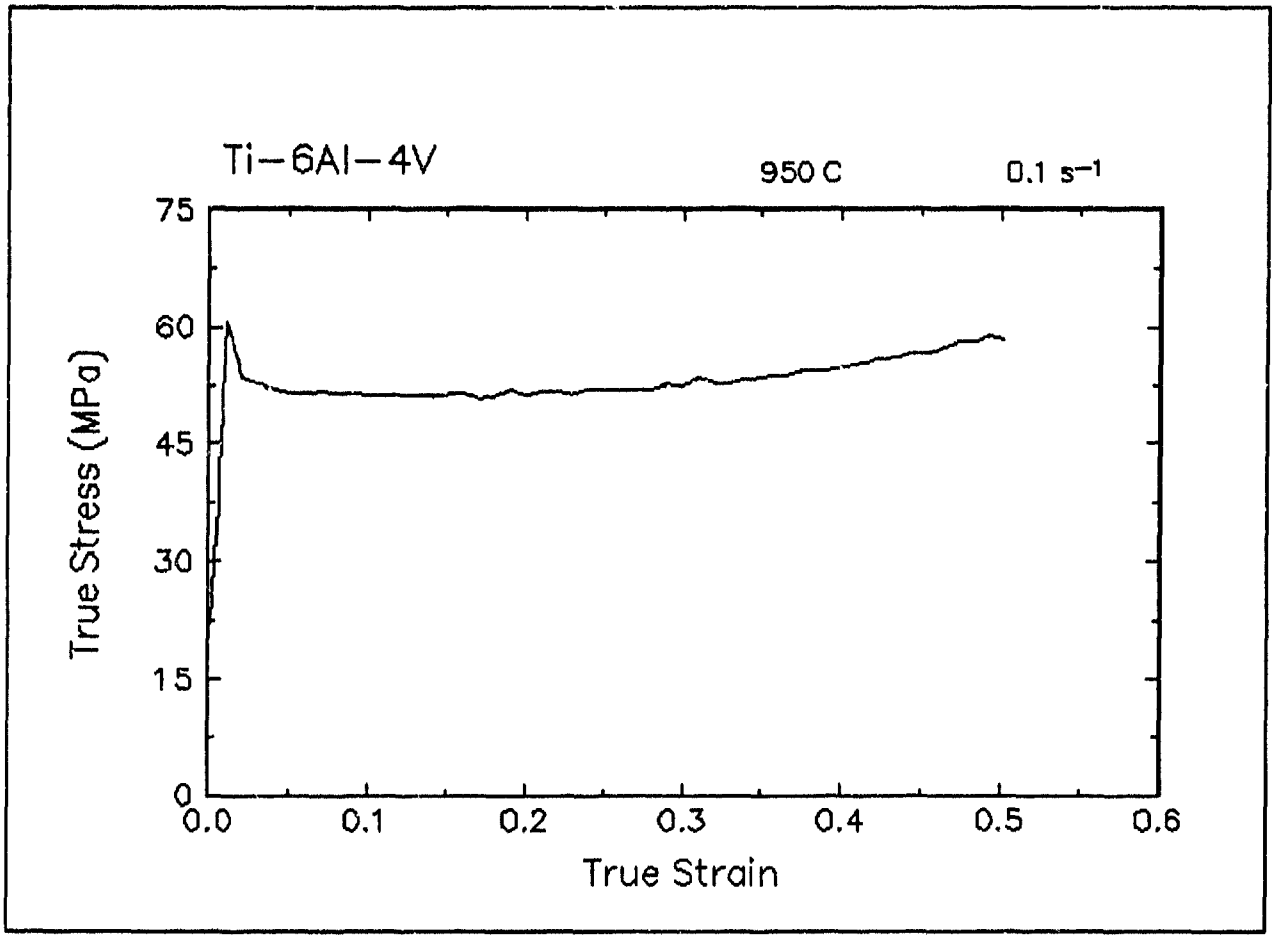

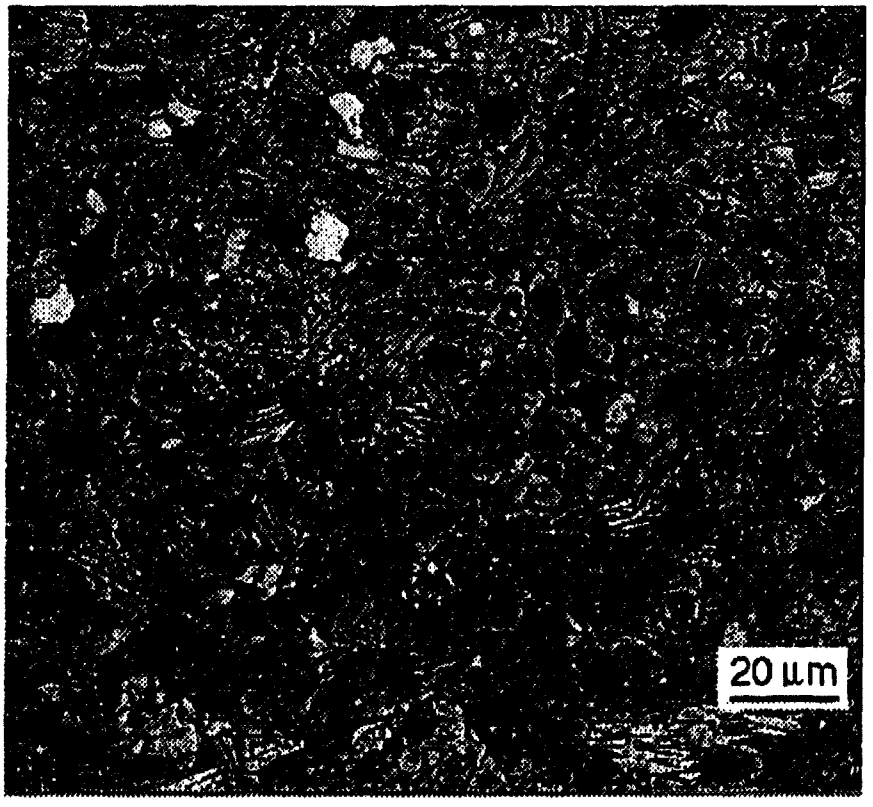

Figure 22. True stress-true strain curve and an optical micrograph from the center of the compressed sample cut through the compression axis, 950 C and 0.1 s^{-1}.

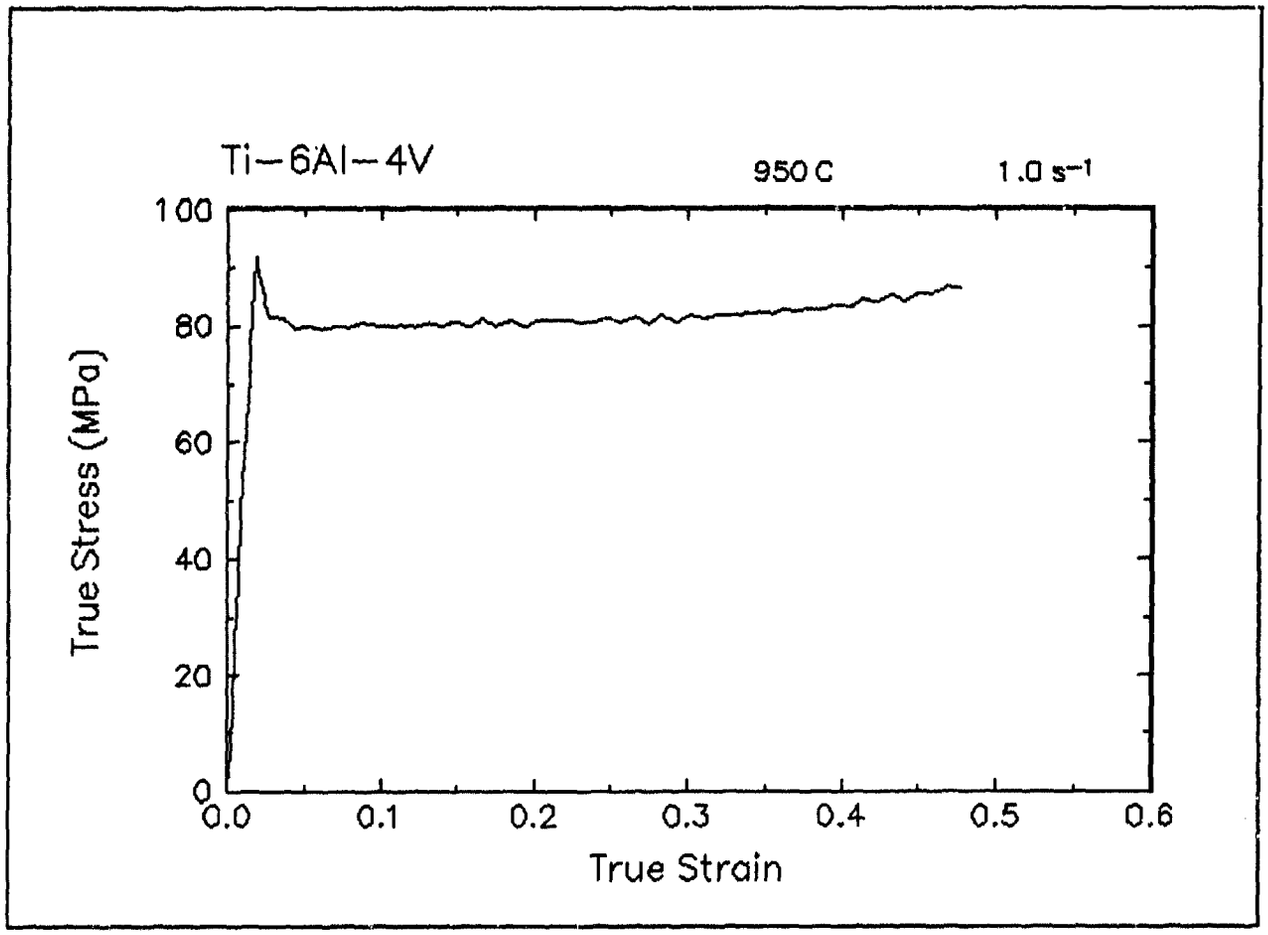

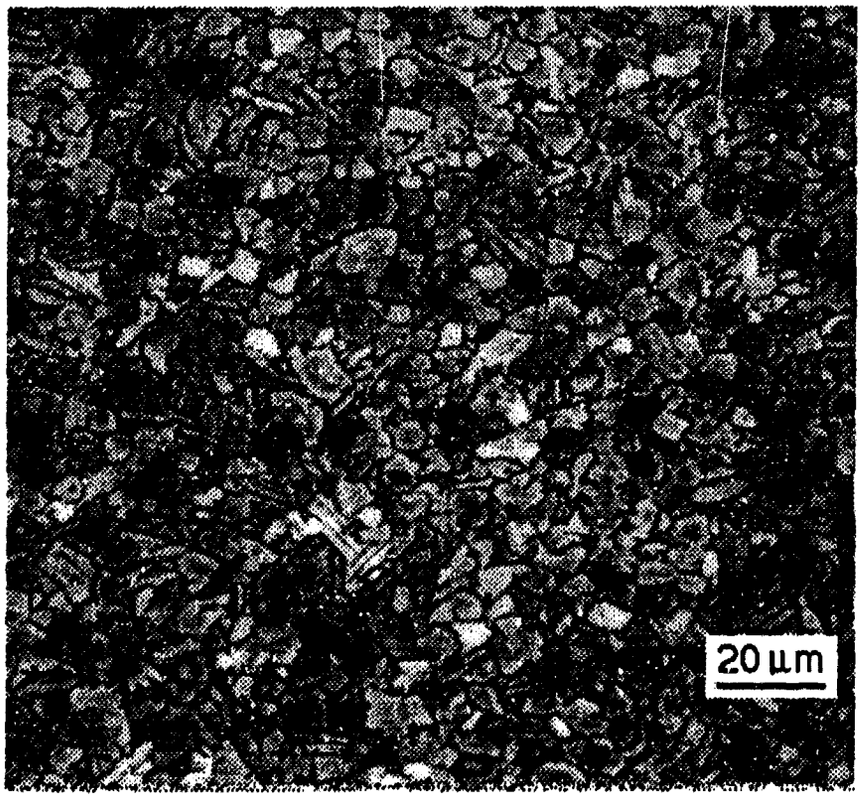

Figure 23. True stress-true strain curve and an optical micrograph from the center of the compressed sample cut through the compression axis, 950 C and 1 s^{-1}.

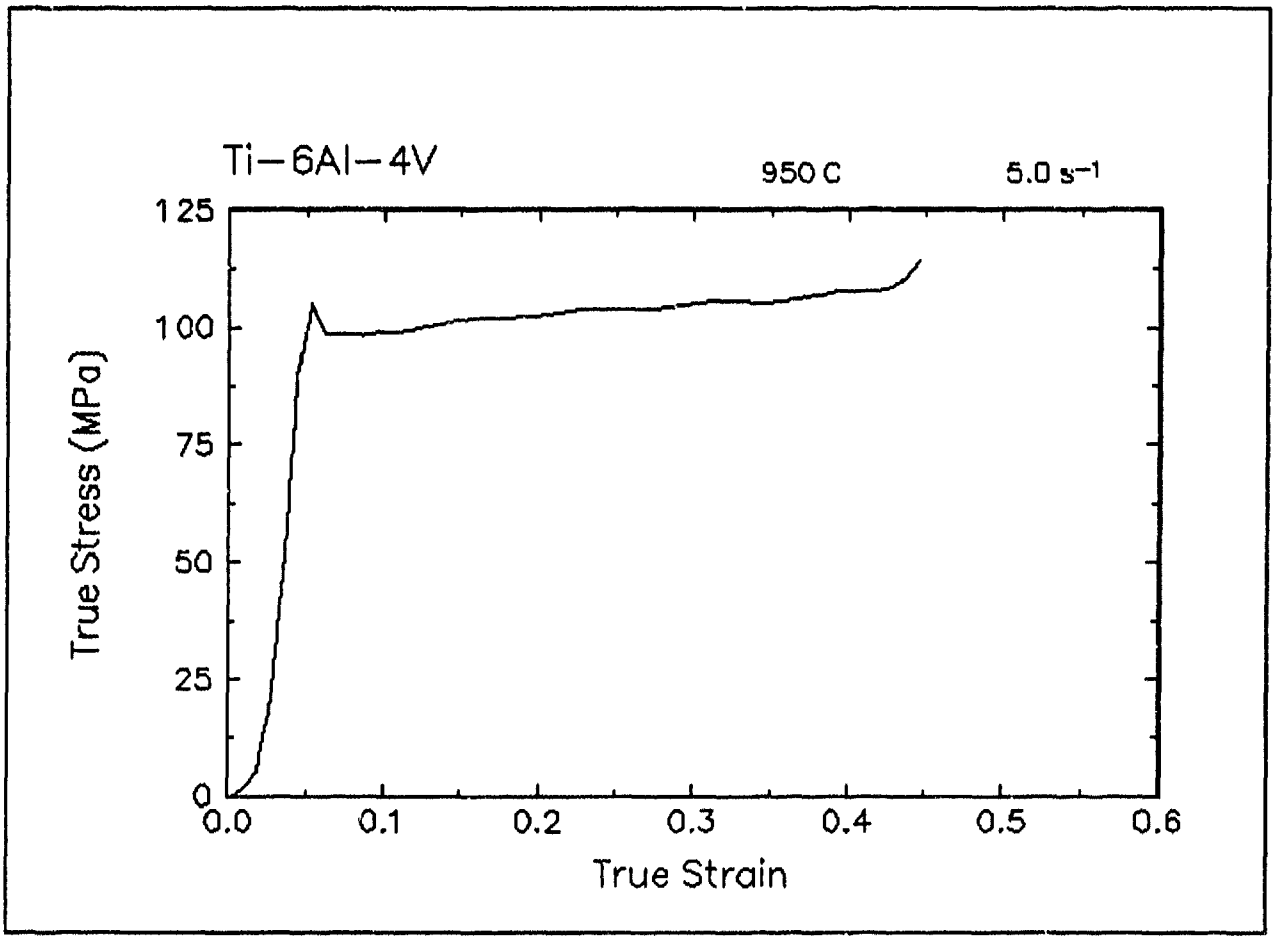

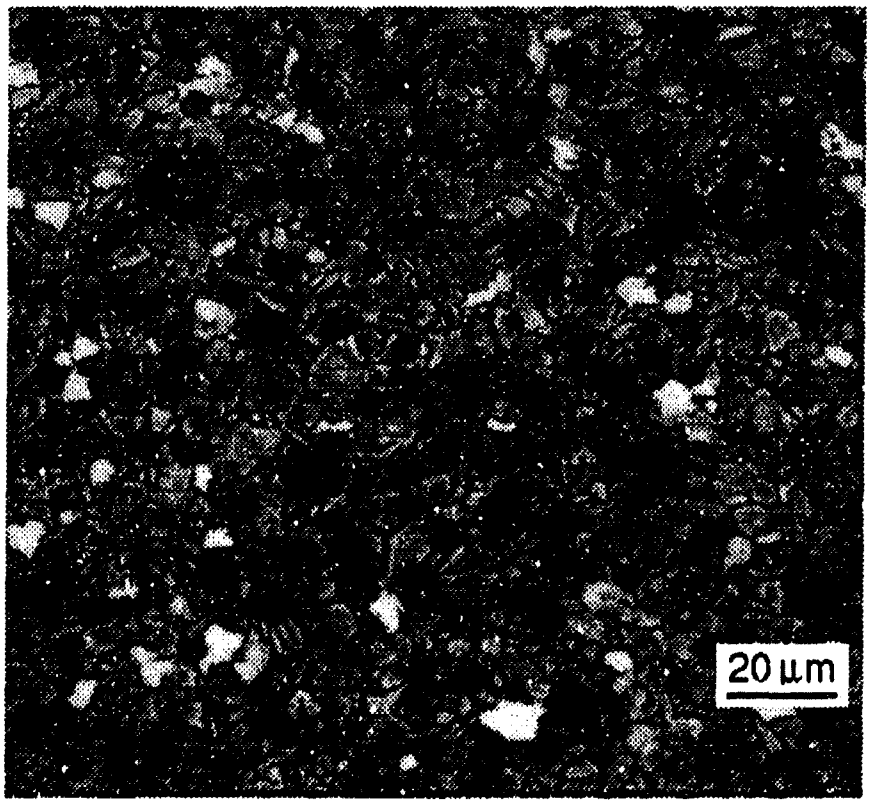

Figure 24. True stress-true strain curve and an optical micrograph from the center of the compressed sample cut through the compression axis, 950 C and 5 s^{-1}.

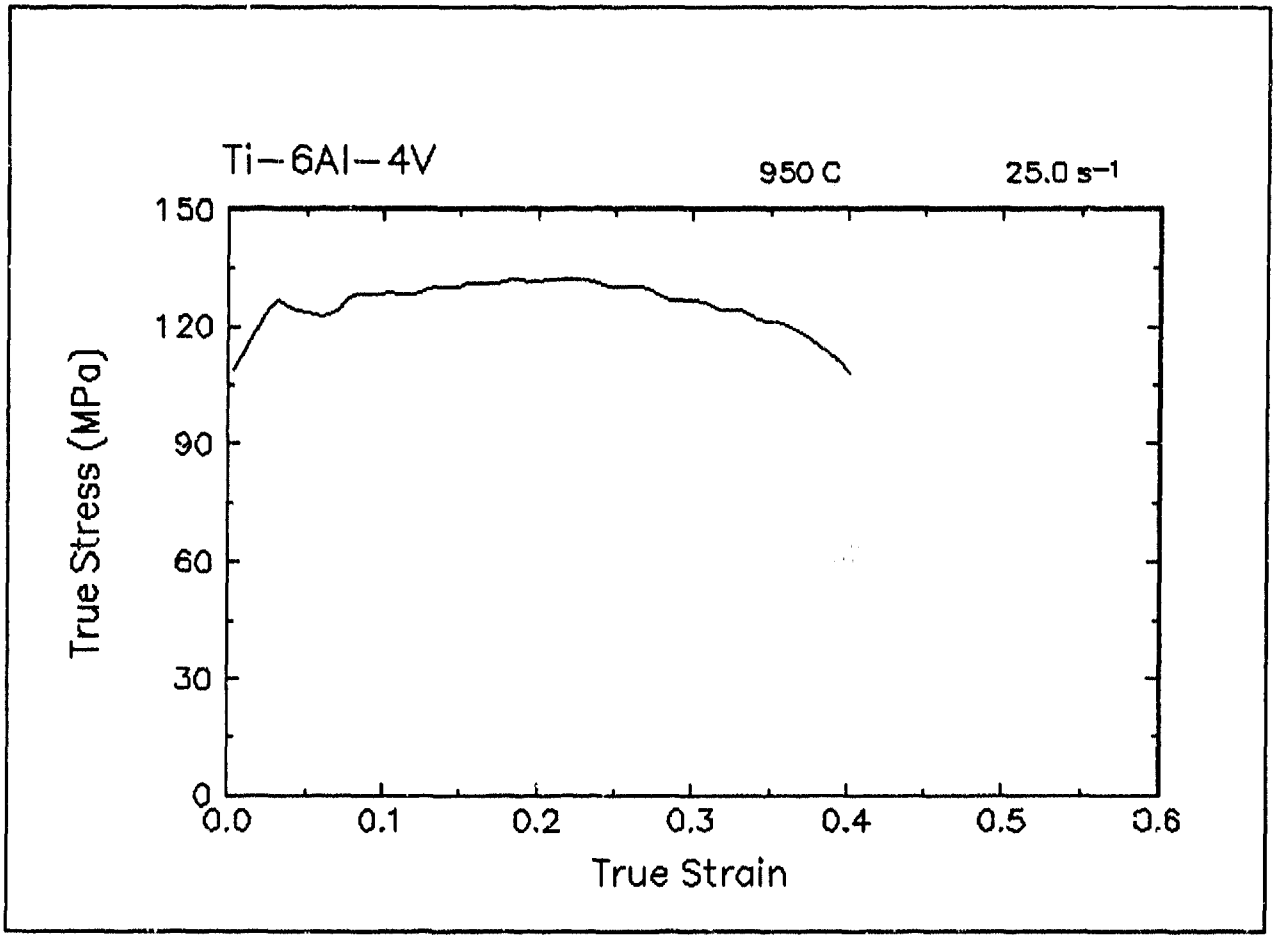

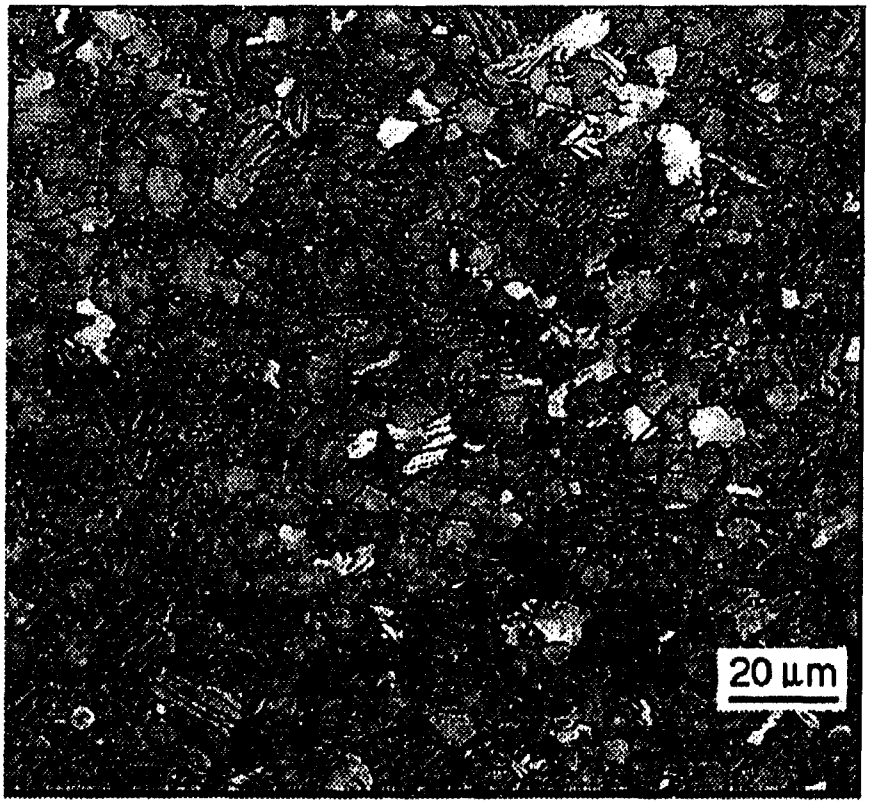

Figure 25. True stress-true strain curve and an optical micrograph from the center of the compressed sample cut through the compression axis, 950 C and 25 s^{-1}.

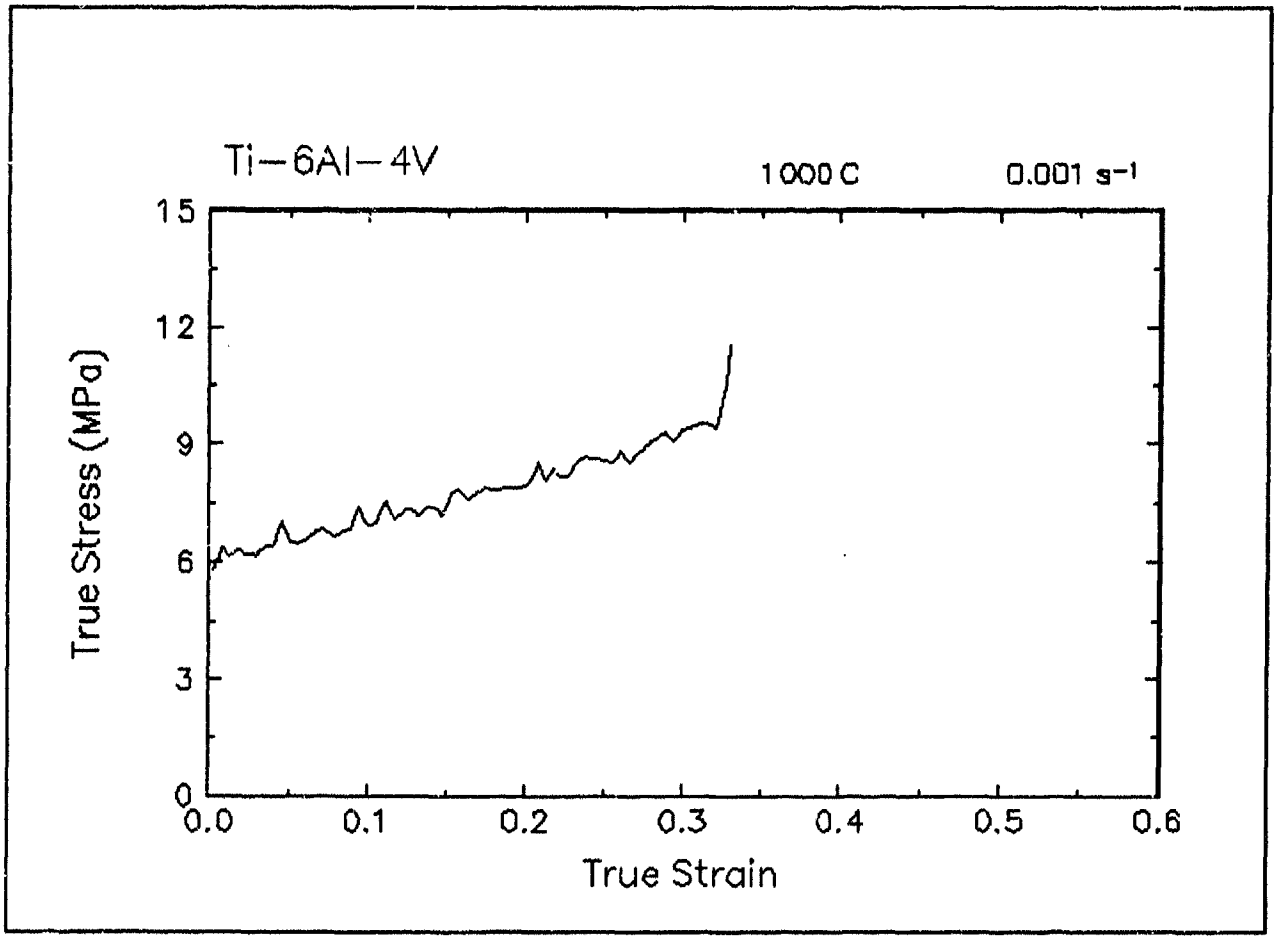

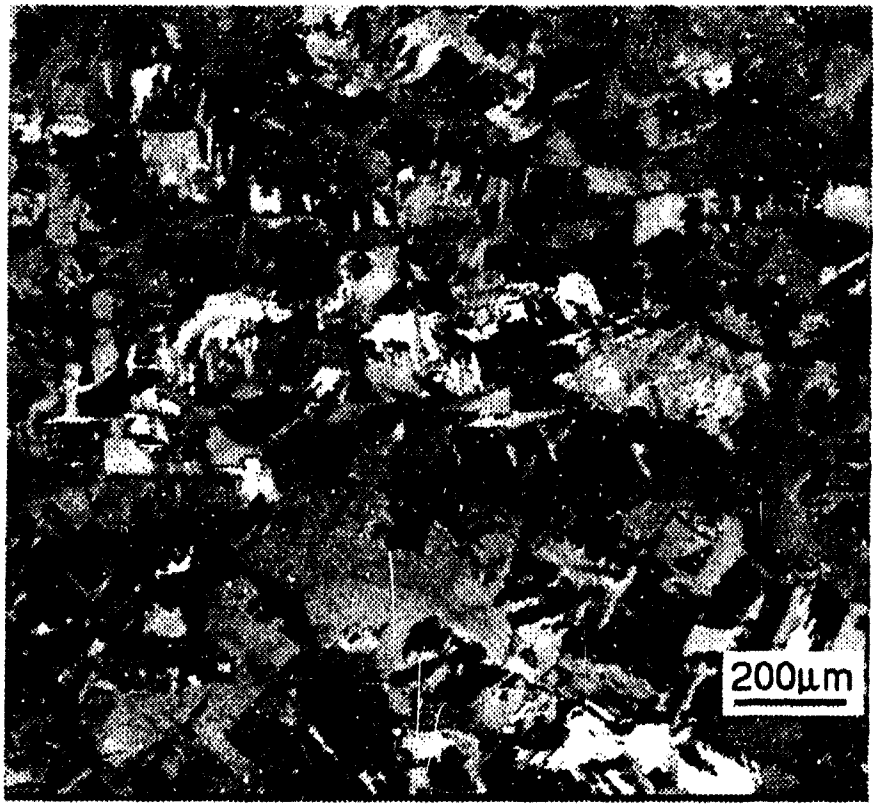

Figure 26. True stress-true strain curve and an optical micrograph from the center of the compressed sample cut through the compression axis, 1000 C and 0.001 s^{-1}.

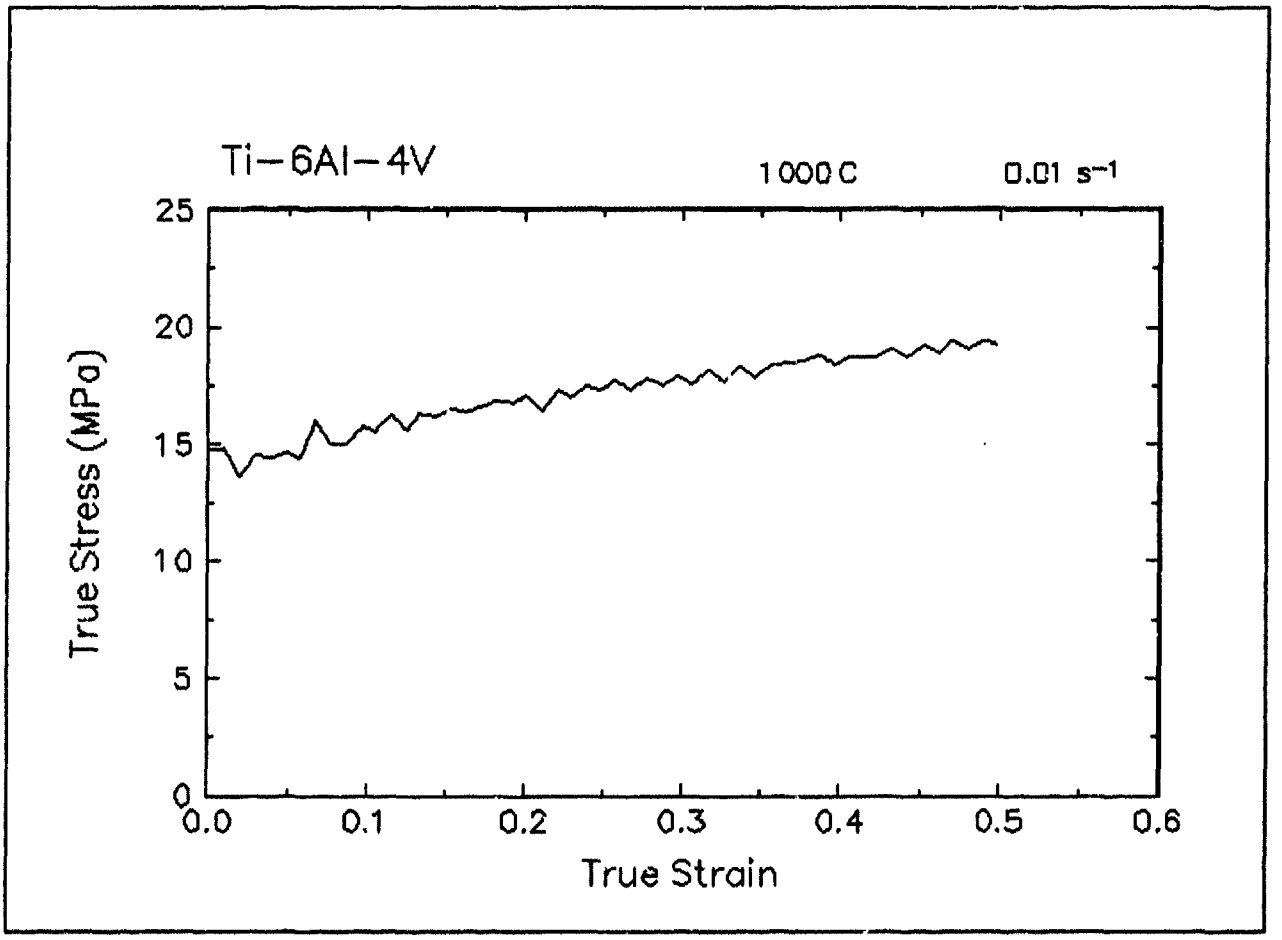

Figure 27. True stress-true strain curve; 1000 C and 0.01 s^{-1}.

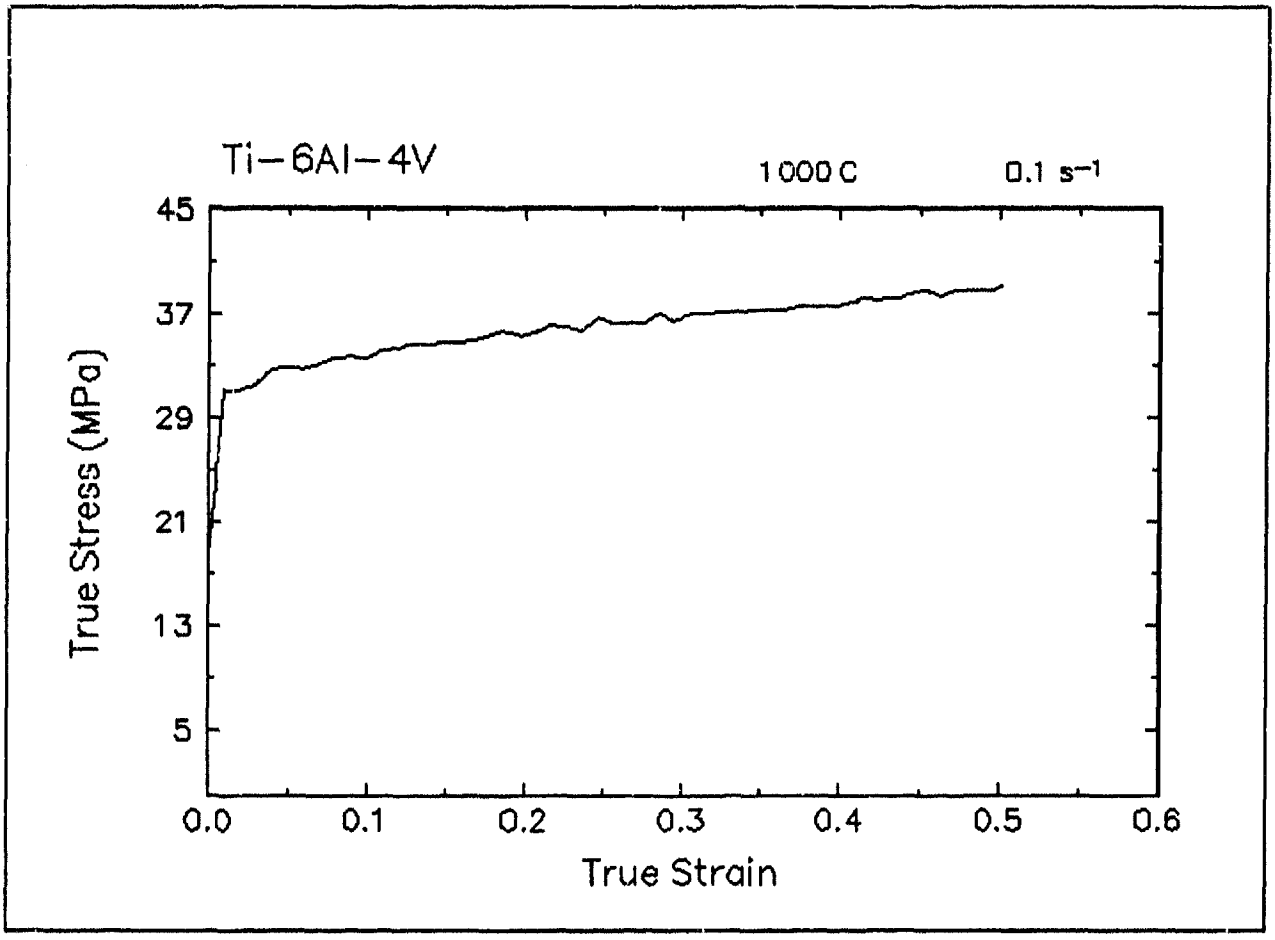

Figure 28. True stress-true strain curve and an optical micrograph from the center of the compressed sample cut through the compression axis, 1000 C and 0.1 s^{-1}.

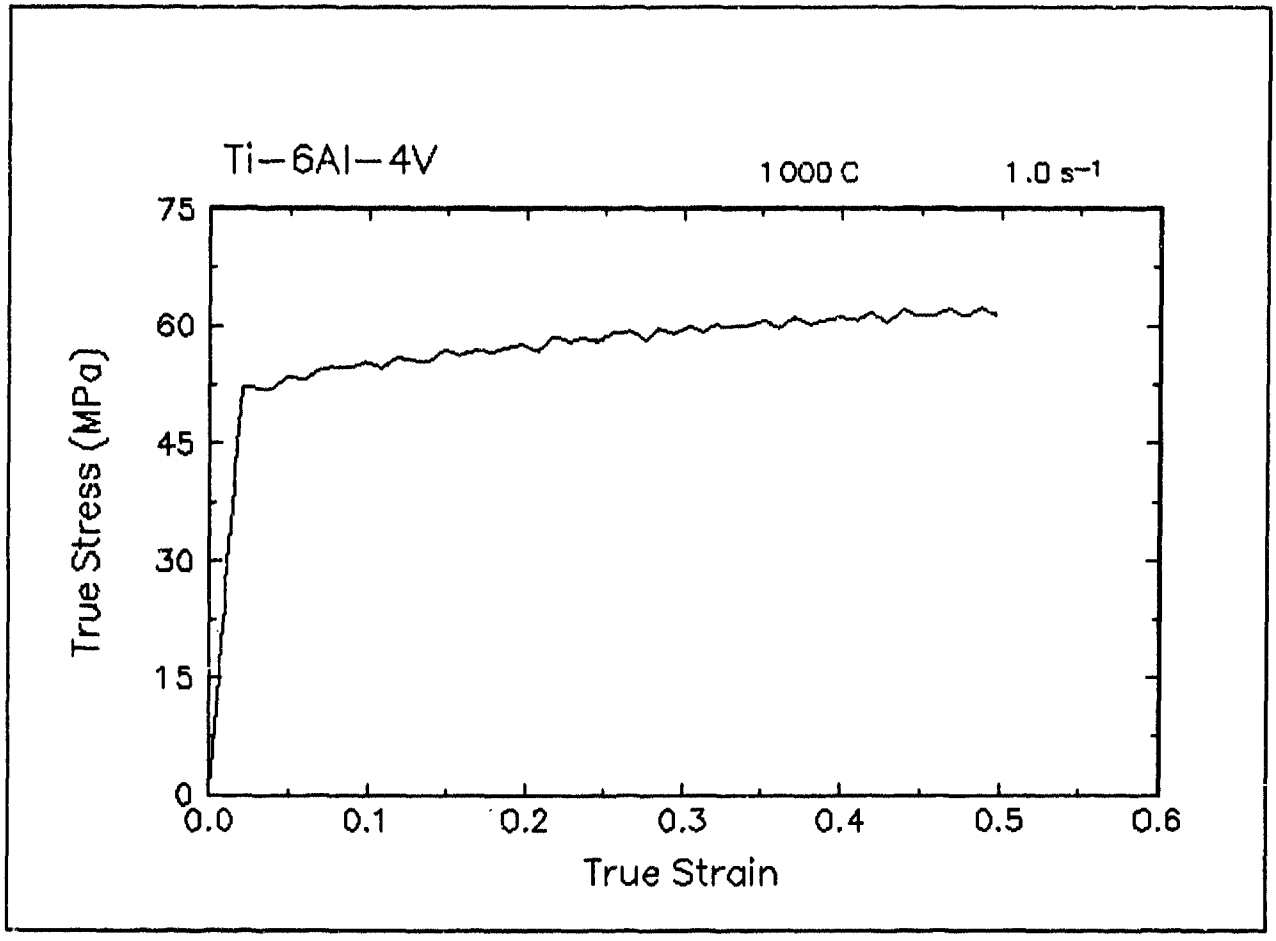

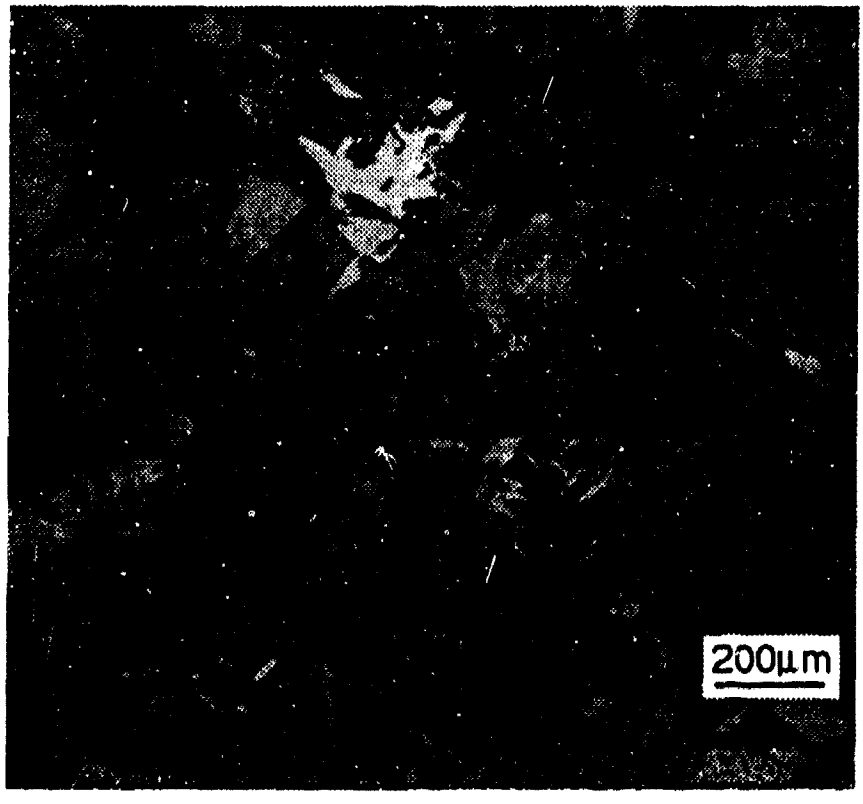

Figure 29. True stress-true strain curve and an optical micrograph from the center of the compressed sample cut through the compression axis, 1000 C and 1 s^{-1}.

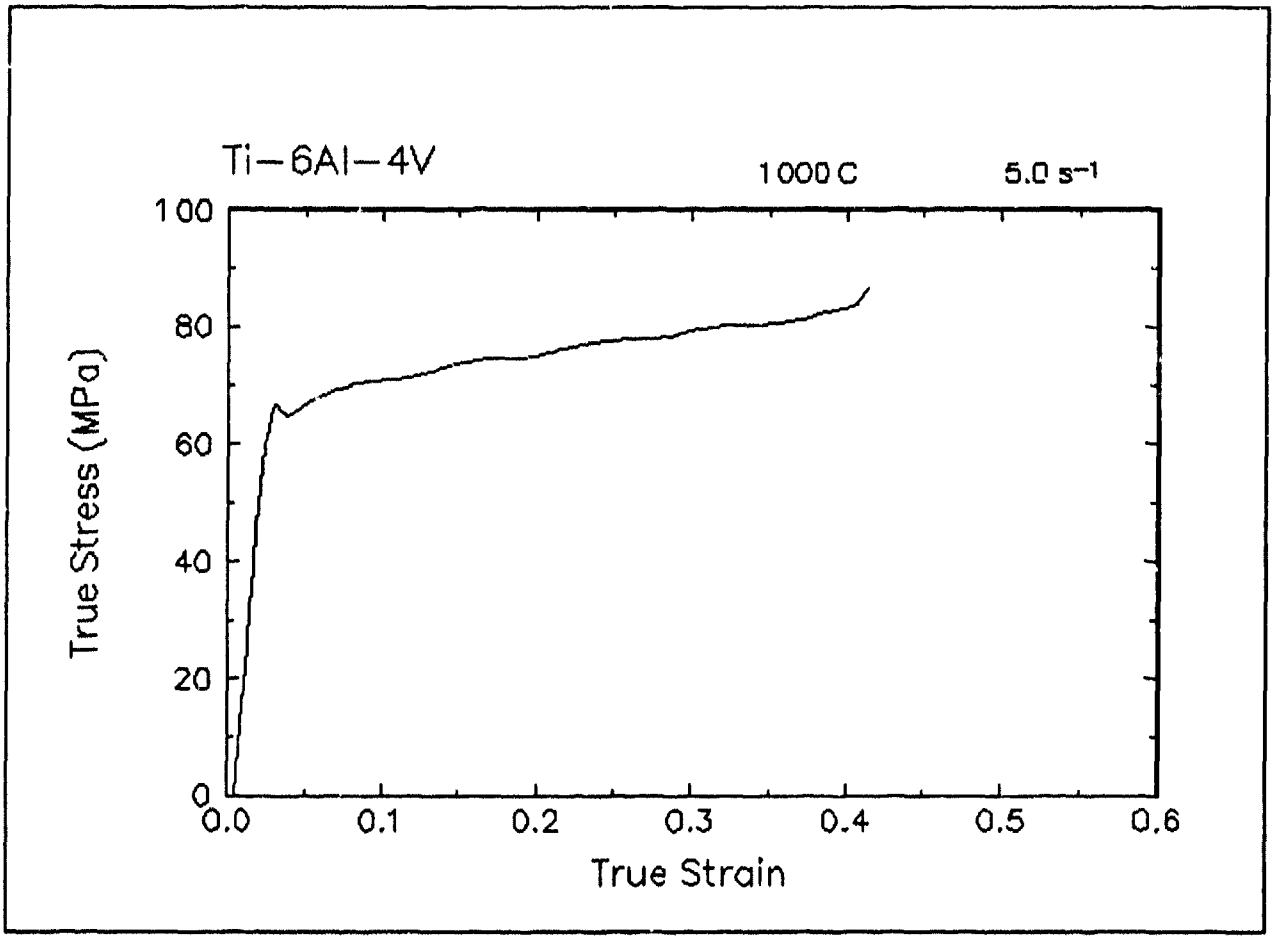

Figure 30. True stress-true strain curve, 1000 C and 5 s^{-1}.

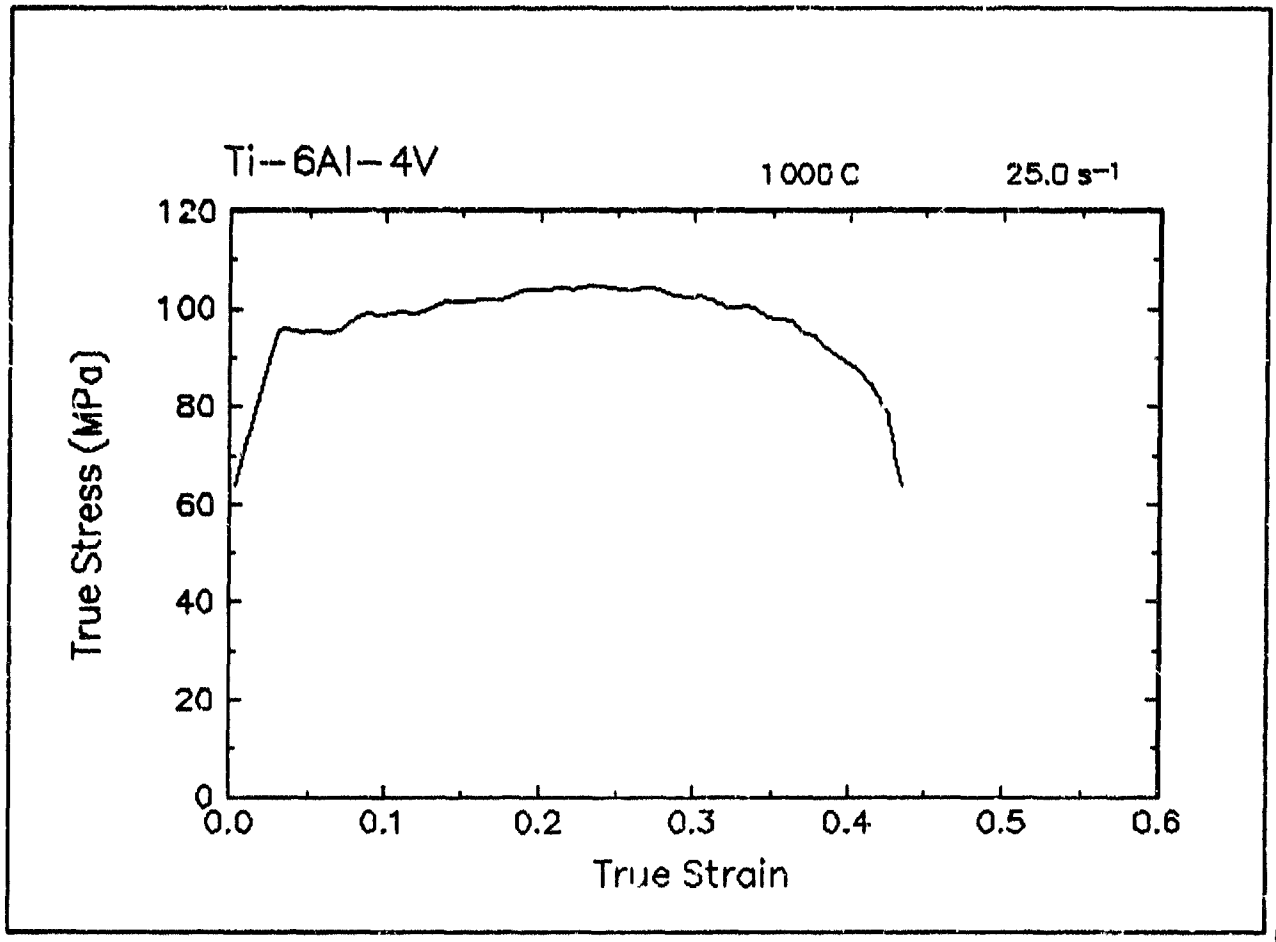

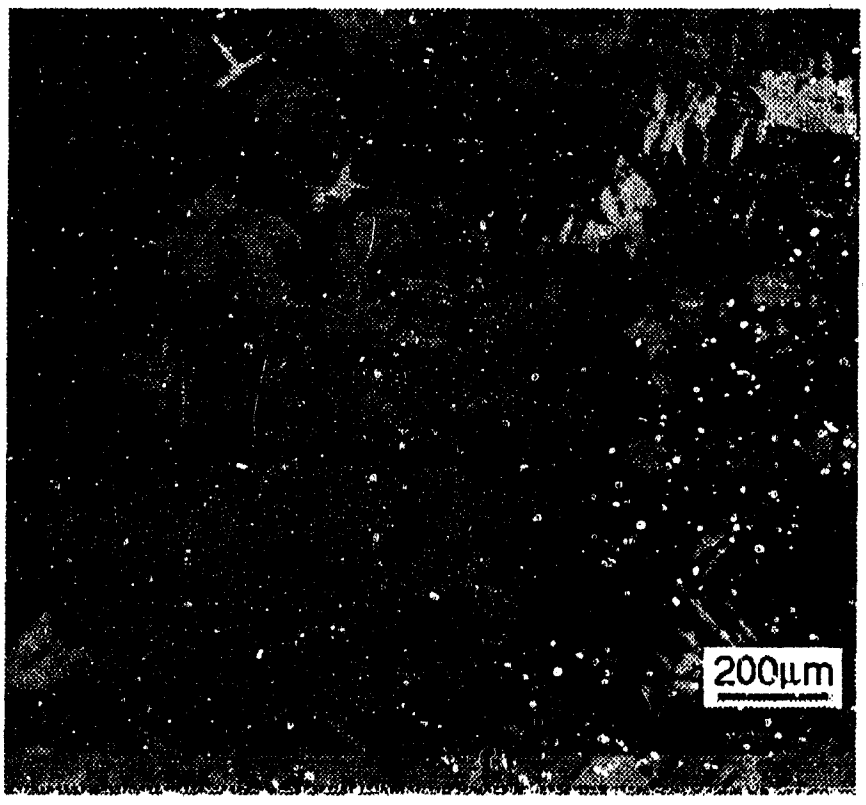

Figure 31. True stress-true strain curve and an optical micrograph from the center of the compressed sample cut through the compression axis, 1000 C and 25 s^{-1}.

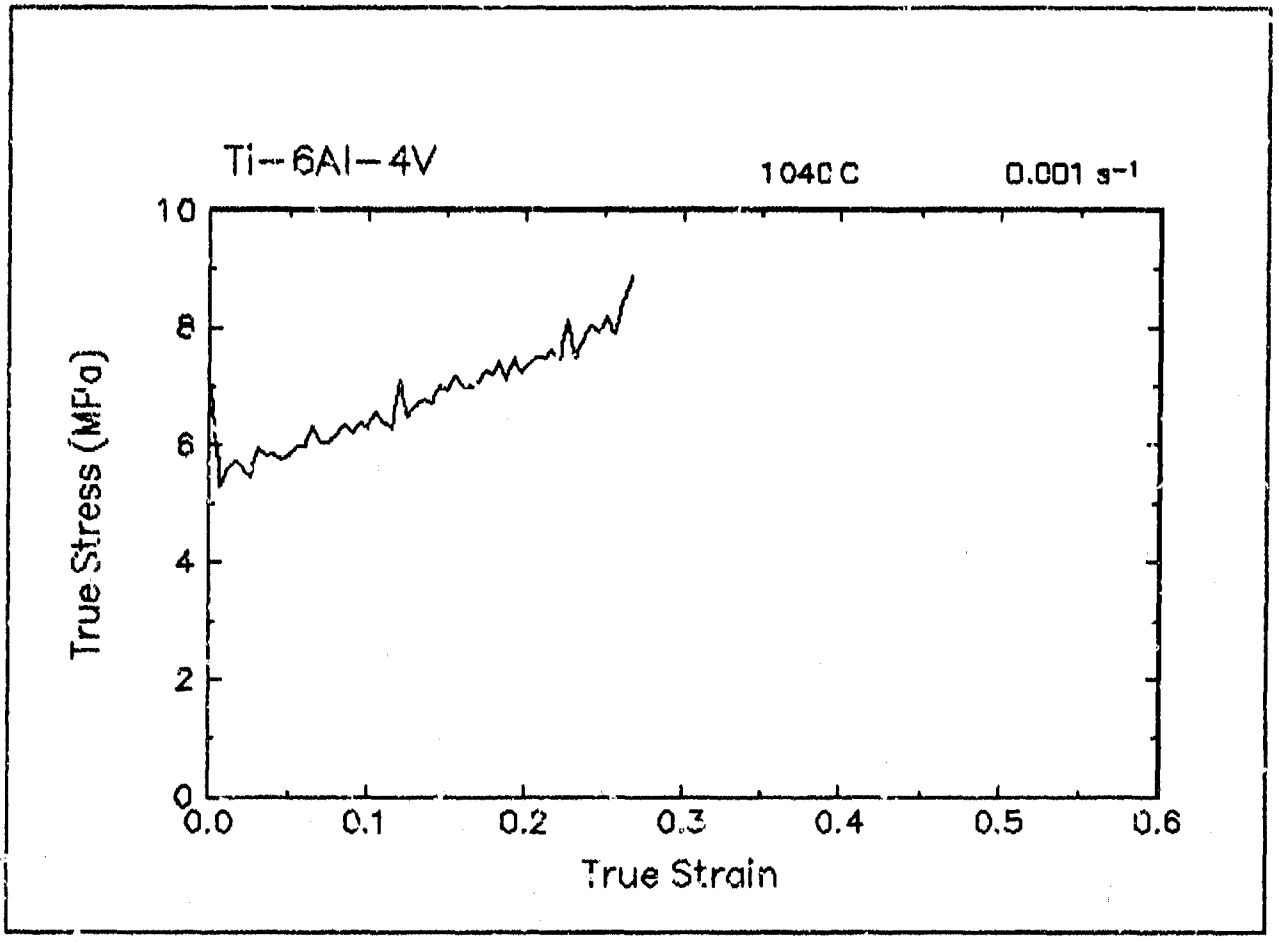

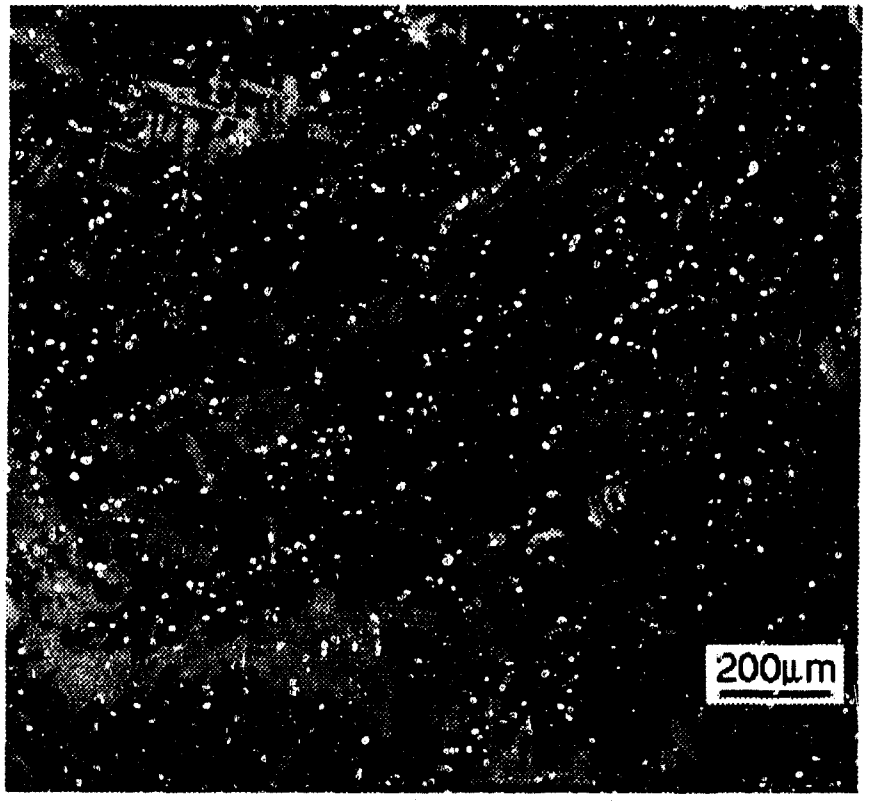

Figure 32. True stress-true strain curve and an optical micrograph from the center of the compressed sample cut through the compression axis, 1040 C and 0.001 s^{-1}.

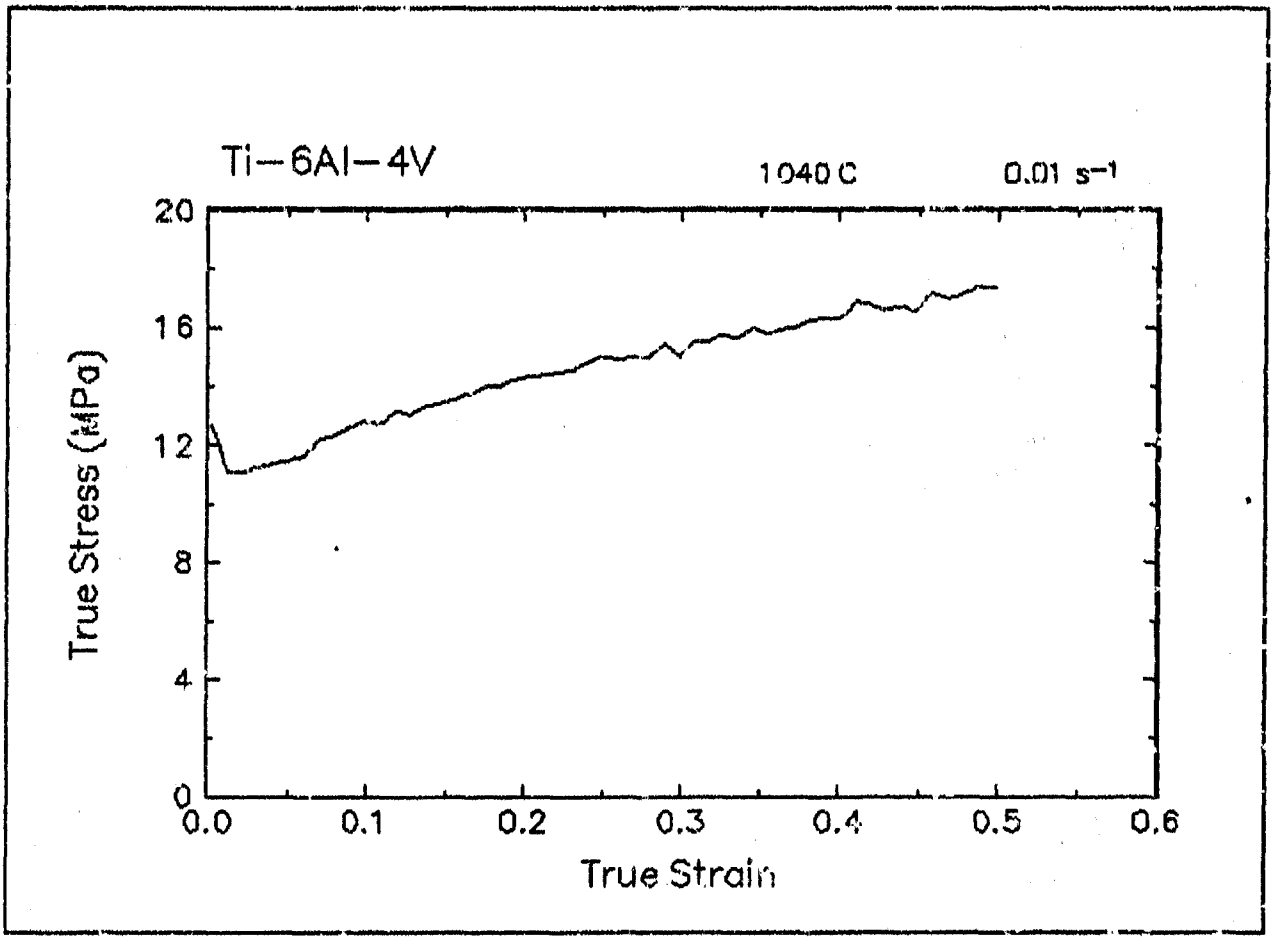

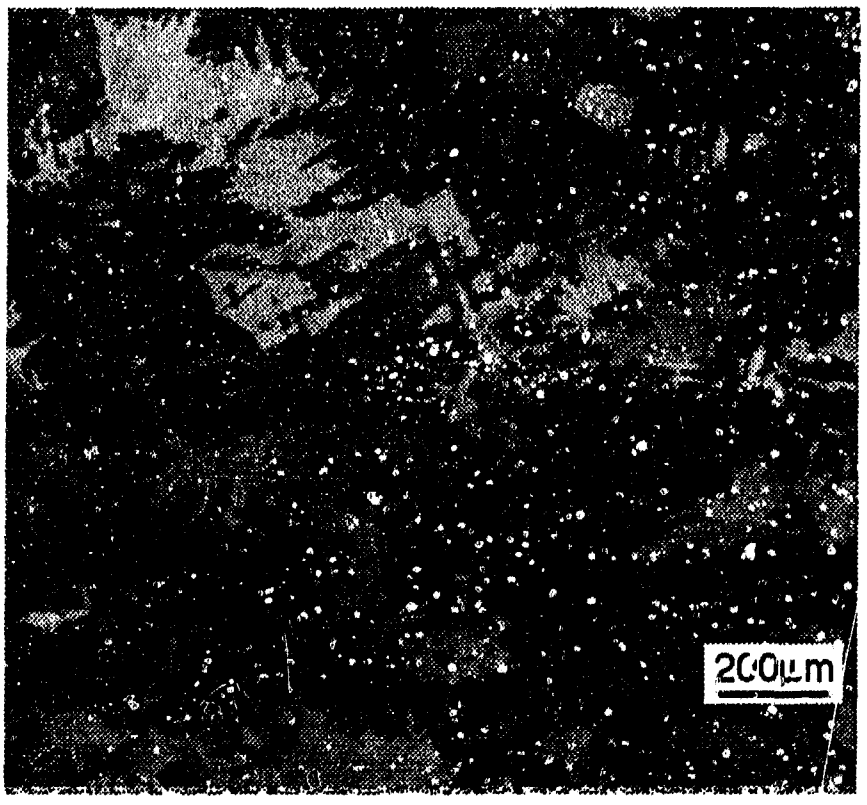

Figure 33. True stress-true strain curve and an optical micrograph from the center of the compressed sample cut through the compression axis, 1040 C and 0.01 s^{-1}.

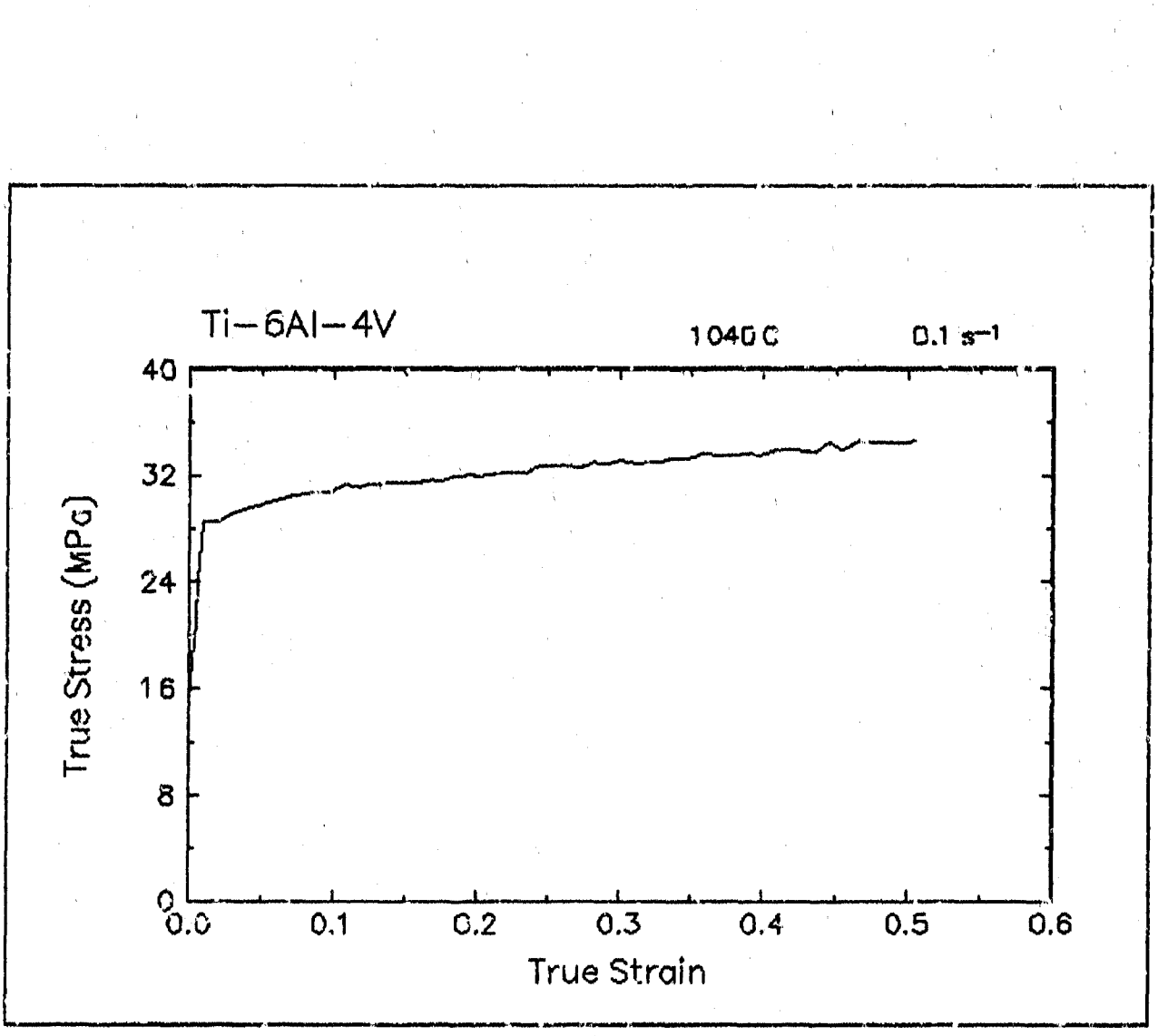

Figure 34. True stress-true strain curve, 1040 C and 0.1 s^{-1}.

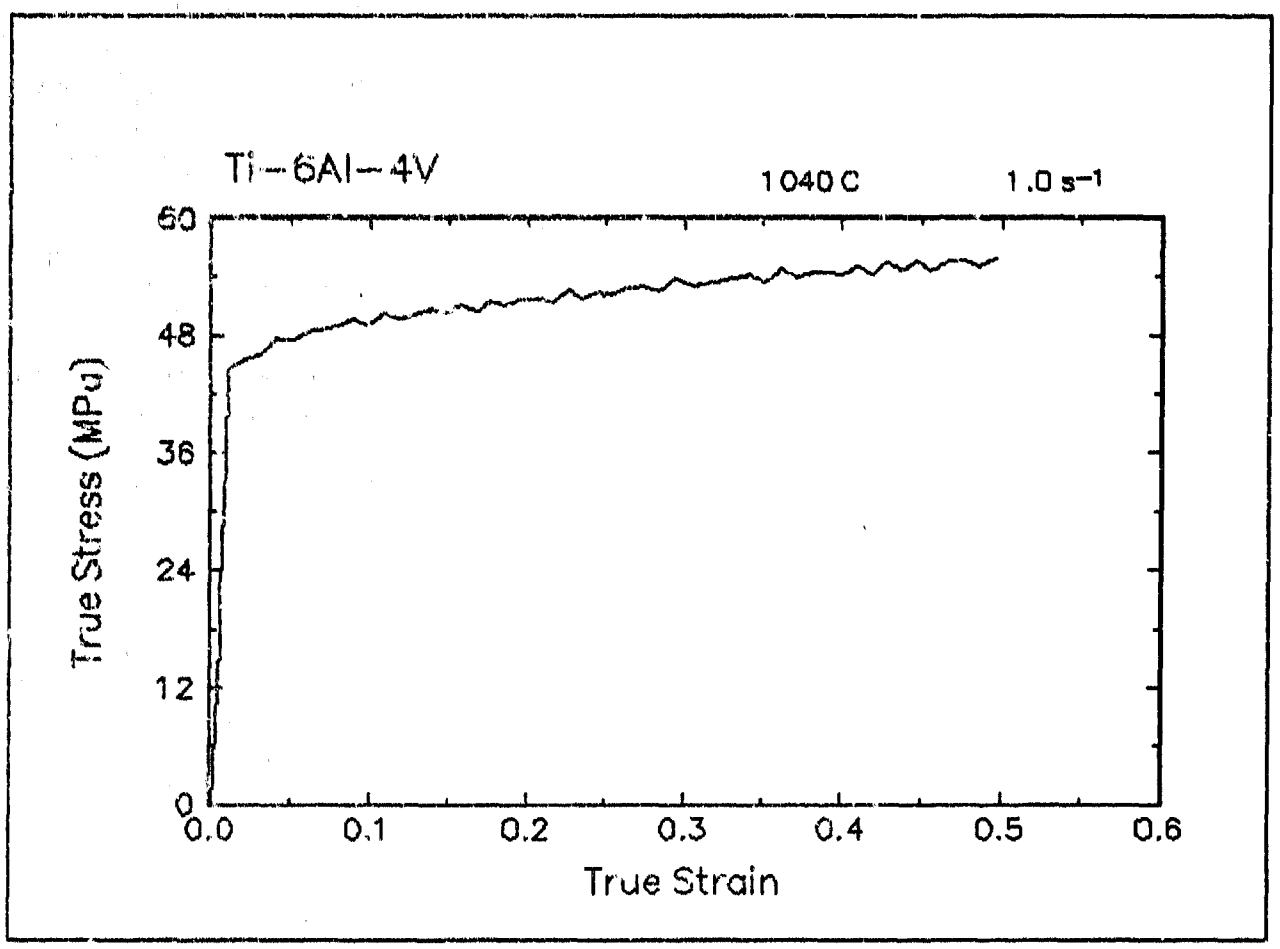

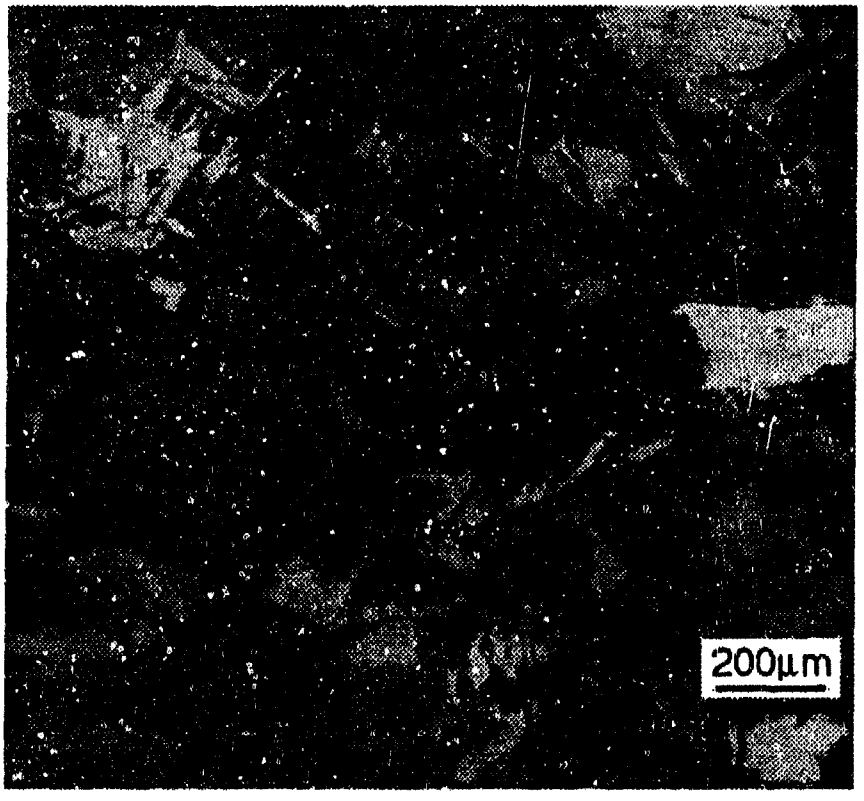

Figure 35. True stress-true strain curve and an optical micrograph from the center of the compressed sample cut through the compression axis, 1040 C and 1 s^{-1}.

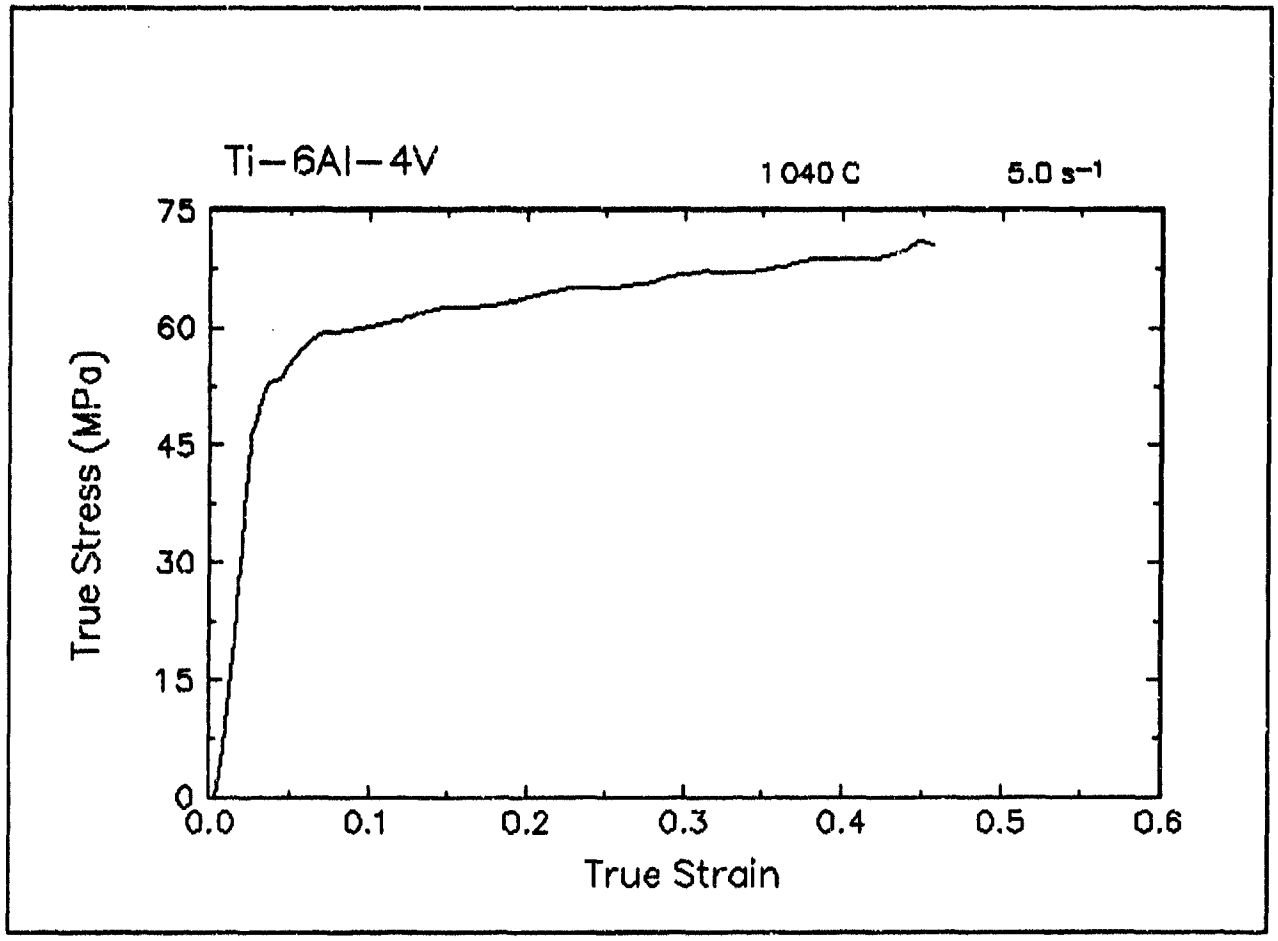

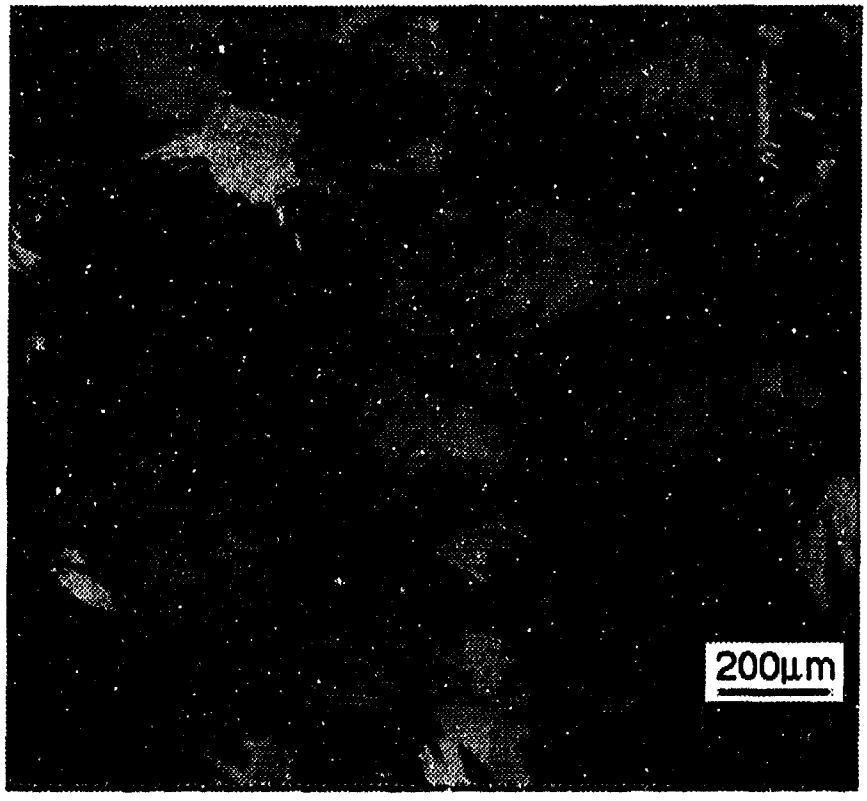

Figure 36. True stress-true strain curve and an optical micrograph from the center of the compressed sample cut through the compression axis, 1040 C and 5 s^{-1}.

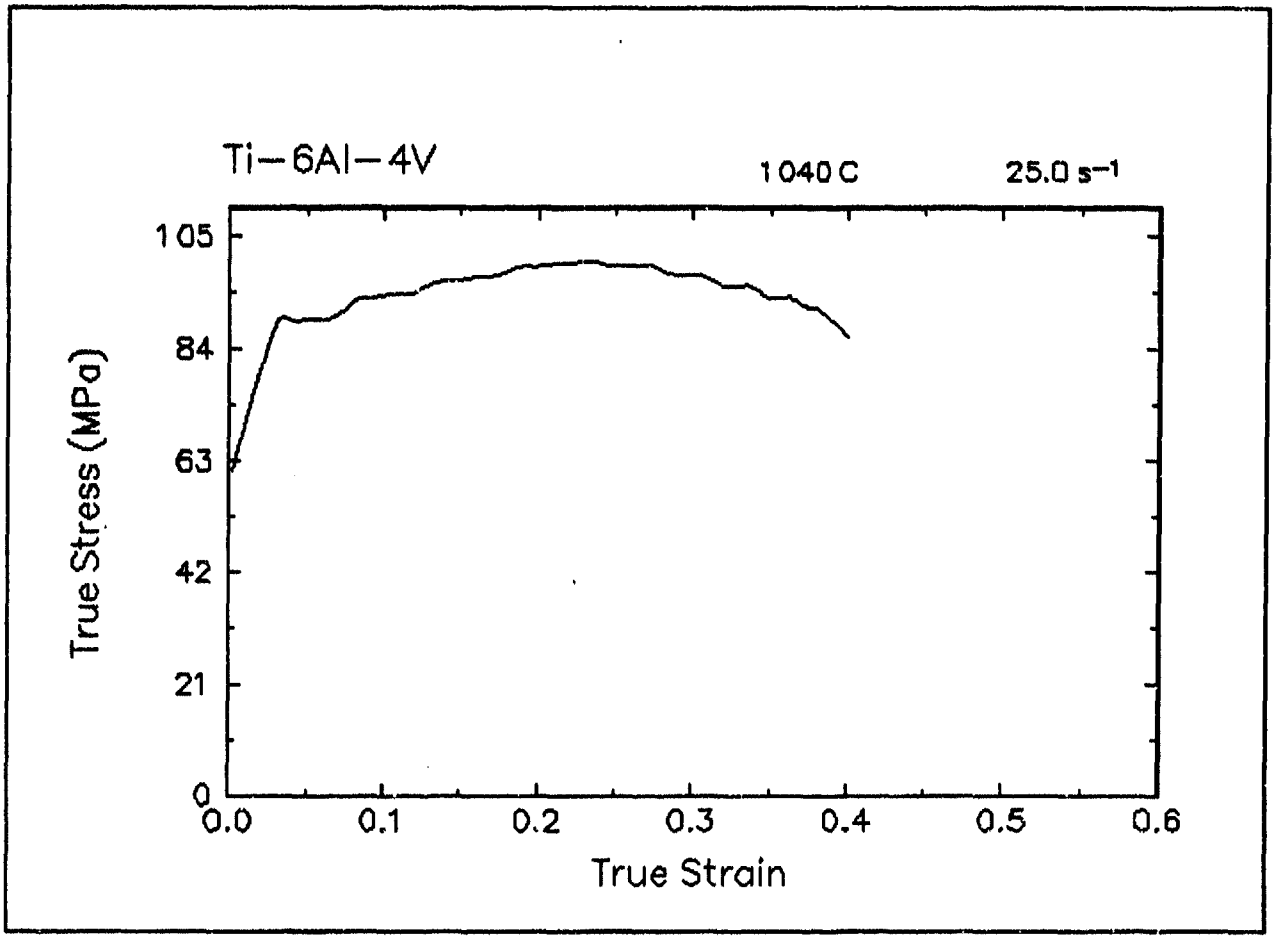

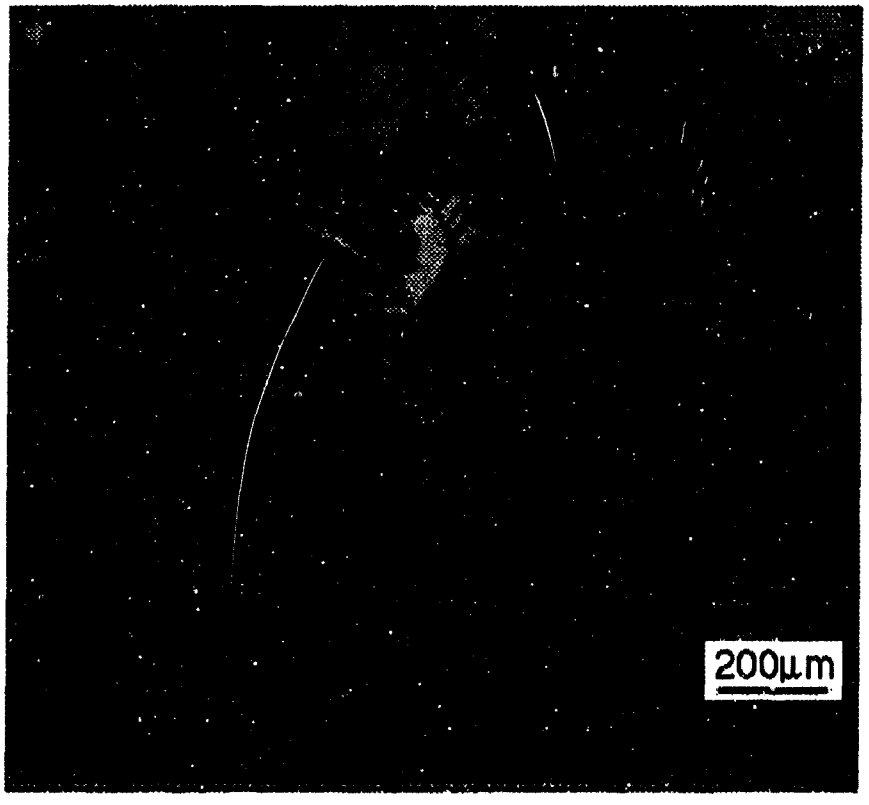

Figure 37. True stress-true strain curve and an optical micrograph from the center of the compressed sample cut through the compression axis, 1040 C and 25 s^{-1}.

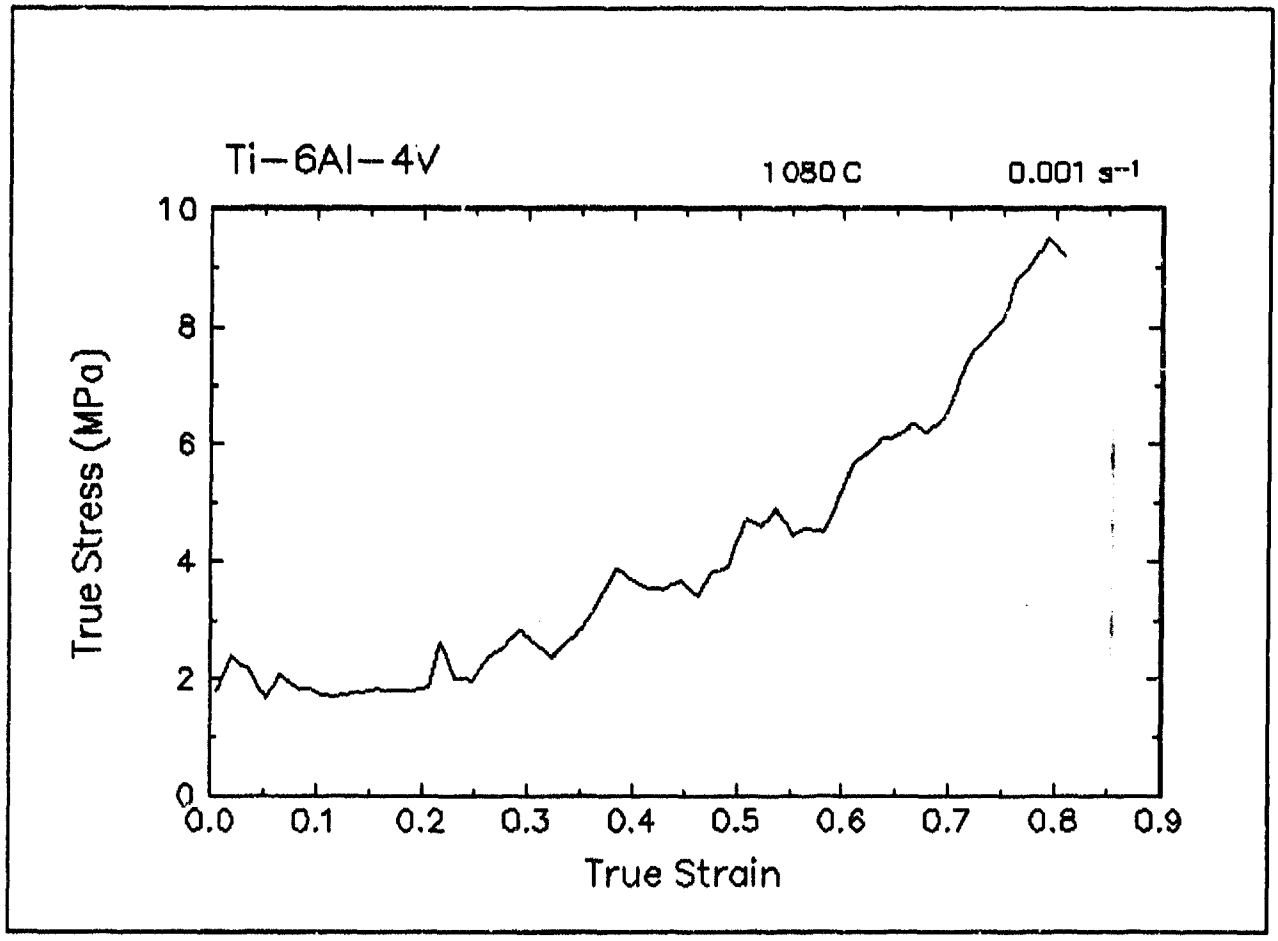

Figure 38. True stress-true strain curve and an optical micrograph from the center of the compressed sample cut through the compression axis, 1080 C and 0.001 s^{-1}.

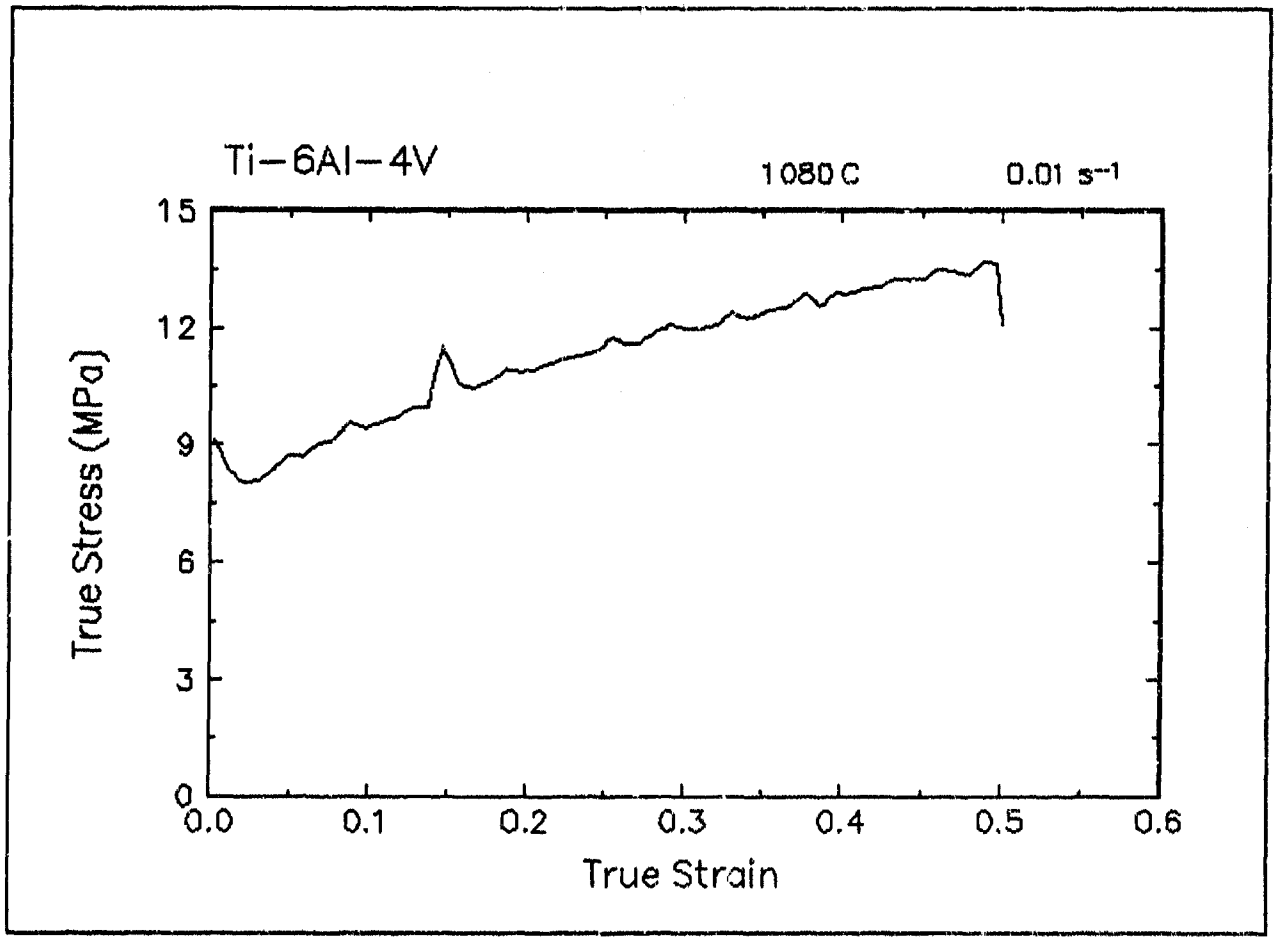

Figure 39. True stress-true strain curve, 1080 C and 0.01 s^{-1}.

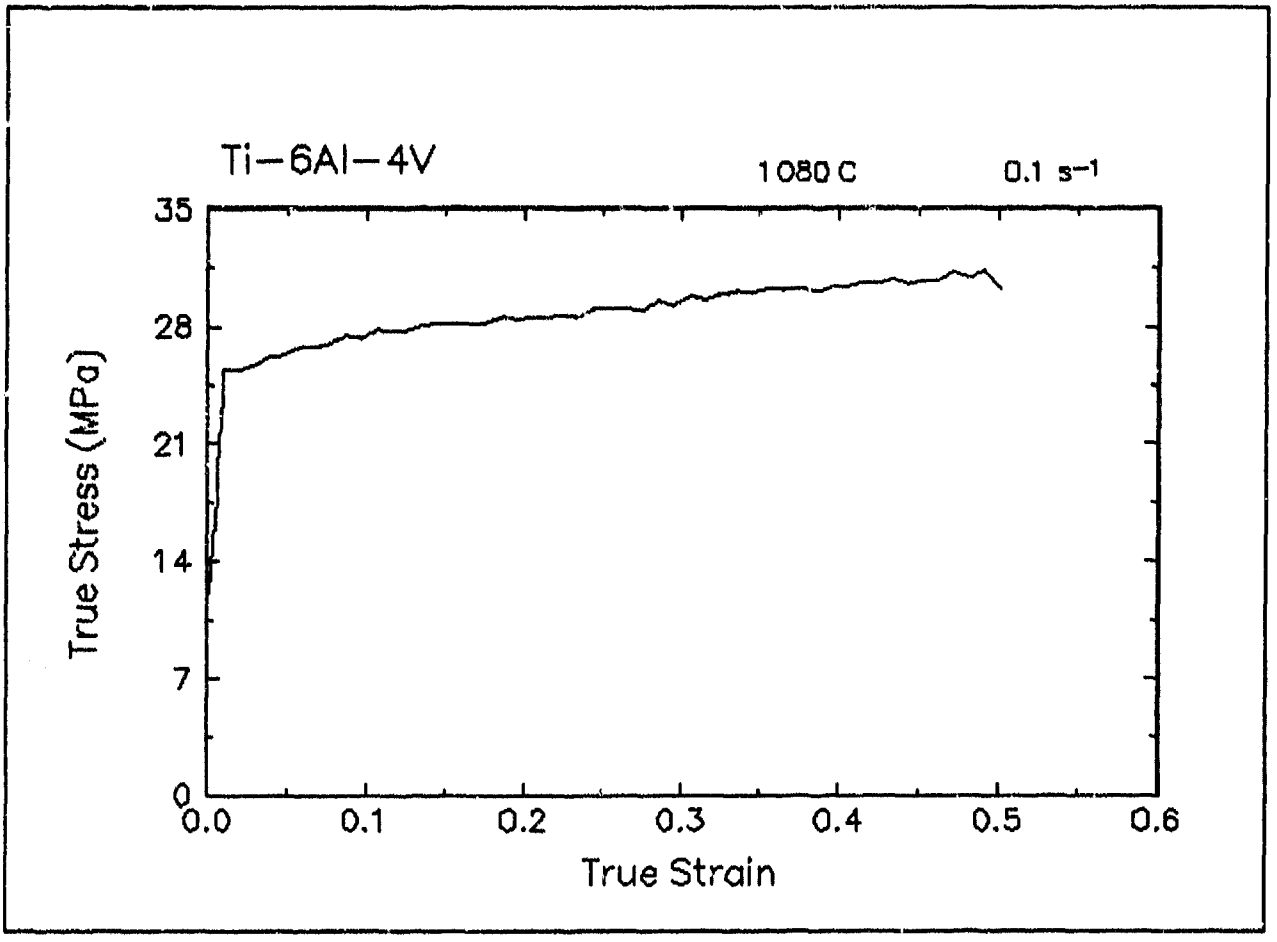

Figure 40. True stress-true strain curve and an optical micrograph from the center of the compressed sample cut through the compression axis, 1080 C and 0.1 s^{-1}.

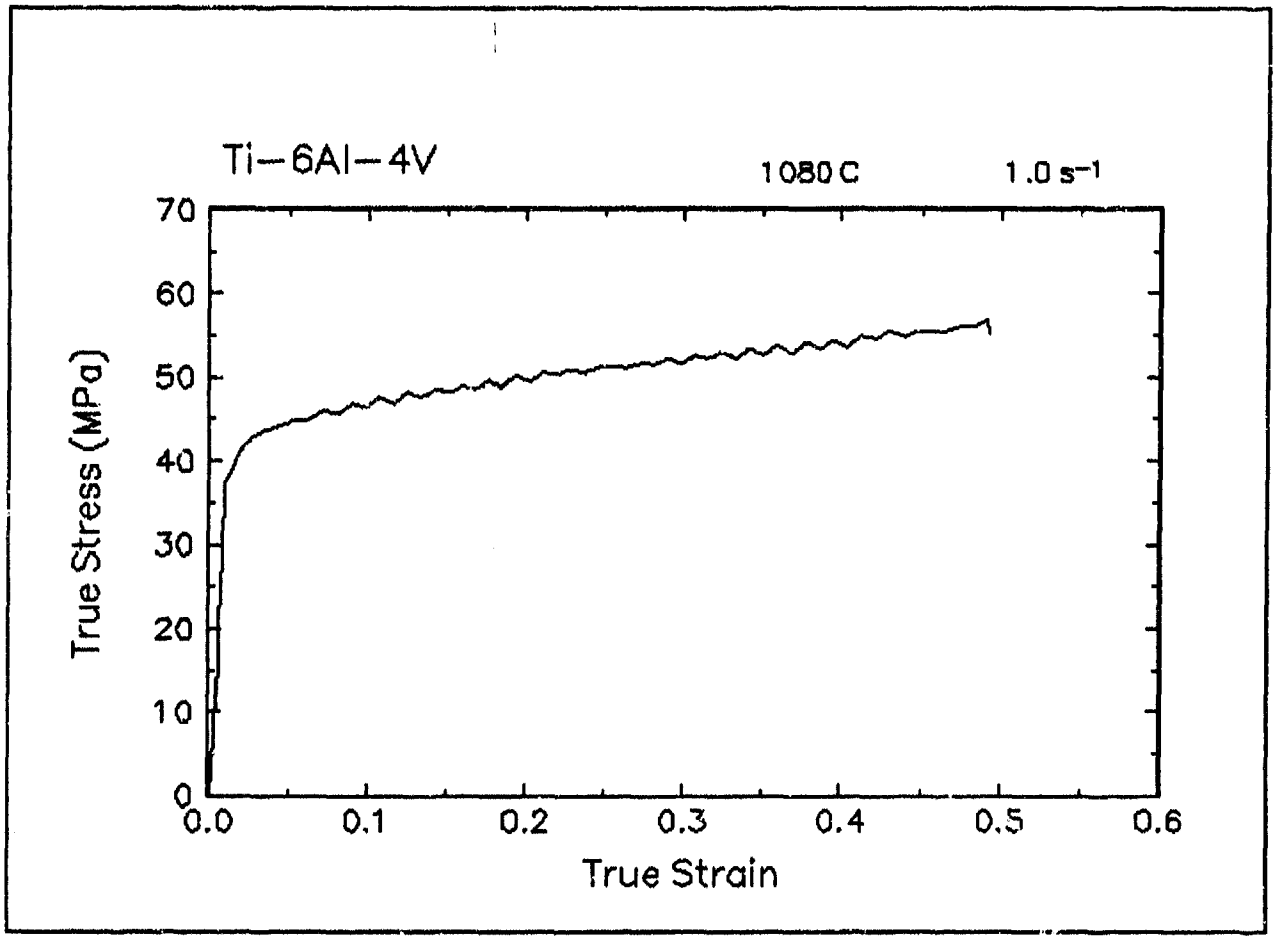

Figure 41. True stress-true strain curve and an optical micrograph from the center of the compressed sample cut through the compression axis, 1080 C and 1 s^{-1}.

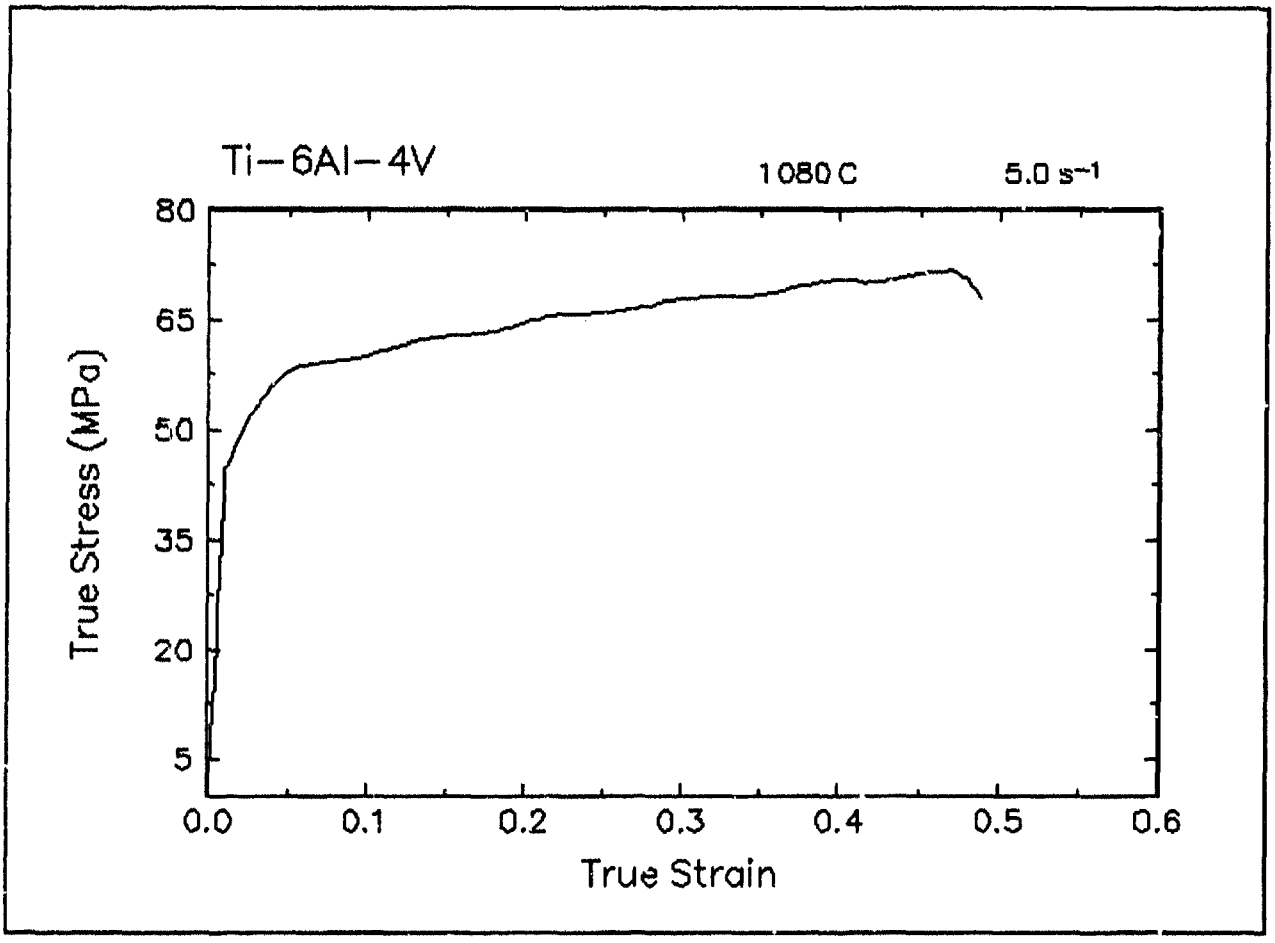

Figure 42. True stress-true strain curve, 1080 C and 5 s^{-1}.

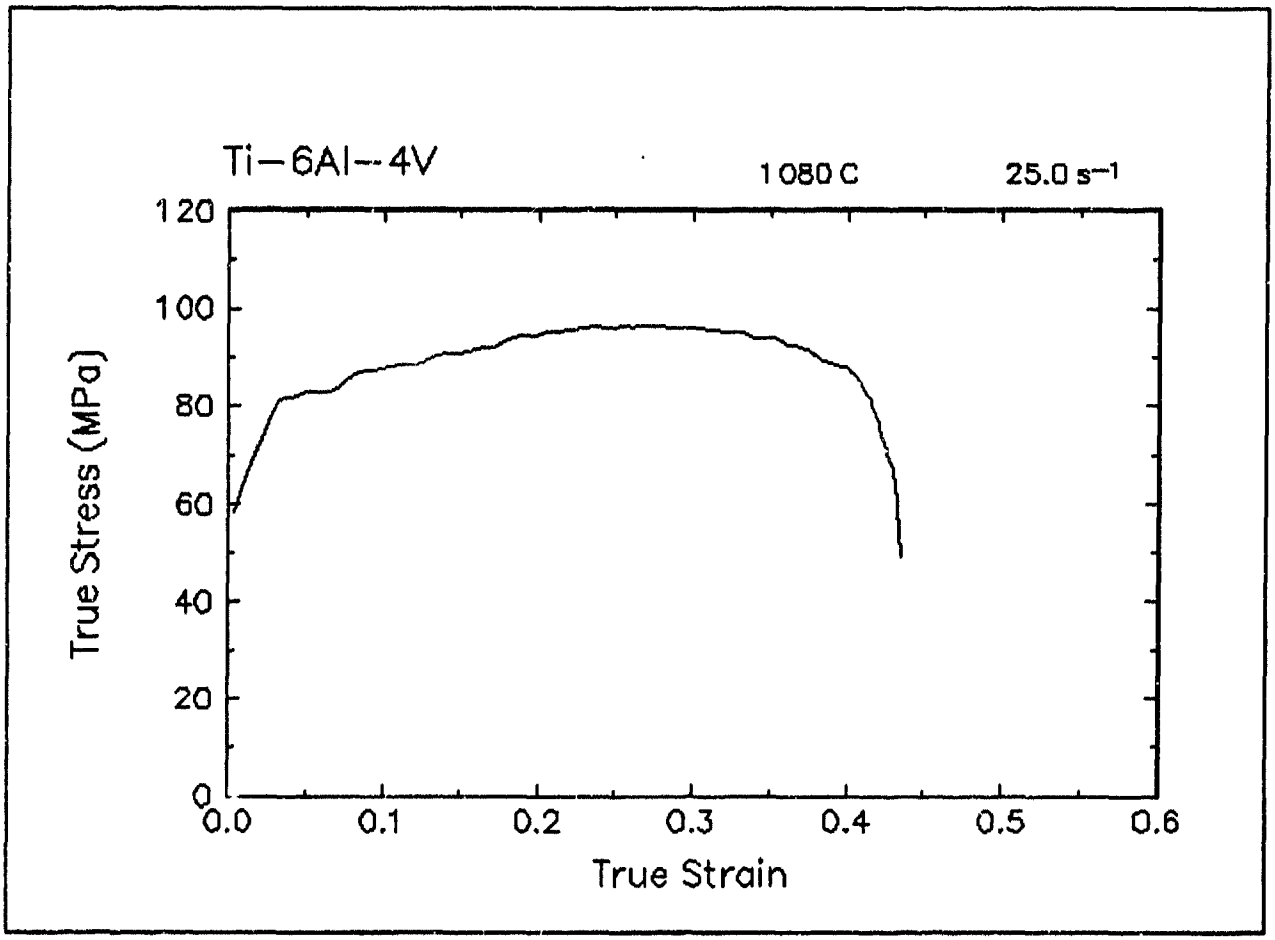

Figure 43. True stress-true strain curve and an optical micrograph from the center of the compressed sample cut through the compression axis, 1080 C and 25 s^{-1}.

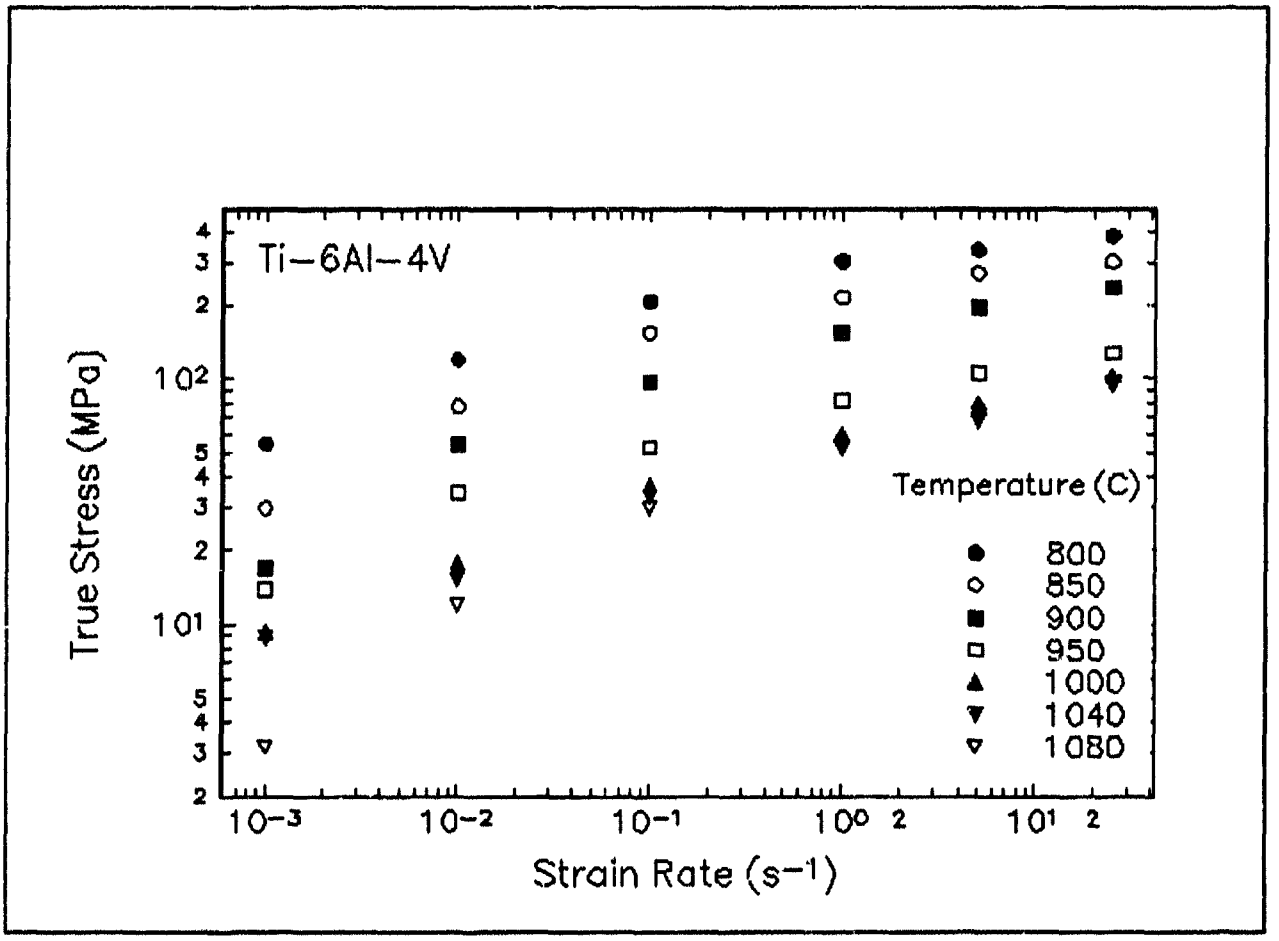

Figure 44. Effect of strain rate on stress in log-log scale at a true strain of 0.3 for Ti-6Al-4V ELI.

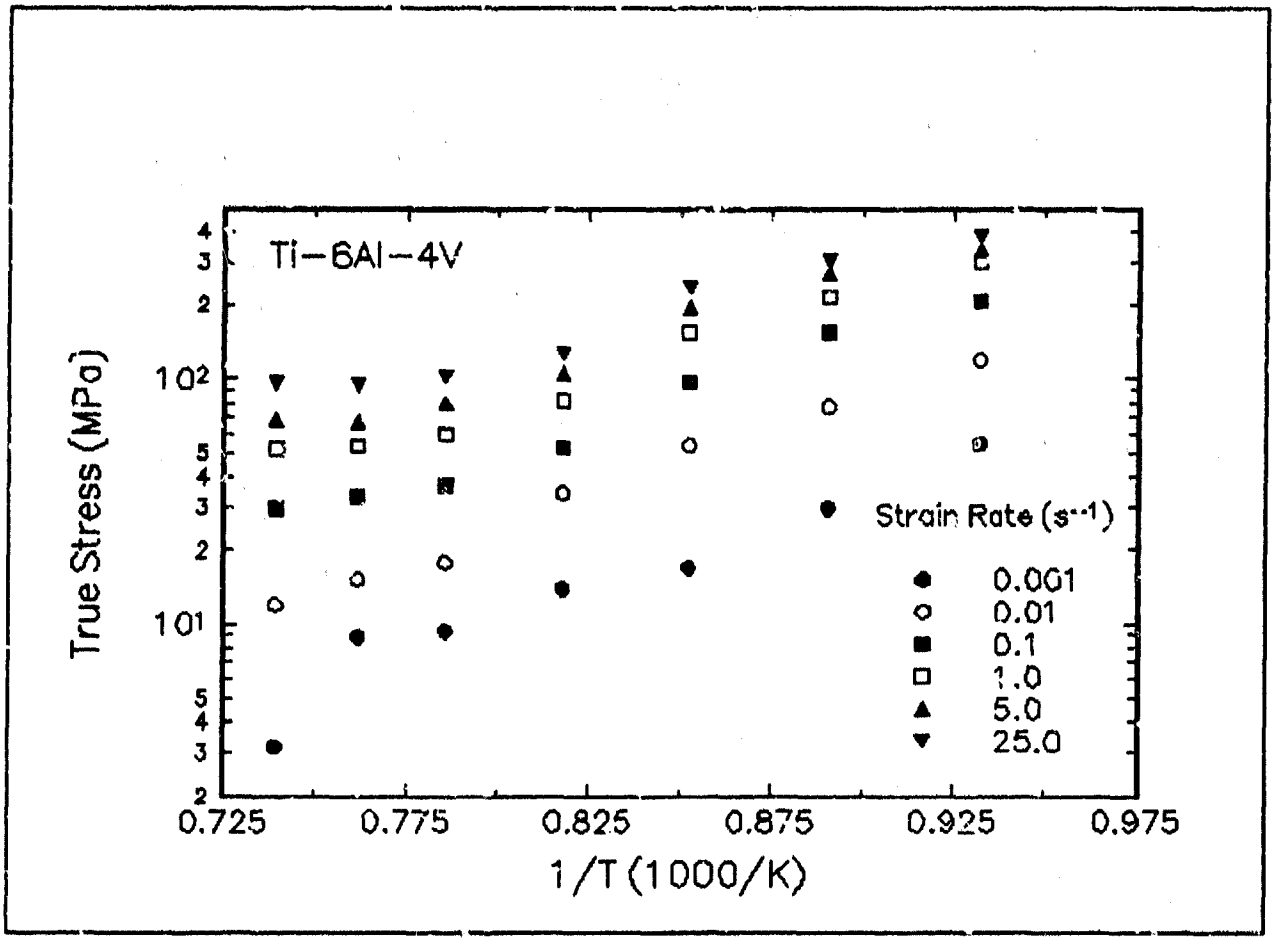

Figure 45. Effect of temperature on stress at a true strain of 0.3 for Ti-6Al-4V ELI.

Summary

Compression tests have been performed on Ti-6Al-4V ELI over a wide range of temperatures and strain rates. The experimental conditions used in this work are representative of those used in metalforming practices. From the stress-strain curves, the flow behavior was characterized and a processing map indicating the optimum processing condition was generated. This condition is approximately 896 C and 0.001 s^{-1}.

The deformed microstructures were characterized from the quenched specimens by optical microscopy and are presented for selective testing conditions together with the stress-strain curves..

Implementation of Data Provided by the Atlas of Formability

The Atlas of Formability program provides ample data on flow behavior of various important engineering materials in the temperature and strain rate regime commonly used in metalworking processes. The data are valuable in design and problem solving in metalworking processes of advanced materials. Microstructural changes with temperature and strain rates are also provided in the Bulletin, which helps the design engineer to select processing parameters leading to the desired microstructure.

The data can also be used to construct processing map using dynamic material modeling approach to determine stable and unstable regions in terms of temperature and strain rate. The temperature and strain rate combination at the highest efficiency in the stable region provides the optimum processing condition. This has been demonstrated in this Bulletin. In some metalworking processes such as forging, strain rate varies within the workpiece. An analysis of the process with finite element method (FEM) can ensure that the strain rates at the processing temperature in the whole workpiece fall into the stable regions in the processing map. Furthermore, FEM analysis with the data from the Atlas of Formability can be coupled with fracture criteria to predict defect formation in metalworking processes.

Using the data provided by the Atlas of Formability, design of metalworking processes, dynamic material modeling, FEM analysis of metalworking processes, and defect prediction are common practice in *Concurrent Technologies Corporation*. Needs in solving problems related to metalworking processes can be directed to Dr. Prabir K. Chaudhury, Manager of Forming Department, by calling (814) 269-2594.